

THE MICHIGAN STATE UNIVERSITY  
IRON-FREE DOUBLE FOCUSING BETA-RAY SPECTROMETER

Thesis for the Degree of Ph. D.

MICHIGAN STATE UNIVERSITY

Libor Jiri Velinsky

1964



MICHIGAN STATE UNIVERSITY  
[REDACTED]  
EAST LANSING, MICHIGAN



## ABSTRACT

### THE MICHIGAN STATE UNIVERSITY IRON-FREE DOUBLE FOCUSING BETA-RAY SPECTROMETER

by Libor Jiri Velinsky

A 30 centimeter radius iron-free  $\pi\sqrt{2}$  beta-ray spectrometer using the Moussa focusing coil configuration and some features of the Vanderbilt University instrument, was designed and constructed. The design, construction and testing of the machine are discussed in detail. With stable environment a  $\pm 2:10^6$  short range and a  $\pm 5:10^5$  long range stability was achieved.

To test the performance of the instrument, the internal conversion spectrum of  $\text{Ba}^{137\text{m}}$  was examined with 0.047% resolution. The relative line intensities obtained were:  $K: L_I: L_{II}: L_{III}: M_I: M_{II,III}: M_{IV,V} = (1^{\pm.04}): (.140^{\pm.007}): (.0207^{\pm.0046}): (.0171^{\pm.0041}): (.0233^{\pm.0030}): (.0145^{\pm.0020}): (.0047^{\pm.0016})$ . The K and L shell results are in agreement with those of Geiger et al. The M shell results are new.

The internal conversion spectrum of  $\text{Bi}^{210}$  was obtained with 0.18% resolution. The relative line intensities are:  $L_I: L_{II}: L_{III}: M_I: M_{II}: M_{III}: N_I: N_{II}: N_{III}: N_{IV-VII}+O_I+P_I = (1^{\pm.034}): (.111^{\pm.007}): (.0094^{\pm.0028}): (.229^{\pm.007}): (.023^{\pm.003}): (.0029^{\pm.0022}): (.0597^{\pm.0038}): (.0069^{\pm.0011}): (.0012^{\pm.0005}): (.015^{\pm.003})$ . The intensity ratios in the L



shell and the  $M_I/M_{II}$  ratio agree with theory for pure M-1 radiation. In both experiments the M shell line intensities fall considerably below Rose's calculated values. The discrepancies are consistent and agree with measurements of Bäckström et al., for  $Hg^{199}$ .

THE MICHIGAN STATE UNIVERSITY  
IRON-FREE DOUBLE FOCUSING BETA-RAY SPECTROMETER

By  
Libor Jiri Velinsky

A THESIS

Submitted to  
Michigan State University  
in partial fulfillment of the requirements  
for the degree of

DOCTOR OF PHILOSOPHY

Department of Physics and Astronomy

1964

## ACKNOWLEDGMENT

It is a pleasure to acknowledge my indebtedness to Professor Sherwood K. Haynes, whose direction, encouragement and patience were invaluable throughout the course of this work. I wish to thank him particularly for allowing me to take a lion's share of the decision-making responsibilities during the design of the spectrometer, for it transformed a straightforward construction project into a creative learning experience. The intimate encounter with the myriad of details involved in this work was invaluable to me.

I am grateful to the members of the staff of the Department of Physics for their help and encouragement and to Mr. R. J. Krisciokaitis for many useful discussions and his assistance, particularly during the stability tests and the data collection runs.

I am indebted to the late Mr. Charles Kingston for his help and his many suggestions pertaining to the mechanical construction of the spectrometer. My thanks also go to N. R. Mercer, R. B. Hoskins, R. W. Cochrane, D. Salemka and N. Rutter, the staff of the machine shop, and to E. F. Brandt and W. Harder, Jr., of the electronics shop, for their part in the construction of the spectrometer.

Last but not least, I wish to express my thanks to my wife Marilyn, whose assistance, encouragement and support were invaluable to me. I dedicate this work to her.

The spectrometer was constructed and operated with the aid of a financial grant from the National Science Foundation.

## TABLE OF CONTENTS

	Page
ACKNOWLEDGMENT. . . . .	ii
LIST OF TABLES. . . . .	vi
LIST OF FIGURES . . . . .	vii
INTRODUCTION. . . . .	1
CHAPTER 1. SURVEY OF BETA-RAY SPECTROMETERS. . . . .	7
CHAPTER 2. ELECTRON OPTICAL PROPERTIES OF AXIALLY SYMMETRIC MAGNETIC FIELDS . . . . .	13
2.1 Basic Definitions and Relationships. . . . .	13
2.2 The Equations of Motion and the Series Representation of the Magnetic Field . . . . .	17
2.3 Focusing Properties of Axially Symmetric Magnetic Fields. . . . .	26
CHAPTER 3. IRON FREE DOUBLE FOCUSING SPECTROMETERS . . . . .	37
3.1 Focusing Coil Configurations . . . . .	37
3.2 Determination of Focusing Coil Parameters . . . . .	41
CHAPTER 4. CONSTRUCTION OF THE SPECTROMETER. . . . .	48
4.1 Introduction . . . . .	48
4.2 Construction of the Focusing Coils . . . . .	51
(a) The Coil Mounts	
(b) The Winding Procedure	
(c) The Coil Terminals and Leads	
4.3 The Vacuum Chamber . . . . .	60
4.4 The Source End Assembly. . . . .	64
4.5 The Counter System . . . . .	67
(a) Introduction	
(b) The Side Window G.-M. Counter	
(c) The Counter Gas Flow System	
(d) The Data Acquisition System	
4.6 The Baffle System. . . . .	77

	Page
4.7 The Focusing Coil Temperature Control System . . . . .	83
(a) Introduction	
(b) The Circulating System	
(c) Thermostatic Control	
4.8 The Vacuum System. . . . .	88
(a) The Vacuum Pumps	
(b) The Vacuum System	
(c) Electrical Controls and Associated Equipment	
CHAPTER 5. FOCUSING COIL CURRENT CONTROL SYSTEM. . .	97
5.1 Introduction . . . . .	97
5.2 Design and Construction of the Transistorized Power Supply. . . . .	98
(a) The Input Section	
(b) The Rough Regulator	
(c) The Fine Regulator Loop	
(d) The A.C. Feedback Loops	
(e) Fine Regulator Construction Notes	
(f) Regulator Operation	
5.3 The Rotating Coil System . . . . .	118
(a) Introduction	
(b) The Field Sensing Coils	
(c) The Rotating Shaft System	
(i) The rotating shaft, its drive and supports	
(ii) The rotating shaft construction notes	
(d) The Permanent Magnet Assembly	
5.4 The Performance of the Current Control System . . . . .	148
CHAPTER 6. EXTERNAL FIELD COMPENSATION . . . . .	153
6.1 Introduction . . . . .	153
6.2 The Compensating Coils . . . . .	154
6.3 The Compensating Coil Power Supply .	155
6.4 Performance. . . . .	158
CHAPTER 7. ALIGNMENT OF THE SPECTROMETER . . . . .	163
7.1 Coil Measurements. . . . .	163
7.2 Computer Runs for the Optimization of the Focusing Field. . . . .	171

	Page
7.3 Alignment of the Spectrometer. . . .	188
7.4 Phasing of the Rotating Coils. . . .	189
CHAPTER 8. COUNTER WINDOW AND SOURCE PREPARATION . .	193
8.1 Counter Window Preparation . . . . .	193
8.2 Source Preparation . . . . .	196
CHAPTER 9. PERFORMANCE OF THE SPECTROMETER	
THE CONVERSION ELECTRON SPECTRUM OF	
Cs - Ba 137 . . . . .	203
9.1 Introduction . . . . .	203
9.2 The Conversion Electron Spectrum of Cs - Ba 137. . . . .	204
9.3 The Experiment . . . . .	207
(a) Source Preparation	
(b) Data Collection	
(c) Data Analysis	
9.4 Results and Conclusions. . . . .	211
CHAPTER 10. THE CONVERSION ELECTRON SPECTRUM OF	
RADIUM D. . . . .	217
10.1 Introduction . . . . .	217
10.2 The Decay of Radium D. . . . .	220
10.3 The Conversion Electrons of Radium D	226
10.4 The Experiment . . . . .	230
(a) Source Preparation	
(b) Data Collection	
(c) Data Analysis	
10.5 Results and Conclusions. . . . .	235
REFERENCES. . . . .	242

# LIST OF TABLES

Table	Page
I. Focusing Coil Data . . . . .	56
II. Coil Winding Cross Sections. . . . .	166
III. Equivalent Radii and the Spacing of Current Filaments for the Focusing Coils . . . . .	166
IV. Axial Spacing of the Focusing Coils. . . . .	187
V. The K Conversion Coefficients and the $K/\Sigma L$ Line Intensity Ratios for $Ba^{137m}$ . . . . .	206
VI. Relative Conversion Line Intensities . . . . .	207
VII. Relative Intensities of the $Ba^{137m}$ Conversion. . . . .	213
VIII. Summary of RaD Conversion Electron Data. . . . .	231
IX. Relative Intensities of the RaD Conversion Lines. . . . .	238

# LIST OF FIGURES

Figure		Page
1.	Transmission as a function of the field coefficient $a_2$ . . . . .	34
2.	Focusing coil arrangement due to Siegbahn and Edvarson . . . . .	38
3.	(a) Focusing coil arrangement due to Moussa (b) Focusing coil arrangement due to Lee- Whiting and Taylor . . . . .	40
4.	Plot of $f\sqrt{\alpha}$ versus $\alpha$ . . . . .	44
5.	Overall view of the completed spectrometer . .	50
6.	Cross-sectional view of focusing coil mounts .	54
7.	Schematic diagram of coil winding apparatus. .	59
8.	Schematic representation of the focusing coil power connections. . . . .	61
9.	Spectrometer vacuum chamber. . . . .	63
10.	The source end assembly. . . . .	66
11.	The source end assembly (photograph) . . . . .	68
12.	The side window G-M counter. . . . .	70
13.	(a) Assembled counter (b) Counter positioned on spectrometer end- plate. . . . .	72
14.	Counter gate assembly. . . . .	74
15.	Counter gas flow system. . . . .	75
16.	Counter gas flow system panel. . . . .	78
17.	Beam defining baffles. . . . .	80
18.	Spectrometer baffle positions. . . . .	82
19.	Focusing coil temperature control system . . .	84
20.	Focusing coil temperature control system. The pump and the heat exchangers . . . . .	86



Figure		Page
21.	Focusing coil temperature control system. The control circuit. . . . .	89
22.	Block diagram of the main vacuum system. . . .	92
23.	High vacuum water cooled baffle. . . . .	93
24.	Vacuum pump control circuit. . . . .	95
25.	Block diagram of spectrometer power supply . .	99
26.	Schematic diagram of the spectrometer power supply . . . . .	103
27.	Schematic diagram of the error signal amplifiers and the phase sensitive detector . . .	109
28.	Schematic diagram of the chopper driving circuit. . . . .	112
29.	Section of the rotating shaft. . . . .	129
30.	Schematic diagram of a shaft section . . . . .	131
31.	Cross-section of the spectrometer end of the rotating shaft . . . . .	136
32.	Cross-section of the central driving pulley. .	139
33.	Photograph of the shaft drive. . . . .	142
34.	Permanent magnet assembly. Mechanical phase control. . . . .	145
35.	Schematic diagram of the compensating coils current regulators . . . . .	157
36.	Residual vertical field. . . . .	159
37.	Decomposition of a rectangular cross-section coil into equivalent current filaments . . .	164
38.	Magnetic field of a circular current. Definition of symbols. . . . .	169
39.	Radial field of the B coil pair as a function of its displacement relative to the median plane of the spectrometer. . . . .	173
40.	Radial field of the C coil pair as a function of its displacement relative to the median plane of the spectrometer. . . . .	174

Figure	Page
41. Radial field of the D coil pair as a function of its displacement relative to the median plane of the spectrometer. . . . .	175
42. Radial field as a function of radius . . . . .	177
43. Variation in $B_z$ as a function of radius (A coils) . . . . .	178
44. Variation in $B_z$ as a function of radius (B coils) . . . . .	179
45. Variation in $B_z$ as a function of radius (C coils) . . . . .	180
46. Variation in $B_z$ as a function of radius (D coils) . . . . .	131
47. Deviation of total axial field from ideal sixth order field (A coils moved). . . . .	183
48. Deviation of total axial field from ideal sixth order field (B coils moved). . . . .	184
49. Deviation of total axial field from ideal sixth order field (C coils moved). . . . .	185
50. Deviation of total axial field from ideal sixth order field (D coils moved). . . . .	186
51. Source evaporator. . . . .	199
52. Internal conversion lines of $\text{Cs}^{137}$ - $\text{Ba}^{137\text{m}}$ . . . . .	210
53. Conversion line intensity ratios as a function of transition energy . . . . .	212
54. The conversion electron spectrum of $\text{RaD}$ . . . . .	233
55. Conversion line intensity ratios as a function of transition energy . . . . .	236
56. Conversion line intensity ratios as a function of transition energy . . . . .	237

## INTRODUCTION

Nuclear physics owes its beginnings to Henri Becquerel<sup>1</sup> and his discovery of the natural radioactivity of uranium compounds. Subsequent interest in this phenomenon led Rutherford and Soddy<sup>2</sup> to suggest that radioactive disintegrations result in changes of atomic species; Rutherford to identify alpha particles as helium nuclei,<sup>3</sup> and from the results of his now famous scattering experiment to propose the nuclear atom.<sup>4</sup> Although stable isotopes were discovered by J. J. Thomson in 1913,<sup>5</sup> it was not until 1932 that the experiments of Curie and Joliot<sup>6</sup> led Chadwick to the discovery of the neutron<sup>7</sup> and thus the completion of the basic inventory of the nucleus. Two years later, in 1934, experiments of Irene Curie and Joliot<sup>8</sup> dealing with the alpha particle bombardment of light nuclei, established the existence of artificially radioactive isotopes. This period also witnessed the proposal of the DeBroglie hypothesis and the next step in the development of the old quantum theory when Erwin Schroedinger formulated the principles of wave mechanics.<sup>9</sup>

These are but few of the events in the history of modern physics that were responsible for the birth of nuclear spectroscopy.

Progress in this field was relatively slow until the end of the second World War, when the availability and use of nuclear reactors and high intensity accelerators made

possible the wholesale discovery of artificially radioactive nuclides and their production in appreciable amounts. It was also during this period that instrumentation became sophisticated enough to enable us to observe the products of nuclear decay with relatively high precision. Since then, a great deal of attention has been devoted to this area of physics. At the present time the amount of information presented to the inquirer every year is nearly astronomical and the problem of rapid recovery of pertinent information from published material is becoming more acute with every passing year.

The purpose of nuclear spectroscopy is the collection, analysis and interpretation of data concerning the positions of the various nuclear energy levels, their quantum numbers and characteristics of decay, to yield information necessary for testing the host of existing nuclear models and theories describing the various aspects of the decays. Only such experimental observation can form a sound basis for justification of theoretical predictions, and only these two, hand in hand, can bring us a closer understanding of some aspects of the nuclear problem.

For most radionuclides, nuclear spectroscopy involves the study of the gamma radiations and the beta emissions from the atom. The study of the beta radiations concerns the identification of the number of beta-ray transitions present, the measurement of their branching ratios and their end-point energies, thereby ascertaining the nuclear energy

levels responsible for these transitions. The measurement of the shapes of the beta-ray spectra provides information about the spin and the parity of the levels involved in the decay.

The primary concern of gamma ray spectroscopy is the measurement of the energies and the intensities of the various gamma ray transitions present in a given decay and, by use of appropriate experimental techniques, the determination of the quantum numbers of the nuclear levels responsible for the decay. Gamma ray spectra can be studied directly by means of scintillation and crystal spectrometers, or indirectly by performing a magnetic momentum analysis of external or internal conversion electrons.

The internal conversion electrons trace their origin to a nuclear process. A nucleus decaying from an excited state can emit a gamma ray whose energy corresponds to the energy difference of the nuclear energy levels involved in the transition. Alternately this energy can be transferred directly to an orbital electron which is then ejected with a kinetic energy corresponding to the energy of the gamma ray less the binding energy of the electron in its orbit. Internal conversion electrons emitted from the various shells and subshells of the atom thus form monoenergetic groups, the study of which can provide information about the nature of the nuclear transition. For instance, the internal conversion coefficients which are defined as the ratio of the transition probability for internal

conversion to the probability of gamma ray emission are found to be sensitive to the multipolarity of the competing gamma radiation.

In cases where the probability of internal conversion is very small, external conversion can be employed where the gamma radiations from the nuclide under study are allowed to fall upon a converter foil and the resulting photoelectrons are analyzed. External conversion can be used to determine the relative intensities of the various gamma rays.

The internal conversion process, electron shakeoff, and the class of decays called orbital capture, give rise to another process which results in the ejection of monoenergetic electron groups: The Auger effect. Following an orbital capture or internal conversion, the atom is left in an ionized state, or, as is often said, there is a primary vacancy in some particular electronic state. This vacancy is filled by a reorganization of the electron population of the atom either in a radiative manner by the emission of X-rays or optical quanta, or, in analogy to the internal conversion process, the energy is transferred to a more weakly bound electron which is then ejected from the atom with a well defined energy. The study of Auger electrons is of interest, since at the present time the amount of accurate theoretical prediction is still quite limited.<sup>10,11</sup> Some recent observations indicate that Auger electron energies are subject to shifts depending on the

chemical composition of the source material.<sup>12</sup> So far these shifts have not been investigated in a systematic manner.

Although the field of nuclear spectroscopy abounds in a wealth of instruments and techniques, an excellent review of which can be found in Siegbahn's book,<sup>13</sup> the beta-ray spectrometer remains one of the basic tools and one of the most versatile; for a wide variety of problems can be studied by the observation and the analysis of the energetics of electron spectra. To be useful, in the light of present day requirements, the beta-ray spectrometer must possess several essential characteristics:

First, there is a need for high resolution. Frequently, many gamma ray transitions are found in the nuclide under observation. The internal conversion process thus yields many groups of monoenergetic electrons, corresponding to the many shells and subshells of the atom where the the conversion process can occur. Furthermore, radiationless transitions that may follow the conversion process give rise to an even larger number of monoenergetic lines of Auger electrons. Often, the great number of such lines in the electron spectrum of a radionuclide causes the lines to be very closely spaced and even to overlap. The interpretation and meaningful, unambiguous analysis of such spectra can only be made if the resolution of the spectrometer is good enough to separate the various groups of electrons.

Second, much of the work done today is with isotopes of low specific activity. High transmission is therefore

desirable to make weak lines observable and to enable the experimenter to collect data with sufficiently good statistics in a reasonable amount of time.

Third, high precision and reproducibility are needed, as the determination of conversion and Auger coefficients requires precise measurements of the intensities and the intensity ratios of the various conversion and Auger spectral lines.

Fourth, high absolute accuracy and the minimization of systematic errors are needed if one is to be able to make meaningful comparisons with the results of other workers in the field and with different observational methods.

The decision to build a magnetic beta-ray spectrometer at Michigan State University was made in the light of interest in the subject matter of electron spectroscopy and of the general versatility of the instrument. The reasons for the choice of the particular instrument that was finally constructed need some amplification and will be found in the succeeding chapters.



## CHAPTER 1

### SURVEY OF BETA-RAY SPECTROMETERS

The various beta spectrometers now in existence can be classified according to the mode of momentum selection into electrostatic and magnetic field deflection instruments. The electrostatic machines have, as a rule, quite good transmission but poor resolution. Their energy range is limited by the potential that can be applied to the deflection elements without electrical breakdown. Attainment of very high precision is also difficult since the deflecting electric field has to be kept always precisely normal to the trajectory of the electrons, or if it is not precisely normal, then the amount of acceleration applied to the electron beam has to be well known and under control. Because of these limitations we shall not consider this type of instrument further.

The beta spectrometers utilizing a magnetic field for momentum analysis can be divided into two main groups, depending on the direction of the applied field relative to the paths of the electrons. In the lens, or helical type of beta spectrometer the net electron motion is parallel to an axially symmetric magnetic field, whereas in the flat, or transverse spectrometers the paths are mainly perpendicular to the applied field. A further distinction

is made among these into iron containing machines and the iron-free machines.

Spectrometers utilizing iron or other ferromagnetic material for shaping their magnetic field appear, at first, to be quite attractive. They are economical in use, for the desired magnetic field can be produced with far less current than in the case of an iron-free spectrometer. Further, the large inductance of the magnet coils is a decided help in stabilizing the field. Fine corrections to the shape of the field can be made relatively easily by means of shims or grinding of the pole faces. Thus once the relatively complex calculations for magnet gap shape are accomplished the actual construction of an iron yoke spectrometer might be expected to be simpler than the construction of its iron-free counterpart. These instruments have, however, some very serious drawbacks which effectively eliminate them from consideration for low energy, high resolution and high precision work:

First, it is difficult to obtain field of precisely axial symmetry, having the proper shape over the entire region of electron trajectories, due to the non-removable inhomogeneities of the iron yoke. Such local variations in the field intensity cause perturbations of the orbits resulting in broadening of the image at the focus.

Second, hysteresis, the nonlinear relationship between the magnet current and the field intensity, requires precise calibration of the magnet over the entire current

range. As the fields generally used for beta spectroscopy are below 1000 gauss and in the case of double focusing spectrometers are highly nonuniform, proton magnetic resonance cannot be used for such measurements and Hall effect devices lack sensitivity at low fields. Rotating coil systems which are used with most of the high precision iron spectrometers have a precision limit of about one part in  $10^4$ . This limit is imposed principally by the magnetic properties of the iron yoke.

Third, the residual remanence of the iron prevents these machines to be used at very low energies, unless a very careful demagnetization procedure is used. Even so, the precision obtainable in this region is rather low.

For these reasons, the iron containing spectrometers will also be dismissed from further consideration. The final choice is to be made therefore among the iron free instruments.

The helical spectrometers fall basically into two categories: The short lens, in which the magnetic field is nonuniform and the source and detector are located outside the field, and the long lens, where the field is more or less uniform and the source and detector are immersed in the field. Both types of spectrometer were developed to a high degree of sophistication after the second World War. One of the most recent and also the best example of a long lens spectrometer is described by Jungerman et al.<sup>14</sup> He reports 0.018% resolution at 0.04% transmission. In spite

of these excellent figures it must be realized, however, that although these machines can be designed to perform close to their theoretical limit and have a very good figure of merit, they do possess several disadvantages for high resolution work at very low energies. The particularly objectionable features are:

First, all lens spectrometers are extremely sensitive to deviations of the focusing field from cylindrical symmetry. This means that the machining work and the coil manufacture on one of these instruments must be of very high order of precision, and hence expensive.

Second, for very high resolution these instruments require a point source, whereas the transverse spectrometers require a line source. Thus the lens spectrometers have eliminated one dimension from the source and therefore the usable intensity for high resolution work will be low.

Third, in these machines the line of maximum convergence of the electron beam, the so-called "ring focus," occurs some distance from the detector. Typically this distance is one-quarter to one-half of the length of the machine. This means that at the detector the beam is divergent and if a maximum of the beam is to be collected the detector must be of large dimensions. This immediately creates the problem of increased background counting rate.

Fourth, examination of the equations governing resolution in lens spectrometers<sup>13</sup> shows that the best resolution is obtained for large angles of divergence of the beam.

This means that the detector is looking at particles that are entering it at an included cone of  $90^\circ$  or more. Such high angle of incidence raises serious problems of detection of low energy electrons. If, for example, a Geiger counter is used for detection it will have to be a large end-window affair with a very thin window. A typical window thickness to be expected in this work is a few micrograms per square centimeter. To contain the gas pressure in the counter, the window must be supported by some means such as a grid, which may cut down the transmission of the window by some 30 to 50 percent even for normal incidence. At large angles, the transmission may be only a few percent.

Due to these rather serious shortcomings, particularly at the very low electron energies, the lens spectrometers were also eliminated from further consideration.

Another variety of beta spectrometer which does not fall exactly into either of the two main classifications is the "orange peel" spectrometer. Essentially it is a three dimensional generalization of the wedge sector field charged particle analyzer found commonly in accelerator laboratories and used as steering magnets. A highly engineered iron free representative of this class is the toroidal spectrometer of Freedman et al.<sup>15</sup> located at the Argonne National Laboratory. This instrument is capable of very high transmission and good resolution. Freedman reports the following characteristics:

Source Diameter	Transmission(%)	Resolution(%)
1/8"	19	0.93
1/8"	16	0.40
1/8"	2.8	0.21
1/4"	16	0.56
3/8"	18	0.88
1mm	13	0.30
1mm	1.6	0.13

The instrument consists of two toroidal sections that can be used either for beta-beta coincidence measurements, or can be arranged in series to give an instrument with higher resolution at a slight loss of transmission.

Aside from the very high cost of such an instrument, due to the extreme precision needed in its manufacture it is not particularly suited for low energy work. It suffers from some of the same objections leveled against the solenoidal spectrometers, in particular, a high angle of incidence of the electron beam at the detector.

None of the spectrometers discussed in this chapter thus far seem to be particularly suitable as judged by the criteria put forth in the Introduction. The remaining type, the iron free transverse spectrometer, offers us the last chance, so to speak, and it does turn out to be the best one. Before we can specify the particular kind of transverse spectrometer that offers the optimum compromise of all the desirable characteristics for low energy work, we must first describe the focusing action of the magnetic field.

## CHAPTER 2

### ELECTRON OPTICAL PROPERTIES OF AXIALLY SYMMETRIC MAGNETIC FIELDS

#### 2.1 Basic Definitions and Relationships

The basic relations of most frequent use in beta spectroscopy can be defined as follows: An electron moving with a velocity  $v$  through a uniform magnetic field  $B$  oriented perpendicular to its trajectory will describe a circular path of radius of curvature  $r$ . Its equation of motion is

$$B e v = \frac{m v^2}{r} \quad (1)$$

where  $m$  is the relativistic mass of the electron

$$m = \frac{m_0}{(1 - v^2/c^2)^{1/2}} \quad (2)$$

The momentum of the electron is given by

$$p = m v = e B r \quad (3)$$

In these equations  $e$  represents the electronic charge.

In iron free spectrometers the value of  $B$  is a well known linear function of the focusing coil current and therefore it is convenient to classify electrons according to their momentum in terms of their  $Br$  value.

The resolution R of an electron line is defined as the relative width at half maximum of the line. In terms of momentum

$$R = \frac{\Delta p}{p} = \frac{\Delta Br}{Br} \quad (4)$$

For a magnetic spectrometer with fixed geometry R is a constant.

The kinetic energy of the electrons whose momentum is Br can be obtained by use of the relativistic expression for energy:

$$E_T^2 = p^2 c^2 + m_0^2 c^4 \quad (5)$$

where  $E_T$  is the total energy of the electron.

Combining equations (5) and (3) we obtain

$$E_T = [(m_0 c^2)^2 + e^2 c^2 (Br)^2]^{1/2} \quad (6)$$

The kinetic energy of the electron is  $E_K = E_T - m_0 c^2$  or

$$E_K = [(m_0 c^2)^2 + e^2 c^2 (Br)^2]^{1/2} - m_0 c^2 \quad (7)$$

$$E_K = m_0 c^2 \left[ \left( \frac{e^2}{m^2 c^2} B^2 r^2 + 1 \right)^{1/2} - 1 \right] \quad (8)$$

This expression is useful for obtaining the kinetic energy of electrons of a given Br value. If the values of the



constants are substituted into equation (8), using  $m_0 = 510.984 \pm 0.016$  Kev the kinetic energy in kilo-electron volts becomes

$$E_K = (510.984 \pm 0.016) \left[ \sqrt{(3442.2 \pm 0.2) \times 10^{-10} B^2 r^2} - 1 \right] \quad (9)$$

Note that equation (8) can be written in terms of relativistic energy units as

$$E = (P^2 + 1)^{1/2} - 1 \quad \Rightarrow \quad E + 1 = P^2 \quad (10)$$

Differentiating this expression gives us a simple equation for energy resolution

$$dE = (P^2 + 1)^{-1/2} P dP = \frac{P^2 dP}{E + 1} \quad (11)$$

$$\frac{dE}{E} = \frac{P^2}{E(E+1)} \frac{dP}{P}$$

$$\frac{dE}{E} = \frac{E + 2}{E + 1} \frac{dP}{P}$$

A good rule of thumb for the resolution in semi-circular spectrometers is

$$R = w/D \quad (12)$$

where  $w$  is the width of the source and  $D$  is the diameter of the spectrometer's mean electron orbit.

Transmission: Electrons ejected from a source are emitted in all directions. The defining slits and other baffles in a beta spectrometer will allow only a certain

fraction of them to come through to the detector. The acceptance solid angle of the spectrometer is usually expressed as a fraction of the total sphere and is called the geometrical transmission, or the gathering power of the instrument.

When the spectrometer is set to observe a given monoenergetic electron line it should be noted that all of the electrons emitted into its acceptance angle may not reach the detector, depending on the adjustment of the detector slit. Transmission  $T$  is defined as the fraction of all of the monoenergetic electrons leaving the source that are actually counted by the detector.  $T$  is usually expressed as percent of the total sphere.

Luminosity and the Figure of Merit: The luminosity of a spectrometer is defined as

$$L = T S \quad (13)$$

where  $T$  is the transmission and  $s$  is the area of the source.

The ratio of luminosity to resolution is a measure of the performance of the spectrometer and is called the figure of merit. Clearly, this ratio should be as large as possible over the entire momentum range of the instrument.

Comparison of the various types of spectrometers shows<sup>13,14,16</sup> that the figure of merit can be much higher for transverse spectrometers than for helical machines.

Dispersion: Dispersion is defined as the change of the position of the image at the detector for a given change in the  $Br$  value of the electron beam.

$$D = \frac{dx}{d(Br)} \quad (14)$$

This quantity is intimately connected with resolution of the spectrometer. The equation shows that an increase in the dispersion while the dimensions of the spectrometer are held fixed, allows us to use wider sources with the resolution remaining constant.

It should be pointed out that the requirements of high resolution and high transmission are really not mutually compatible, as all electron optical systems suffer from aberrations. Therefore the design of a spectrometer is essentially a search for the best compromise among the desirable properties and the minimization of the optical aberrations.

## 2.2 The Equations of Motion and the Series Representation of the Magnetic Field

The focusing properties of magnetic fields having axial symmetry have been studied in detail by several authors. Svartholm and Siegbahn developed the appropriate equations for the design of a double focusing spectrometer in 1946.<sup>17</sup> Later that year Svartholm published a paper concerning the aberrations of such focusing fields.<sup>18</sup> In 1947, Shull and Dennison<sup>19</sup> developed the same equations employing a somewhat different approach, and attempted to calculate conditions favorable for higher than second order focusing. Quite recently, Lee-Whiting and Taylor tackled the problem in a very thorough manner, in preparation for the construction

of the one meter radius beta spectrometer located in Chalk River, Canada.<sup>20</sup>

In the following review, an attempt has been made to integrate the material presented in the quoted articles, and show the development of the various equations of motion from first principles. In the process, the quoted references were used freely. The notation used is something of a mixture, but is nearest the notation used by Lee-Whiting and Taylor. Indeed, toward the end of this section the Lee-Whiting and Taylor notation was deliberately chosen to enable the interested reader to peruse the original material with a minimum of difficulty.

Consider a magnetic field, rotationally symmetric about the  $z$  axis and having the  $x$ - $y$  plane (at  $z = 0$ ) as the plane of symmetry. A circular orbit in the symmetry plane and concentric with the  $z$  axis will be called a central orbit or the optic circle. Consider a charged particle in such a field. The most appropriate coordinates for this problem are the cylindrical coordinates,  $r, \phi, z$ . The magnetic field is a function of  $r$  and  $z$ , independent of  $\phi$  :

$$\vec{B} = \vec{B}(r, z) \quad (15)$$

the Lorentz force equation is

$$\vec{F} = e \vec{v} \times \vec{B} \quad (16)$$

here  $e$  is the electronic charge, as before and  $\vec{v}$  is the velocity:

$$v^2 = (r\dot{\phi})^2 + \dot{r}^2 + \dot{z}^2 \quad (17)$$

The magnetic field is definable in terms of a vector potential as

$$\vec{B} = \nabla \times \vec{A} \quad \text{with the auxiliary condition} \quad \nabla \cdot \vec{A} = 0 \quad (18)$$

Clearly, only the  $\phi$  component of  $\vec{A}$  will be nonzero.

This component will be denoted simply by  $A$ . Equation (18) now assumes the explicit form

$$B_r(r, z) = - \frac{\partial A}{\partial z} \quad (19)$$

$$B_z(r, z) = \frac{1}{r} \frac{\partial(rA)}{\partial r} \quad (20)$$

Combination of equations (16), (17), (19) and (20) gives the time dependent equations of motion of the particle

$$\frac{d}{dt} (m\dot{r}) = m r \dot{\phi}^2 + e \dot{\phi} \frac{\partial(rA)}{\partial r} \quad (21)$$

$$\frac{d}{dt} (m\dot{z}) = e r \dot{\phi} \frac{\partial A}{\partial z} \quad (22)$$

$$\frac{d}{dt} (m r^2 \dot{\phi}) = - e r \dot{z} \frac{\partial A}{\partial z} - e \dot{r} \frac{\partial(rA)}{\partial r} \quad (23)$$

Integral of equation (23) is a constant of motion, the component of momentum corresponding to the coordinate  $\phi$  :

$$\frac{d}{dt} (m r^2 \dot{\phi} + e r A) = 0 = \frac{d}{dt} u \quad (24)$$

or

$$\dot{\phi} = \frac{u - e r A}{m r^2} \quad (25)$$

The equations of motion can now be rewritten in the form:

$$m \ddot{r} = - \frac{\partial}{\partial r} \left[ \frac{1}{2m} \left( \frac{u}{r} - e A \right)^2 \right] \quad (26)$$

$$m \ddot{z} = - \frac{\partial}{\partial z} \left[ \frac{1}{2m} \left( \frac{u}{r} - e A \right)^2 \right] \quad (26^1)$$

These equations are identical with Svartholm and Siegbahn equations 6 and 7.<sup>17</sup> In preparation to transformation of the equations of motion into dimensionless form, let us first change the independent variable from time to the angle  $\phi$ , since ultimately we are more interested in the path of the electron as a function of the angle rather than time.

To condense the equations further, define

$$U = U(r, z) = \frac{1}{2m} \left( \frac{u}{r} - e A \right)^2 \quad (27)$$

treating  $u$  as a constant. Then

$$r'' + \frac{\dot{\phi}'}{\dot{\phi}} r' = - \frac{1}{m \dot{\phi}^2} \frac{\partial U}{\partial r} \quad (28)$$

$$z'' + \frac{\dot{\phi}'}{\dot{\phi}} z' = - \frac{1}{m \dot{\phi}^2} \frac{\partial U}{\partial z} \quad (28^1)$$

Differentiation with respect to  $\phi$  is denoted by primes.

Transformation into dimensionless form is accomplished by using the parameters

$$\delta = \frac{r - r_0}{r_0}, \quad \xi = \frac{z}{r_0} \quad (29)$$

where  $r_0$  is the radius of the mean orbit.

We need an explicit expression for  $\dot{\phi}$ . Note that equations (25) and (27) give  $\dot{\phi} = \frac{1}{mr} \sqrt{2mU}$  and that for an electron traveling on the mean orbit,  $r = r_0$  and  $z = 0$ , we shall have stationary motion if the relation

$$B_z(r_0, 0) = -\frac{p_0}{er_0} \quad \text{is satisfied.} \quad (30)$$

For such an orbit we can write  $\dot{\phi}_0 = v_0/r_0$  and hence

$$\dot{\phi} = \frac{1}{mr} \sqrt{2mU} = \dot{\phi}_0 G(\delta, \xi) \quad (31)$$

where the new function  $G(\delta, \xi)$  is defined as

$$G(\delta, \xi) = \frac{r_0}{mr v_0} \sqrt{2mU} \quad (32)$$

The relation (29), (30) and (31) combine to give the dimensionless equations of motion

$$\delta'' + \left[ \frac{1}{G} \frac{\partial G}{\partial \delta} \delta' + \frac{1}{G} \frac{\partial G}{\partial \xi} \xi' \right] \delta' = - \left[ (1+\delta)^2 \frac{1}{G} \frac{\partial G}{\partial \delta} + 1 + \delta \right] \quad (33)$$

$$\xi'' + \left[ \frac{1}{G} \frac{\partial G}{\partial \delta} \delta' + \frac{1}{G} \frac{\partial G}{\partial \xi} \xi' \right] \xi' = - (1+\delta)^2 \frac{1}{G} \frac{\partial G}{\partial \xi} \quad (33^1)$$

These are identical with equations 16 of Svartholm.<sup>18</sup>

As the focusing field enters these equations through the function  $G$  and in particular, the product  $rA$ , the solution must be approached by expressing  $G$  explicitly in terms of  $\delta$ ,  $\xi$ , and  $B_0$ . The order of the calculation is then determined by the number of terms that are retained in the expansion of  $G$ . Furthermore, since we are not interested in trajectories coincident with the mean orbit, we must allow the electron a variation in the initial momentum,

100

101

102



position and angle subtended with the tangent to the mean orbit. A set of such initial conditions imposed on the electron at its starting position  $\phi = 0$  can be written as

$$p = p_0 (1 + \epsilon) \quad (34)$$

$$\delta_0 = h \quad ; \quad \xi_0 = t \quad (35)$$

$$\delta'_0 = \left( \frac{\partial \delta}{\partial \phi} \right)_0 = H \quad ; \quad \xi'_0 = \left( \frac{\partial \xi}{\partial \phi} \right)_0 = T \quad (36)$$

Note that the velocity vector of a particle traveling parallel to a tangent to the mean orbit is

$$\vec{v}_0 = [ r_0 (\delta + 1) \dot{\phi} ] \hat{\phi}$$

and the velocity vector for a particle which deviates from the tangent by having radial and axial components of velocity nonzero is

$$\vec{v} = (r_0 \dot{\phi} \delta') \hat{r} + (r_0 \dot{\phi} \xi') \hat{z} + [r_0 (\delta + 1) \dot{\phi}] \hat{\phi}$$

The angle between these vectors is given by

$$\cos \gamma = \frac{\vec{v}_0 \cdot \vec{v}}{|\vec{v}_0| |\vec{v}|}$$

or explicitly in terms of the initial values

$$\cos \gamma = \left\{ 1 + \frac{H^2 + T^2}{(1 + h)^2} \right\}^{-1/2} \quad (37)$$

Recalling the expressions for  $G$ ,  $U$  and  $u$ :

$$\begin{aligned} G(\delta, \xi) &= \frac{r_0}{m r v_0} \sqrt{2 m \mathcal{U}} \\ \mathcal{U} &= \frac{1}{2 m} \left( \frac{u}{r} - e A \right)^2 \\ u &= m r^2 \dot{\phi} + e r A \end{aligned}$$

note that for stationary motion on the mean orbit  $u$  has the value

$$u = m r_0 v_0 + e r_0 A_0 \quad (38)$$

This expression is modified by introducing the initial conditions so that

$$\begin{aligned} m v_0 &\rightarrow (1 + \epsilon) m v_0 \\ r_0 &\rightarrow (1 + h) r_0 \\ v_0 &\rightarrow v_0 \cos \gamma \end{aligned}$$

The function  $u$  then has the form

$$u = (1 + \epsilon)(1 + h) \cos \gamma (m r_0 v_0) + e r_0 A_0 \quad (39)$$

and the function  $G$  assumes the explicit form

$$G(\delta, \xi) = \frac{1}{(1 + \delta)^2} \left\{ (1 + \epsilon)(1 + h) \cos \gamma + \frac{e}{m v_0 r_0} (r_0 A_0 - r A) \right\} \quad (40)$$

In this equation  $rA$  can be expanded in the neighborhood of the mean orbit. The resulting series is used in conjunction with the equations of motion (33) to obtain the desired solutions of  $\delta$  and  $\xi$  as a function of  $\phi$ . Lee-Whiting and Taylor<sup>20</sup> have performed such calculations and have carried them numerically up to the sixth order. Since their treatment is not only the most recent and thorough, but also mathematically the most elegant, we shall sketch its main features here: It is convenient to define another function,  $F$ , and express it in terms of  $G$ :

$$F(\delta, \xi) = (1 + \delta)^2 G(\delta, \xi) \quad (41)$$

The equations of motion (33) are therefore also modified.

The new equations are

$$\delta'' + \left\{ \frac{1}{F} \frac{\partial F}{\partial \delta} \delta' + \frac{1}{F} \frac{\partial F}{\partial \xi} \xi' - \frac{2}{(1+\delta)} \delta' \right\} \delta' = -(1+\delta)^2 \frac{1}{F} \frac{\partial F}{\partial \delta} - (1+\delta) \quad (42)$$

$$\xi'' + \left\{ \frac{1}{F} \frac{\partial F}{\partial \delta} \delta' + \frac{1}{F} \frac{\partial F}{\partial \xi} \xi' - \frac{2}{(1+\delta)} \delta' \right\} \xi' = -(1+\delta)^2 \frac{1}{F} \frac{\partial F}{\partial \xi} \quad (42^1)$$

The product  $rA$  is now expanded in the neighborhood of the mean orbit as

$$rA = r_0 A_0 - \frac{m v_0 r_0}{e} \sum_{m,n=0}^{\infty} C_{mn} \xi^m \delta^n \quad (43)$$

In this expansion note that not all coefficients are permitted to have nonzero values. The field that we assumed at the beginning of this section has a plane of symmetry at  $z = 0$ . Therefore also  $\xi = 0$  there. This makes all odd  $m$  coefficients equal to zero. Furthermore on the mean orbit  $rA = r_0 A_0$ . Thus  $C_{00} = 0$ . Equation (30) requires that  $C_{01} = 1$ . Introduction of the particle's initial conditions results in

$$rA = r_0 A_0 - \frac{m v_0 r_0}{e} \sum_{m,n=0}^{\infty} C_{mn} \left\{ \xi^m \delta^n - t^m h^n \right\} \quad (44)$$

and the function  $F$  now assumes the form

$$F(\delta, \xi) = (1+\epsilon)(1+h) \cos \gamma + \sum_{m,n=0}^{\infty} C_{mn} \left\{ \xi^m \delta^n - t^m h^n \right\} \quad (45)$$

The equations of motion are then solved using this equation.

Before further calculations can be done we must

establish relationships among the  $C$  coefficients. To do this we shall require that Maxwell's equations be satisfied. Thus

$$\frac{\partial B_r}{\partial \xi} = \frac{\partial B_z}{\partial \delta} \quad (46)$$

Now using equations (19)  $B_r = -\frac{\partial A}{\partial z}$  and (20)  $B_z = \frac{1}{r} \frac{\partial(rA)}{\partial r}$  and equation (43), we express (46) in terms of the expansion and equate the coefficients of  $\xi^m \delta^n$ . The resulting equations

$$(m+2)(m+1) \left\{ C_{(m+2)(n+1)} + C_{(m+2)n} \right\} = -(n+2) \left\{ (n+3) C_{m(n+3)} + n C_{m(n+2)} \right\} \quad (47)$$

for  $n \geq 0$ .

$$(m+2)(m+1) C_{(m+2)0} = -2 C_{m2} + C_{m1} \quad (48)$$

are the Lee-Whiting and Taylor equations 12 and 13. The coefficients  $C_{on}$  are independent and if they are specified, all others can be obtained from the above recurrence relations.

The focusing field  $B$ , in the plane of symmetry ( $z = 0$ ) and in the neighborhood of the mean orbit, can be expressed in terms of a Taylor series expansion

$$B(r, 0) = B(r_0, 0) \sum_{n=0}^{\infty} a_n \delta^n \quad (49)$$

Where the coefficient  $a_0 = 1$ , and the  $a_n$  are given by

$$a_n = \frac{r_0^n}{n! B(r_0)} \left( \frac{d^n B}{d r^n} \right)_{r_0} \quad (50)$$

The relationship between the  $a_n$  and the  $C_{on}$  is found from equations (20) and (49)

$$B(r,0) = \frac{1}{r} \frac{\partial(rA)}{\partial r} = B(r_0,0) \sum_{n=0}^{\infty} a_n \delta^n$$

or explicitly

$$\frac{1}{r_0(\delta+1)} B(r_0) r_0^2 \sum_{n=0}^{\infty} \frac{n}{r_0} C_{on} \delta^{n-1} = B(r_0) \sum_{n=0}^{\infty} a_n \delta^n \quad (51)$$

Again, equating coefficients of equal powers gives the recurrence relationship

$$n C_{on} = a_{n-1} + a_{n-2} \quad (52)$$

This expression is valid for  $n \geq 1$ , provided that we define  $a_{-1} = 0$ .

### 2.3 Focusing Properties of Axially Symmetric Magnetic Fields

Consider the first order solutions to a field having the form

$$B(r,0) = B(r_0,0) \{ 1 + a_1 \delta \} \quad (53)$$

Substitution of the explicit form of the function  $F$  into the equations of motion (42) gives, to first order

$$\delta'' + 2 C_{02} \delta = \epsilon \quad (54)$$

$$\xi'' + 2 C_{20} \xi = 0 \quad (54^1)$$

The solutions of these equations are

$$\delta = \frac{H}{\sqrt{2C_{02}}} \sin \sqrt{2C_{02}} \phi + h \cos \sqrt{2C_{02}} \phi + \frac{\epsilon}{2C_{02}} \{ 1 - \cos \sqrt{2C_{02}} \phi \} \quad (55)$$

$$\xi = \frac{T}{\sqrt{2C_{20}}} \sin \sqrt{2C_{20}} \phi + t \cos \sqrt{2C_{20}} \phi \quad (55^1)$$

The initial conditions (34), (35) and (36) are included in the above equations.

These solutions are somewhat more general than the results given by Svartholm and Siegbahn, who assumed that the electron starts from a point on the mean orbit with momentum  $p_0$ . If we restrict ourselves to such initial conditions, then  $h = t = 0$  and  $\epsilon = 0$ . Equations (55) reduce to

$$\delta = \frac{H}{\sqrt{2C_{02}}} \sin \sqrt{2C_{02}} \phi \quad (56)$$

$$\xi = \frac{T}{\sqrt{2C_{20}}} \sin \sqrt{2C_{20}} \phi \quad (56^1)$$

Clearly, at the source  $\phi = 0$  and the initial coordinates of the electron are  $\delta = h = 0$ ,  $\xi = t = 0$ ; as we said before. The electron beam is focused at an angle when  $\delta$  and  $\xi$  are again equal to zero. That is

$$\sqrt{2C_{02}} \phi = \sqrt{2C_{20}} \phi = k\pi \quad (57)$$

We shall consider only the first focal point and let  $k = 1$ .

The radial and axial focusing angles are

$$\psi_{\delta} = \frac{\pi}{\sqrt{2 C_{02}}} \quad (58)$$

$$\psi_{\xi} = \frac{\pi}{\sqrt{2 C_{20}}} \quad (58^1)$$

The recurrence relation for the C coefficients, equation (48) gives

$$C_{02} + C_{20} = \frac{1}{2} \quad \text{since } C_{01} = 1. \quad (59)$$

Combining (58) and (59):

$$\frac{1}{\psi_{\delta}^2} + \frac{1}{\psi_{\xi}^2} = \frac{2(C_{02} + C_{20})}{\pi^2} = \frac{1}{\pi^2} \quad (60)$$

which is the Svartholm and Siegbahn equation.

A special case of this is the uniform magnetic field spectrometer. There  $B(r,0) = B(r_0,0)$ , the radial focusing angle is  $\pi$ , and

$$\psi_{\delta} = \frac{\pi}{\sqrt{2 C_{02}}} = \pi \quad \text{hence } C_{02} = \frac{1}{2} \quad \text{and } C_{20} = 0$$

Therefore  $\psi_{\xi}$  is indeterminate and no axial focusing takes place.

To obtain the dispersion in this case, consider the radial displacement of the image for an electron of initial momentum  $p = p_0(1 + \epsilon)$ . This means that we use solution (55) with  $h = 0$ :

$$\delta = \frac{r - r_0}{r_0} = H \sin \phi + \epsilon (1 - \cos \phi) \quad \text{now set } \phi = \pi$$

102

102

102

102

102

102

102

102

102



The radial displacement is

$$r - r_0 = 2 \epsilon r_0 \quad (61)$$

Conditions for first order double focusing are found by solving equations (57) and (58) explicitly. Then  $C_{02} = C_{20} = 1/4$ , and the focusing angles are

$$\psi_\delta = \psi_\xi = \pi\sqrt{2} \quad (62)$$

In analogy to (47) we have for this case

$$r - r_0 = 4 \epsilon r_0 \quad (63)$$

For double focusing the dispersion is therefore doubled.

The value of the field coefficient  $a_1$  is found from the recurrence relation (52)

$$2C_{02} = a_1 + a_0$$

as  $a_0 = 1$ ,  $a_1 = -1/2$ . The field form for first order double focusing is therefore

$$B(r, 0) = B(r_0, 0) \left(1 - \frac{1}{2} \delta\right). \quad (64)$$

The solutions (56) written for the double focusing case

$$\delta = H\sqrt{2} \sin \frac{\phi}{\sqrt{2}} \quad \text{and} \quad \xi = T\sqrt{2} \sin \frac{\phi}{\sqrt{2}}$$

show that  $\delta$  and  $\xi$  have maximum values for  $\phi = \frac{\pi}{\sqrt{2}}$ .

These are approximately the maximum deviations of the particles from the mean orbit. We have a way, therefore, to find the transmission by considering the projections of

the particle momentum  $\vec{p}$  on the  $z = 0$  plane and the plane defined by  $\vec{p}_0$  and a line parallel to the  $z$  axis. Taking the tangents of the angles that these projections subtend with  $\vec{p}_0$  we have

$$\tan \gamma_r = \frac{r_0 \dot{\phi} \delta'}{r_0 \dot{\phi}} = \delta' \quad (65)$$

$$\tan \gamma_z = \frac{r_0 \dot{\phi} \xi'}{r_0 \dot{\phi}} = \xi' \quad (65^1)$$

and using the initial conditions,

$$\delta' = H, \quad \xi' = T$$

the transmission, in terms of a fraction of the total sphere, is

$$\tau \approx \frac{2 \gamma_{r \max} \cdot 2 \gamma_{z \max}}{4\pi} = \frac{H_{\max} \cdot T_{\max}}{\pi} \quad (66)$$

In the case of uniform field this expression is modified due to the absence of axial focusing. Same considerations as above give the same value for radial angle:  $\tan \gamma_r = \delta' = H$ . The axial angle must be limited, however, either by the spectrometer chamber height or by the height of the detector slit. The transmission is therefore

$$\tau_{\text{uniform field}} \approx \frac{2 \gamma_{r \max} \cdot 2 \gamma_{z \text{ detector}}}{4\pi}$$

and a comparison of the two cases shows

$$\frac{\tau_{\text{double foc.}}}{\tau_{\text{uniform fld.}}} = \frac{\gamma_{z \max}}{\gamma_{z \text{ det.}}} , \quad \gamma_{z \text{ det}} < \gamma_{z \max} \text{ for practical instruments.}$$

Thus the double focusing feature is much preferable over the uniform field case.

Second order calculation: First of all, we assume that in the Taylor expansion of the field  $a_1 = -1/2$  exactly. The field has the form, to second order

$$B(r,0) = B(r_0,0) \left\{ 1 - \frac{1}{2} \delta + a_2 \delta^2 \right\} \quad (67)$$

and we are interested in finding the values of  $a_2$  for which double focusing will occur at  $\phi = \pi\sqrt{2}$ . Neglecting higher order corrections to the dispersion, we shall use the following initial conditions at  $\phi = 0$ :

$$\begin{aligned} \delta &= h, & \delta' &= H, & \vec{p} &= p_0 \\ \xi &= t, & \xi' &= T \end{aligned} \quad (68)$$

The orbital equations are formed as before, by keeping the terms in the function  $F(\delta, \xi)$  and in the equations of motion to second order. The equations are then approximated by substituting the first order solutions into the second order terms. Shull and Dennison<sup>19</sup> have performed this calculation starting from the time dependent equations of motion by perturbation methods. Although Lee-Whiting and Taylor<sup>20</sup> list the complete equations of the orbit as a function of the angle  $\phi$  it is of more interest to examine the coordinates of the image point for an electron whose initial conditions are given by (68). To obtain the simplest expression we make an angle transformation

$$\phi_1 = \phi/\sqrt{2}$$

as the focusing angle is  $\pi\sqrt{2}$ . Then we shall also have

$$H_1 = H\sqrt{2} \quad \text{and} \quad T_1 = T\sqrt{2}$$

In terms of these quantities, the coordinates of the image points are

$$\begin{aligned} \delta(\phi_1 = \pi) = & -h + \frac{1}{3}(1 - 8a_2)H_1^2 + \left(\frac{8}{3}a_2 - 1\right)T_1^2 + \\ & + \frac{2}{3}(1 - 2a_2)h^2 + \left(\frac{4}{3}a_2 - 1\right)t^2 \end{aligned} \quad (69)$$

$$\zeta(\phi_1 = \pi) = -t + 2\left(\frac{8}{3}a_2 - 1\right)H_1T_1 + \frac{8}{3}a_2ht. \quad (69^1)$$

In these equations, the terms involving  $h$  and  $t$  depend on the width and the height of the source, respectively; and the terms containing  $H_1$  and  $T_1$  depend on the size of the aperture. Examination of the equations shows that no single value of  $a_2$  will eliminate all of the aberrations. Values of  $1/8$ ,  $1/2$ ,  $3/8$  and  $3/4$  make some of the terms vanish, but it is not easy to see which, if any, of these values would result in an overall minimum in the aberrations. Some progress can be made by realizing that the terms in  $H_1$  and  $T_1$  are the dominant ones, and that in the event that long sources are to be used so  $t$  is no longer much less than one, the radial aberration due to source height can be limited by curving the source. We can allow the term in  $t^2$  to be balanced out by the term in  $h$ :

$$\left(\frac{4}{3}a_2 - 1\right)t^2 - h = 0 \quad (70)$$

This will hold for infinitesimally narrow sources only.

For sources of finite width an aberration proportional to

the source width still remains.

Let us consider the dominant terms of equation (69). The image or line width can be written as

$$\begin{aligned} A &= \frac{1}{3} (1 - 8a_2) H_1^2 + \left( \frac{8}{3} a_2 - 1 \right) T_1^2 \\ &= \frac{1}{6} (1 - 8a_2) H^2 + \frac{1}{2} \left( \frac{8}{3} a_2 - 1 \right) T^2 \end{aligned} \quad (71)$$

In general the question that must be answered is the following: What aperture opening will result in the least aberration and the greatest transmission? If we restrict ourselves to a rectangular aperture, transmission is given approximately by the equation (66), and the problem reduces to finding values of  $H$  and  $T$ , for  $A$  constant, for maximum transmission. Under these conditions

$$H^2 = \frac{A}{\frac{1}{3}(1-8a_2)} \quad ; \quad T^2 = \frac{A}{\frac{1}{3}(8a_2-3)}$$

and hence

$$\tau \approx \frac{H \cdot T}{\pi} = \frac{\sqrt{3}}{\pi} \frac{A}{\sqrt{(1-8a_2)\left(\frac{8}{3}a_2-1\right)}} \quad (72)$$

The transmission has two singularities, at  $a_2 = 1/8$  and at  $a_2 = 3/8$ . If we rearrange the equation somewhat

$$\tau \frac{\pi}{A\sqrt{3}} = \frac{1}{\sqrt{|1-8a_2| \left| \frac{8}{3}a_2-1 \right|}}$$

and plot its values as a function of  $a_2$  we obtain a graph as shown in Figure 1. Assuming a rectangular aperture, the values of  $1/8$  or  $3/8$  for  $a_2$  are the most advantageous. The other possible choices  $1/2$  and  $3/4$  are clearly at a disadvantage.

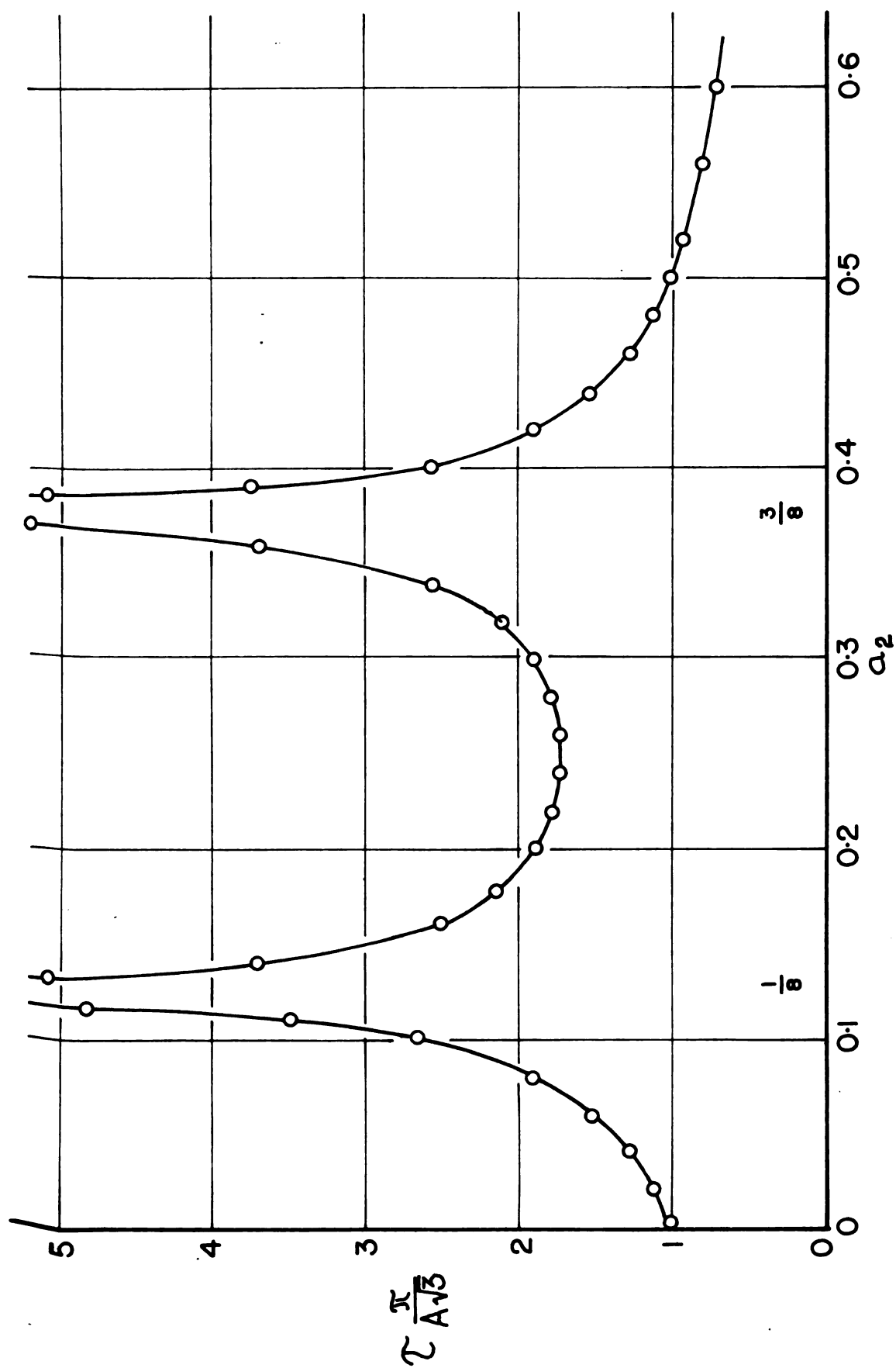


FIGURE 1. TRANSMISSION AS A FUNCTION OF THE FIELD COEFFICIENT  $Q_2$ .

Examine equation (71) for the two favorable cases:

$$a_2 = \frac{1}{8} \quad , \quad A = -\frac{2}{6} T^2$$

$$a_2 = \frac{3}{8} \quad , \quad A = -\frac{2}{6} H^2$$

These are the residual aberrations. Thus in the case  $a_2 = 1/8$  we are permitted large radial departure and must limit the axial aperture, whereas in the case  $a_2 = 3/8$ , the conditions are reversed. Unless we take into account the complete equations (69), there is no apparent advantage of one of these choices over the other.

The full equations are

for  $a_2 = 1/8$

$$\delta(\pi) = -h - \frac{2}{3} T_1^2 + \frac{1}{2} h^2 - \frac{5}{6} t^2$$

$$\xi(\pi) = -t - \frac{4}{3} H_1 T_1 + \frac{1}{3} h$$

large radial  
departure in

for  $a_2 = 3/8$

$$\delta(\pi) = -h - \frac{2}{3} H_1^2 + \frac{1}{6} h^2 - \frac{1}{2} t^2$$

$$\xi(\pi) = -t + h t$$

large axial

It is clear that  $a_2 = 3/8$  is the better choice, since it results in a smaller axial aberration and if we compare the coefficients of  $t^2$  in the two cases we see that it permits about 30 percent higher sources to be used at the same resolution (line width).

Higher order corrections: For the choice of field expansion coefficients  $a_1 = -1/2$  and  $a_2 = 3/8$ , the higher order calculations resulting in the optimum choices of

$a_3$ ,  $a_4$  and so on, become rapidly quite involved and tedious. The reason for undertaking these computations is that higher order corrections to the radial and axial aberrations will result in further increases of transmission while the resolution is kept constant. About thirty percent in transmission can be gained by fitting the field accurately up to  $a_4$ . Lee-Whiting and Taylor have performed these calculations up to  $a_6$  giving an optimum field of the form

$$B(r,0) = B(r_0,0) \left\{ 1 - \frac{1}{2} \delta + \frac{3}{8} \delta^2 - 0.299 \delta^3 + \right. \\ \left. + 0.24 \delta^4 - 0.202 \delta^5 + 0.177 \delta^6 + \dots \right\} \quad (73)$$

In conclusion, it is clear that to realize a double focusing instrument with small aberrations and no undue hardships of manufacture, we should strive for an accurate fit to the second order field shape with  $a_1 = -1/2$  and  $a_2 = 3/8$ , and approximate the higher order field near the mean orbit by suitable positioning of the field producing currents. This assumes, of course, that sufficient funds are not available to manufacture a set of focusing coils to the standard of precision necessary for fitting the higher order field. The adjustment method seems to have worked quite well in the case of the Michigan State University spectrometer.



## CHAPTER 3

### IRON-FREE DOUBLE FOCUSING SPECTROMETERS

#### 3.1 Focusing Coil Configurations

The demonstrated superiority of the iron-free instruments over the iron-containing machines for high precision and high resolution work has resulted in a great amount of interest in them and many are to be found in all corners of the world. In view of the large amount of design effort invested in these instruments since their invention in the nineteen forties we would expect a variety of ways employed in producing the desired shape of the focusing magnetic field. This is not the case. At this time there are basically two methods for shaping the focusing field of the type described in the last chapter. The first method was developed by Siegbahn and Edvarson.<sup>21</sup> It consists of two coaxial solenoids in the shape of tight circular cylinders. A schematic cross-section of this type of coil is given in Figure 2. These so-called "Siegbahn" type spectrometers have been built by Siegbahn and Edvarson in Sweden, by Wapstra and DeVries in Holland,<sup>22</sup> by Mladjenovic in Yugoslavia<sup>23</sup> and by Hollander et al.<sup>24</sup> in this country at Berkeley.

Although attractive from mechanical viewpoint for their simplicity, these instruments have some drawbacks.

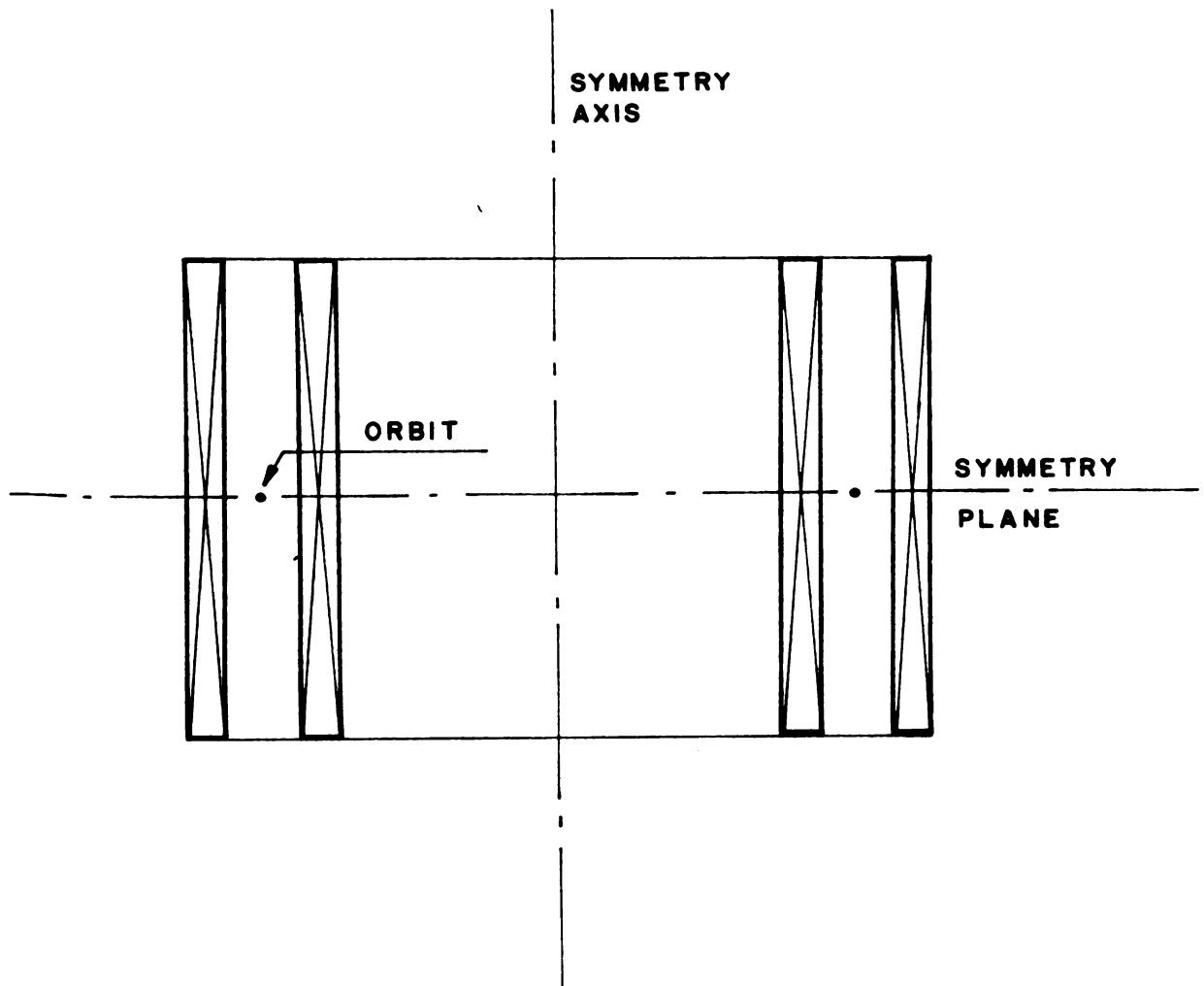


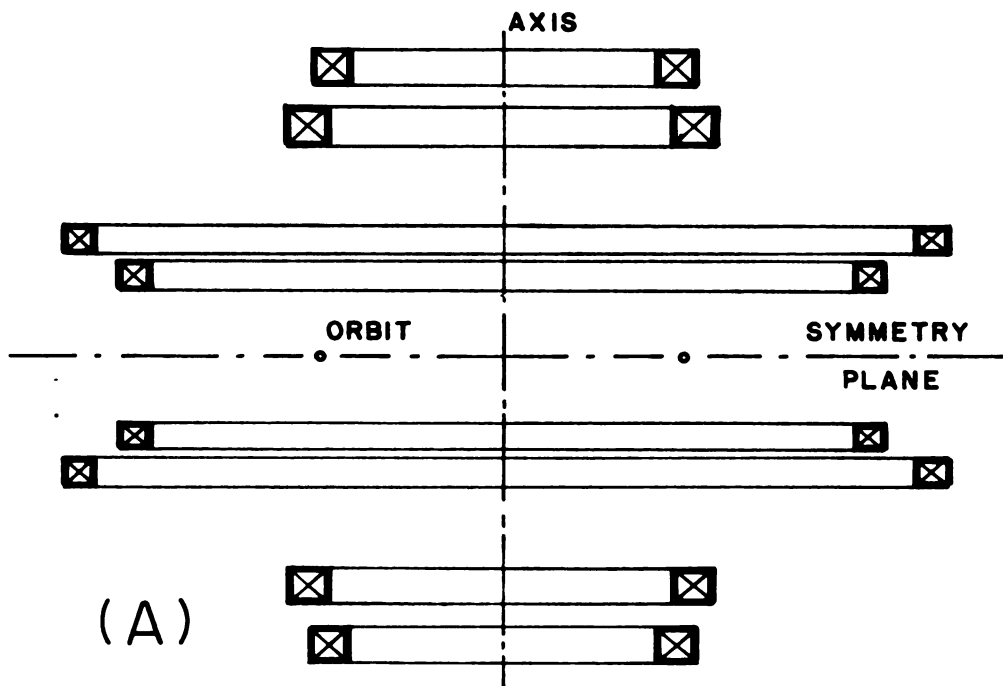
FIGURE 2. FOCUSING COIL ARRANGEMENT

DUE TO SIEGBAHN AND EDVARSON .

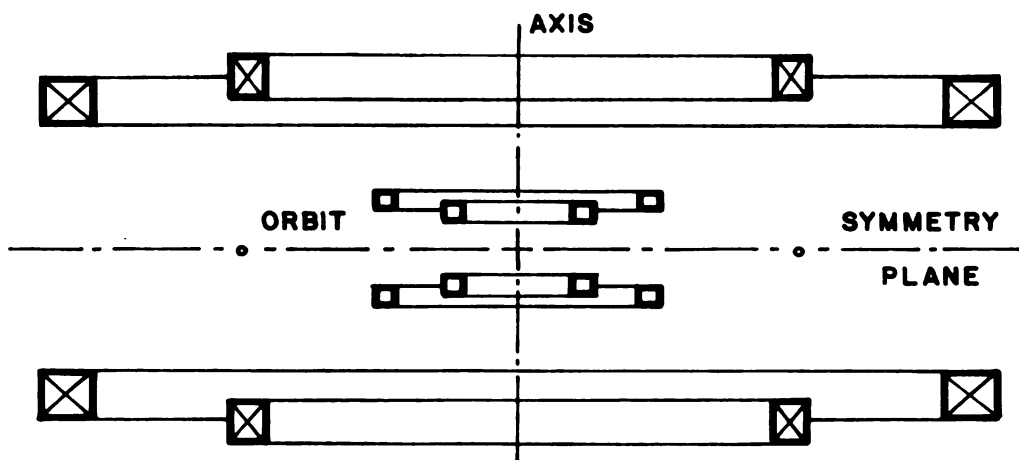
One of these is the difficulty of realizing the proper field shape for matching field coefficients higher than the second order. To solve this problem, most likely, the density of coil turns would have to be made a function of  $z$  and would have to be accurately computed beforehand, as adjustments on a finished instrument are all but impossible. The coaxial solenoid design also limits the radial departure of the electrons from the mean orbit and due to the positions of the coils; these machines have a very restricted accessibility to the source and the counter.

The second method of obtaining the proper field shape uses several pairs of symmetric thin coils. Two main designs are currently in use, one due to Moussa and Belliard,<sup>25,26</sup> and the other due to Lee-Whiting and Taylor.<sup>27</sup> Their respective coil configurations are shown in Figure 3. Both schemes use four pairs of coils. There is in essence no difference between these two in terms of their ability to produce focusing fields matched to orders higher than the second. The advantage will lie with the instrument of larger mean orbit radius and the higher degree of engineering and general precision of construction that is invested in it. The Canadian design<sup>28</sup> does have a slight edge on the Moussa design in that it is more accessible and that the coil configuration yields a zero total field at the origin of the spectrometer's coordinate system thus allowing the use of photomultipliers for coincidence studies.

A spectrometer patterned along the design of Moussa



(A)



(B)

FIGURE 3. (A) FOCUSING COIL ARRANGEMENT  
DUE TO MOUSSA.

(B) FOCUSING COIL ARRANGEMENT  
DUE TO LEE-WHITING AND TAYLOR.

was built at Vanderbilt University by Haynes et al.<sup>29</sup> This instrument was constructed before the Canadian design was finished. It differs from the Moussa spectrometer in having a larger mean radius, 300 millimeters as compared with 210 millimeters of the Moussa machine, operates with low voltage-high current coils and uses field rather than current regulation.

The spectrometer constructed at Michigan State University was originally intended to be a direct copy of the Vanderbilt machine; however, profiting from experience gained with the Vanderbilt spectrometer, it was possible to manufacture a more precise set of focusing coils, thus enabling the Michigan instrument to have better optical properties. Furthermore, the author has at times disregarded the Vanderbilt design altogether, in favor of new and hopefully, better one. Thus, although the basic dimensions of the two instruments are the same, there are many differences between them that justify a complete description.

### 3.2 Determination of Focusing Coil Parameters

The determination of focusing coil radii and distances from the  $z = 0$  plane can be carried out by detailed computer-assisted calculations fitting the sixth order ideal field, as was done by the Canadian Chalk River group,<sup>28</sup> or by a somewhat more empirical approach following a scheme worked out by Moussa and Bellicard.<sup>25</sup> Since our spectrometer was patterned originally after the French design, its basic focusing coil dimensions were calculated using the Moussa

and Bellicard method. The following few pages show the basic steps involved in this calculation.

Moussa and Bellicard fitted a field having the shape

$$B(r,0) = B(r_0,0) \left( \frac{r_0}{r} \right)^{1/2} \quad (74)$$

This shape gives a fairly good approximation to an optimum focusing field, even to the sixth order, provided that the radial deviations from the mean orbit are small. The method consists of calculation of the field due to a chosen number of circular current filaments spaced symmetrically about the median plane and the comparison of this field with the desired one. The parameters of the current filaments (radii and axial positions) are adjusted in progressively finer steps until the desired degree of fit is reached. A brief outline of this method is presented below:

Consider a circular filament of radius  $R$ , spaced a distance  $z$  from the plane of symmetry at  $z = 0$ . We can define dimensionless parameters  $\alpha$  and  $\beta$  such that

$$\alpha = \frac{r}{R} \quad ; \quad \beta = \frac{z}{R} \quad (75)$$

The axial field produced by such a filament at a point anywhere except on the filament itself can be written as an expression involving elliptic integrals of the first and second kind

$$B_z = \frac{\mu_0 I}{2\pi R} \frac{1}{\sqrt{(1+\alpha)^2 + \beta^2}} \left[ \frac{1 - \alpha^2 - \beta^2}{(1-\alpha)^2 + \beta^2} E + K \right] \quad (76)$$

The derivation of this expression will be found in Chapter VII.

The modulus of the elliptic integrals E and K is

$$k^2 = \frac{4\alpha}{(1+\alpha)^2 + \beta^2} \quad (77)$$

The field can be therefore schematically expressed as

$$B_z = \frac{\mu_0 I}{2\pi R} f(\alpha, \beta) \quad (78)$$

The function  $f(\alpha, \beta)$  can be tabulated for chosen ranges of  $\alpha$  and  $\beta$ , i.e., the radial and axial range of departure of the electrons from the mean orbit. Moussa gives a table of values of  $f$  for  $0 \leq \alpha \leq 1.3$  ;  $0 \leq \beta \leq 1.2$

Since in this case the field to be fitted is  $B_z \cdot (r)^{1/2} = \text{Constant}$ , the product  $f(\alpha, \beta) \cdot (\alpha)^{1/2}$  can be plotted against  $\alpha$ , using  $\beta$  as a parameter to obtain a family of curves, as shown in Figure 4. The  $B_z \sqrt{r} = \text{constant}$  field will be matched even for a single pair of coils at a point of zero slope on these curves. The presence of sizeable curvature of these curves shows that spectrometer constructed in this way would permit only a very narrow radial departure from the mean orbit.

To obtain a good fit over an extended region of space, more coil pairs are needed. The choice of the  $\alpha$  and  $\beta$  parameters is made as follows: Points on the various curves are chosen in regions of minimum curvature and at points where the slopes will sum to zero. This will

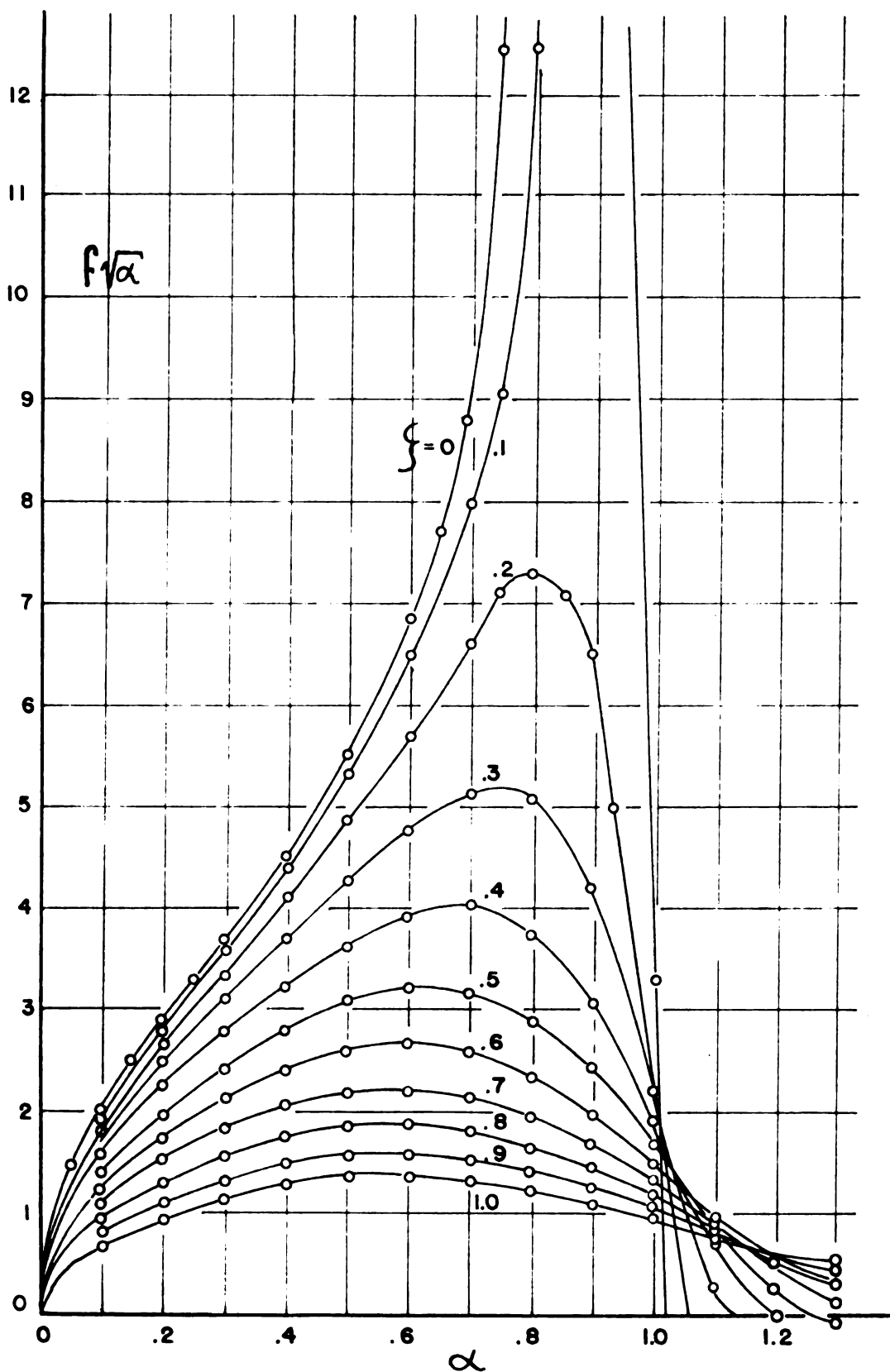


FIGURE 4. PLOT OF  $f\sqrt{\alpha}$  VERSUS  $\alpha$ .



clearly require that an even number of coil pairs is chosen. Ideally, the curvatures for the various coil pairs should also cancel. This procedure permits an infinity of possible solutions. The number can be reduced by placing constraints on the values of  $R$  and  $z$ . The coils must not encroach on the electron orbits and they should not be so far away from the mean orbit that an exorbitant amount of power is required to produce a given focusing field. Since the  $B_r$  value as given by equation (4) is  $nI \propto f(\alpha, \beta)$ , the number of ampere turns needed for a given  $B_r$  varies as

$$\frac{1}{\propto f(\alpha, \beta)}$$

This expression shows that while curves with large values of  $\beta$  have small curvature and seem to be the logical choice for coil parameters, they may in fact be unsatisfactory, due to low values of  $f(\alpha, \beta)$  and consequently, high power consumption.

Bellicard and Moussa therefore made a choice of two filament pairs, related to the mean radius by the parameters

$$\alpha_1^\circ, \beta_1^\circ \quad ; \quad \alpha_2^\circ, \beta_2^\circ$$

The radii of these coils are

$$R_1 = \frac{r_0}{\alpha_1^\circ} \quad , \quad R_2 = \frac{r_0}{\alpha_2^\circ} \quad (79)$$

and their distances from the symmetry plane are

$$z_1 = R_1 \beta_1^\circ \quad , \quad z_2 = R_2 \beta_2^\circ \quad (80)$$

For any point on the symmetry plane

$$\alpha_1 = \frac{r}{R_1} = \frac{\alpha_1^0}{r_0} r$$

$$\alpha_2 = \frac{r}{R_2} = \frac{\alpha_2^0}{r_0} r$$

$$\beta_1 = \frac{z_1}{R_1} = \beta_1^0$$

$$\beta_2 = \frac{z_2}{R_2} = \beta_2^0$$

and the total axial field at this point is

$$\begin{aligned} B_z &= \frac{\mu_0}{2\pi} \frac{n_1 I_1}{R_1} f(\alpha_1, \beta_1) + \frac{\mu_0}{2\pi} \frac{n_2 I_2}{R_2} f(\alpha_2, \beta_2) \\ &= \frac{\mu_0}{2\pi} \frac{n_1 I_1}{R_1} \left\{ f(\alpha_1, \beta_1) + \frac{n_2 I_2}{n_1 I_1} \frac{R_1}{R_2} f(\alpha_2, \beta_2) \right\} \end{aligned} \quad (81)$$

The ratio of ampere turns for the two coil pairs is adjusted to give  $B_z \sqrt{r} = \text{constant}$  for a chosen deviation from the mean orbit. In Moussa and Bellicard's case the limits chosen were  $r_1 = 0.9r_0$  and  $r_2 = 1.1r_0$ .  $B_z$  is now calculated covering a larger than the above range of  $r$  values ( $0.7r_0 \leq r \leq 1.3r_0$ ) and the deviations from the "ideal" field suggest corrections of the  $R_1$ ,  $R_2$ ,  $z_1$  and  $z_2$  values.

Moussa and Bellicard were thus led to a final configuration of four pairs of filaments with the following parameters:

$$\begin{aligned} \alpha_0^1 &= 0.6 & , & \beta_0^1 = 0.2 \\ \alpha_0^2 &= 1.05 & , & \beta_0^2 = 0.9 \end{aligned} \quad (82)$$

for the ampere turn ratio  $\frac{n_2 I_2}{n_1 I_1} = 1.813$  ,

$$\alpha_1^0 = 0.51 \quad , \quad \beta_0^1 = 0.25$$

$$\alpha_2^0 = 1.1 \quad , \quad \beta_0^2 = 1.2 \quad (83)$$

for the ampere turn ratio  $\frac{n_2 I_2}{n_1 I_1} = 2.035$  .

The Vanderbilt and the Michigan State spectrometers use these values of  $\alpha$  and  $\beta$  , and the ratios of ampere turns for determination of coil radii and  $z$  values. In addition, however, the Michigan State machine was optimized by calculating the best  $z$  values for the measured radii of the focusing coils, to fit the optimum sixth order field. Such a fit was achieved for a limited region around the mean orbit. An account of the optimization procedure can be found in Chapter VII.

## CHAPTER 4

### CONSTRUCTION OF THE SPECTROMETER

#### 4.1 Introduction

The Michigan State University spectrometer is located in the north-west corner of the first floor of a relatively new physics building. Below it, in the basement, are located ultrasonics laboratories. Above it, on the second floor, are offices and classrooms. Thus there are no large masses of iron, such as magnet yokes, in the immediate vicinity of the machine. Even so, the location is to some extent unfortunate, particularly for a low energy machine. The building is constructed of reinforced concrete and steel, which causes the earth's magnetic field to be quite nonuniform at the spectrometer location. After an initial magnetic survey of the room by means of a saturable strip (fluxgate) magnetometer\* it was found necessary to shim the field by placing three steel compressed-gas tanks in the north-west corner of the room to gain better uniformity. Other disturbing factors affecting the field are steel doors located next to the spectrometer room and a parking lot approximately seventy-five feet from the machine. Both of these cause a small but measurable change

---

\*Distributed by Magnaflux Corporation, Chicago, Illinois.

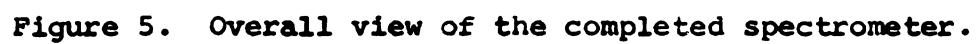
The image area is mostly blank, suggesting the photograph of the spectrometer was not captured or is obscured. There is a small black rectangular mark on the left edge of the page.

Figure 5. Overall view of the completed spectrometer.

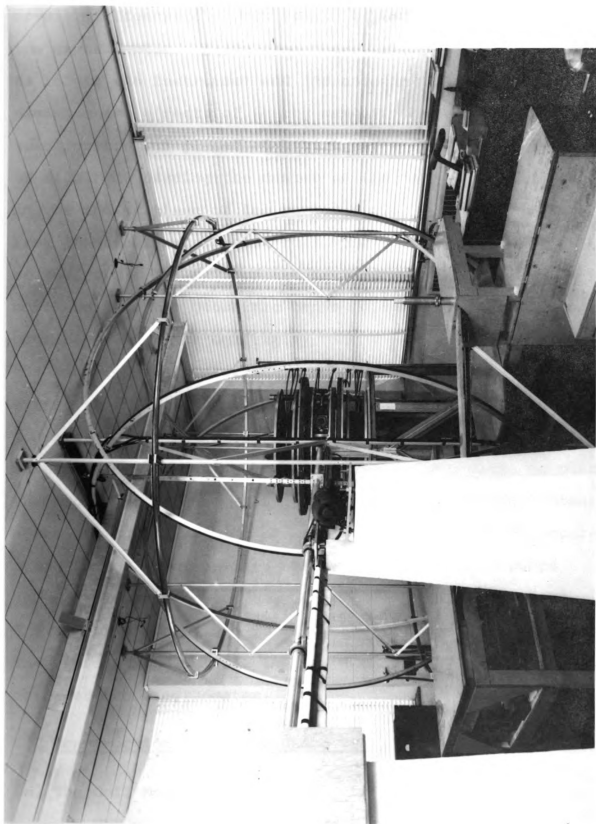


Figure 5

in the magnetic field at the spectrometer, of the order of 0.1 millioersted. Both remain beyond the control of the experimenter. Aside from these, every effort was made to locate the instrument and its associated equipment to minimize the effects of nearby magnetic materials: The spectrometer was placed on a high table constructed mostly of aluminum, placing the center of the machine approximately in the median plane of the room, as far away as possible from the steel reinforcing rods in the floor and ceiling of the room. The axis of the machine was set somewhat north-west of the geometric center of the floor, as a compromise between the uniformity of the earth's field and the need for space near the machine. Enough room was necessary to install the focusing field control system, which consists in part of a long rotating shaft and a fairly sizeable permanent magnet. It is desirable, of course, to place the magnet as far from the spectrometer as possible. Other accessory apparatus made of steel, but needed for the operation of the spectrometer: two mechanical vacuum pumps and the electric motors operating the cooling system and the rotating shaft, had to be located near the spectrometer. They were placed outside the space enclosed by the degaussing coils of the spectrometer.

#### 4.2 Construction of the Focusing Coils

##### (a) The Coil Mounts

The nonuniform field needed by the spectrometer

is produced by four pairs of coils, mounted along the symmetry axis of the spectrometer. The members of each pair are mirror images of each other and are spaced at approximately equal distances from the plane of symmetry of the machine. The decision was made to essentially duplicate the coils used by the Vanderbilt machine, with the exception of trying to make them with better accuracy.

The coil mounts themselves have the shape of annular rings machined from castings of #12 aluminum alloy. The shoulders and the flange surfaces upon which the coil windings are placed were machined to an accuracy of  $\pm 0.001$  inches. A cross sectional view in Figure 6 shows the relative sizes of the coil mounts. Note that the flanges are extended far enough to reach supporting rods which hold the spectrometer assembly aligned. Each coil mount is equipped with a groove containing a 3/8 inch copper tubing, for temperature control of the coils. On the four smaller coils, where heat transfer from the windings to the mount proved to be poor, the cooling tube is sealed in by Wood's metal to improve its thermal contact with the coil mount.

#### (b) The Winding Procedure

The coils were wound from soft temper electrolytic tough pitch copper ribbon. Varnish coated Fyberoid fish Paper\* was used as insulation. Copper ribbon rather than wire was used to provide more uniform current distribution

---

\*Fyberoid Fish Paper, product of Wilmington Fibre Specialty Company, New Castle, Delaware.



Figure 6. Cross-sectional view of focusing coil mounts.

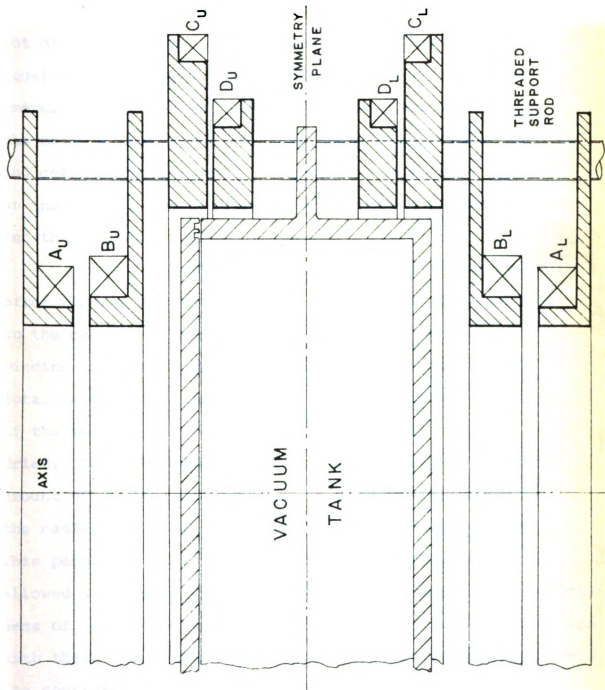


Figure 6

throughout the cross section of the winding.

The winding procedure was as follows: The coil form was first mounted on a specially prepared spider and affixed to a slow speed lathe. During the winding the coil turned on a horizontal axis. Two annular rings were cut out of a large sheet of fish paper, with the inner diameter equal to the diameter of the coil mount and the outer diameter somewhat larger than the anticipated outer edge of the coil. These rings were coated with insulating varnish and cemented to the face of the coil mount, thus forming an insulating layer between the edges of the copper ribbon and the aluminum mount.

In order that the mean radius of the finished coils, after winding and bakeout, be as nearly as possible equal to the calculated radii, it was necessary to estimate the winding thickness. This implies knowledge not only of the total amount of copper and paper in the winding, but also of the thickness of the varnish and its expansion as it dried. The coil mounts were made undersize, so a certain amount of insulation had to be wound on each to build up the radius before the first turn of copper was started. This permitted an adjustment for varnish properties and allowed a closer control in matching coil pairs. The thickness of insulation thus added can be found in Table I. Even with these precautions the finished radii of the coils deviate considerably from the ideal values. Primarily this is due to the uncertainty in thickness of the varnish impregnated

TABLE I. Focusing Coil Data

Coil Pair	$A_u / A_l$	$B_u / B_l$	$C_u / C_l$	$D_u / D_l$
Mount	9.704	10.204	22.396	18.946
Radius	9.7035	10.204	22.396	18.945
Copper				
Width	2.000	2.000	1.400	1.400
Copper				
Thickness	0.0121	0.0121	0.0167	0.0167
Insulation				
Thickness	0.0056	0.0056	0.0067	0.0040
Number of				
Turns	116	116	57	64
Buildup				
Factor	0.0006	0.0006	0.0006	0.0006
Mount Buildup	0.0275	0.0275	0.1170	0.1130
before Winding	0.0250	0.0275	0.1125	0.1183
Finished	11.7920	12.3073	23.8490	20.426
Radius	11.795	12.306	23.837	20.442
Winding	2.061	2.076	1.336	1.367
Thickness	2.067	2.075	1.329	1.379
Mean	10.7618	11.2694	23.1810	19.7415
Radius	10.7618	11.2688	23.1728	19.7526
Ideal				
Radius	10.7320	11.2485	23.1588	19.6850

All dimensions are in inches.

Subscripts refer to upper and lower set of coils, relative to the  $z = 0$  plane.

paper. The amount of varnish remaining on the insulation layers depends greatly on the tension maintained during the winding process. These deviations are unfortunate, but it should be pointed out that a deviation from ideal radius for a coil PAIR is much less serious than a mismatch between members of the pair. Therefore greater care was taken in matching the radii of the coil pairs and, as Table I shows, this has largely been accomplished.

Care was also taken to choose the copper and insulation dimensions to obtain as nearly a square current carrying cross section as possible. A square cross section can be represented for the purpose of calculations as a single current carrying filament, which is nearly equivalent to the physical coil. A rectangular cross section coil, on the other hand, needs two filaments for an equivalent representation.<sup>30</sup> With such coils the matching of the focusing field shape becomes more complicated.

With these preparations completed, a piece of copper ribbon about three feet long was cut at a 45 degree angle and silver soldered to the remainder of the conductor to serve as the inner lead-in. The joint was carefully smoothed out to the same thickness as the rest of the ribbon, insulated with tape, varnished and clamped at a predetermined point on the coil mount. The place on the coil mount was chosen to allow both leads from the same coil to be placed flat on top of each other, thus reducing their magnetic field, and to have the leads from all eight coils come out

in the same azimuthal direction. The plane of the leads was chosen to fall near the counter, in the space between the counter and the source. This choice minimizes the effect of stray fields on the electron orbits.

Figure 7 shows a schematic diagram of the main parts of the winding apparatus. Provisions are made for controlling the copper ribbon tension and the amount of varnish carried to the coil by the insulation. The winding itself was a slow procedure. The coil was moved in approximately 120 degree intervals, with the conductor always securely clamped to prevent slippage. Micrometer readings were taken at three points around the circumference of the coil and the buildup of radius was recorded at frequent intervals. By varying the tension on the copper ribbon and the amount of varnish left on the insulation it was possible to control this radius buildup from coil to coil and consequently to match coil pairs and approximate the ideal radii. The change in radius of the winding contributed by the presence of the varnish was called the buildup factor for the coil. Typically the buildup factor was 0.0006 inches per turn.

After the appropriate number of turns was placed on each coil it was bound off with cloth tape, saturated with insulating varnish and again clamped securely. The finished coils were baked overnight and then painted with air drying varnish for protection. The coils then underwent an insulation check and also a dimensional check consisting of an extended series of micrometer measurements.

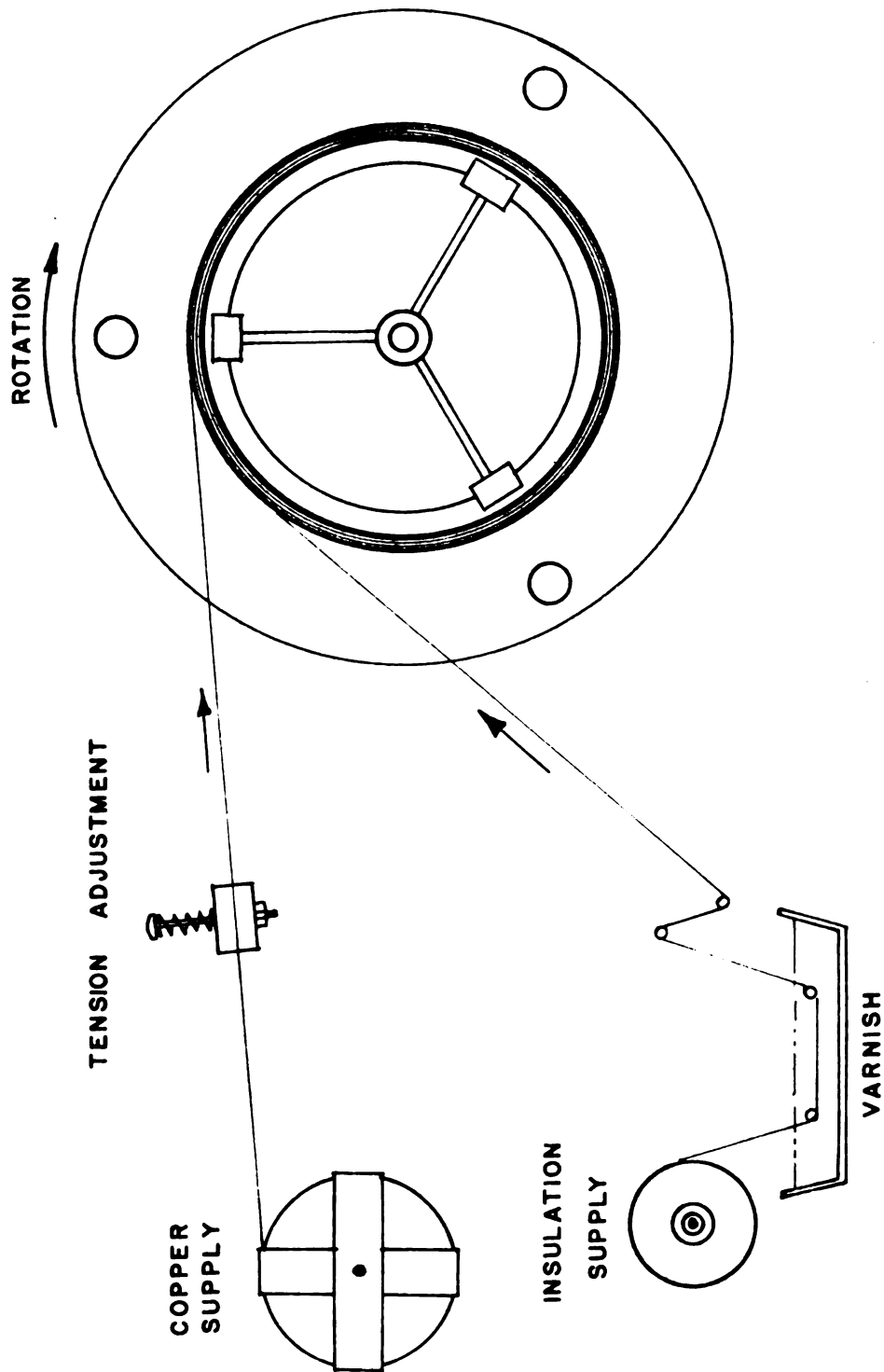


FIGURE 7. SCHEMATIC DIAGRAM OF COIL WINDING APPARATUS.

Later on some of the protective coating was removed and the coils were checked turn by turn for the possibility of internal shorts.

#### (c) The Coil Terminals and Leads

The coil mounts for each pair of focusing coils are identical. Mirror symmetry arrangement thus requires that one coil of each pair be turned upside down. As all coils carry current in the same direction, the four inverted coils had to be wound in the opposite sense and care had to be taken that leads to all eight coils come out in the same direction.

The coil leads were dressed as follows: First, the inner and outer leads of each coil were insulated from each other by individual wrapping with fish paper. Then they were placed tightly on top of each other and fastened together by tape. Thus each coil has a two conductor lead-in, with the conductors carrying current in opposite directions, which reduces their fringing field.

The main lead-in bus bar is also made of two conductors fastened side by side to a plastic strip. The conductors are brass strips one-quarter of an inch thick and two inches wide. Figure 8 shows a cross section of the lead-in bus and the connections to the focusing coils.

#### 4.3 The Vacuum Chamber

The spectrometer vacuum chamber is made from one inch thick tempered aluminum. It is cylindrical and roughly



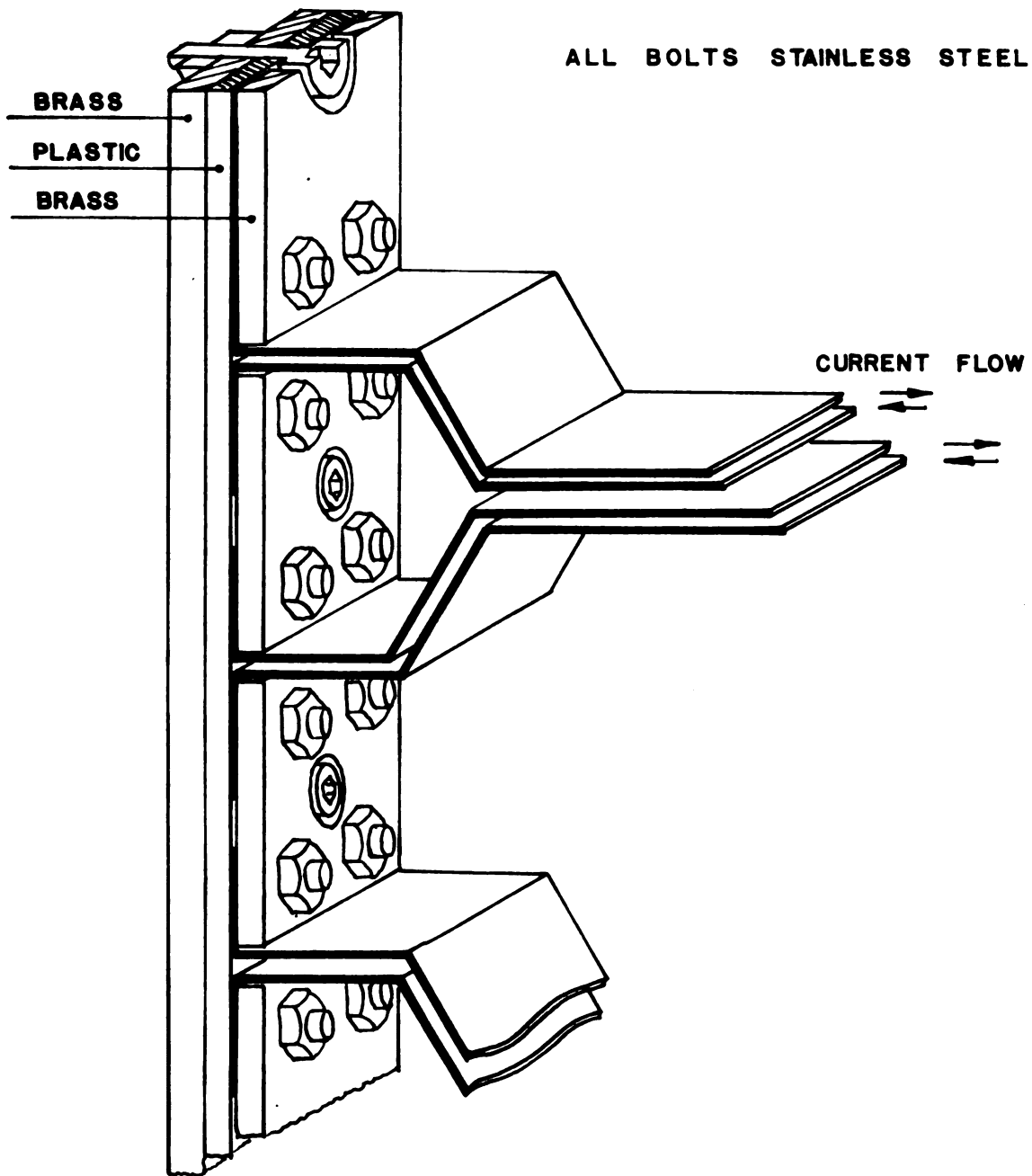


FIGURE 8. SCHEMATIC REPRESENTATION OF THE FOCUSING COIL POWER CONNECTIONS.

pie-shaped, formed by heliarc welding the various wall sections to a flat circular base. A cross-sectional drawing of the chamber is shown in Figure 9. The chamber is mounted on the spectrometer mounting screws by an annular flange welded to the curved part of its walls and located at its midsection. The internal chamber height is eleven inches.

The upper edge of the chamber walls is machined flat and free of tool marks to form a good sealing surface for an O ring. The final smooth surface was achieved by hand lapping. The chamber is closed off by a lid, also made of one inch tempered aluminum and conforming to the pie shape of the chamber. The perimeter of the lid has two O ring grooves milled in it. Although original plans called for a double O ring seal, in practice only one O ring was found necessary. The O ring itself proved to be of non-standard length and all attempts at securing adequate quality custom-made rings failed, primarily, I believe, due to poor control over the vulcanizing process used by the manufacturers. The joints in the rings tended to have a knobby texture, with at least one place where the ring was thinner than normal, thus preventing a seal. Finally a satisfactory O ring was made from 3/16 inch diameter O ring stock. After careful measurement for length, to obtain a finished ring slightly shorter than the groove, the ends were cut on a bevel and ground flat on a high speed grinding wheel. The faces were then very carefully cemented together. An O ring made in this simple way has operated

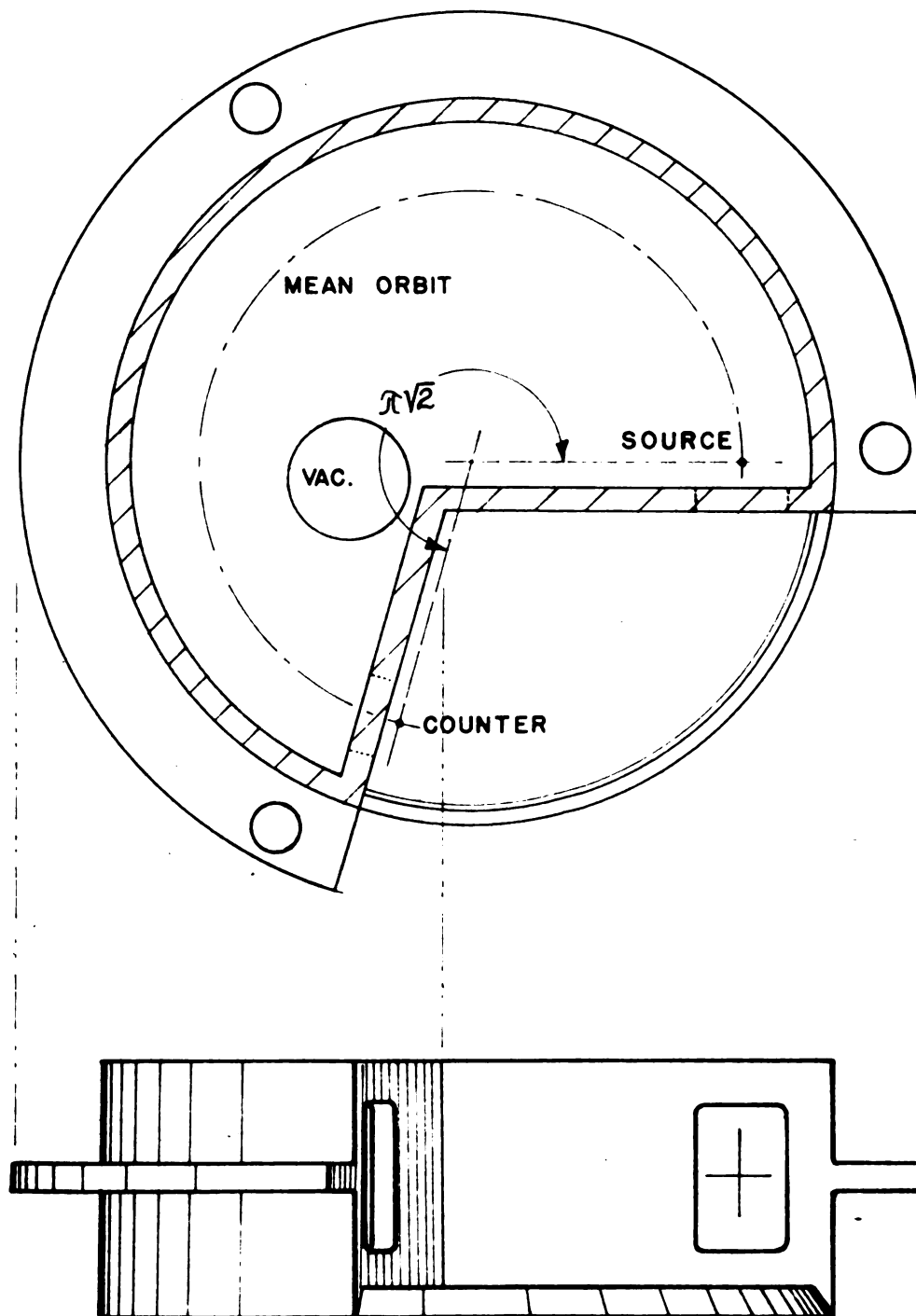


FIGURE 9. SPECTROMETER VACUUM CHAMBER.

satisfactorily now for several years.

The two flat portions of the chamber walls are positioned at an angle of  $270^\circ$  with respect to each other. The faces of these wall sections are machined flat and bear 3.5 inch by 7 inch holes, centered on the proposed mean orbit of the machine, for mounting the source and the counter assemblies.

The outlet to the vacuum pumps is located near the counter end of the spectrometer chamber, to take advantage of differential pumping in the event of counter window leakage. The opening allows a connection six inches in diameter.

#### 4.4 The Source End Assembly

A vacuum lock and a source holder were designed to enable the operator to change sources without breaking the main vacuum of the spectrometer and to position the source accurately in a fixed radial and axial position. The source lock consists basically of an all bronze 2.5 inch diameter gate valve, the type usually used for water service, modified to make it suitable for use with a vacuum system. The seating surfaces of the valve were machined flat, with recesses for rubber gaskets and the stem was isolated from atmosphere by strategically placed O rings. In practice this valve was found to be quite leak tight with the obvious advantage of being non-magnetic and inexpensive. The gate valve is soft soldered onto a half inch thick brass end plate that fits over the source end opening of the spectrometer tank and is sealed to it by means of a rectangular

O ring. A separate vacuum line connection is made to the body of the valve permitting evacuation of the lock prior to opening.

Referring to Figure 10, a schematic drawing of the source lock and holder, note that the end-plate contains a tapered hole, concentric with the gate valve and with its axis lying in the plane of symmetry of the spectrometer. The smaller radius of the opening is on the spectrometer side of the end-plate. The diameter of the hole is machined to be a slip fit for the source holder. Tapering the hole allows source position adjustment without binding.

The outside face of the gate valve is soldered to a three inch length of cylindrical brass bellows, terminating in a collar equipped with an internal O ring. The outside of the collar has the shape of a square with vee grooves machined into the perimeter. A half inch thick brass frame fits over the collar, with about a quarter inch of space separating the two. The outside frame is firmly attached to the end-plate by four brass rods located at its corners. Adjusting screws threaded into the sides of the frame and fitting into the grooves in the collar allow radial and axial adjustment of the source.

The sources themselves are mounted on small aluminum rings 1.25 inches in diameter. The rings are held in a recessed end of a thin walled aluminum tube, approximately three inches long. To minimize back scattering, most of the walls of this tube have been drilled away.

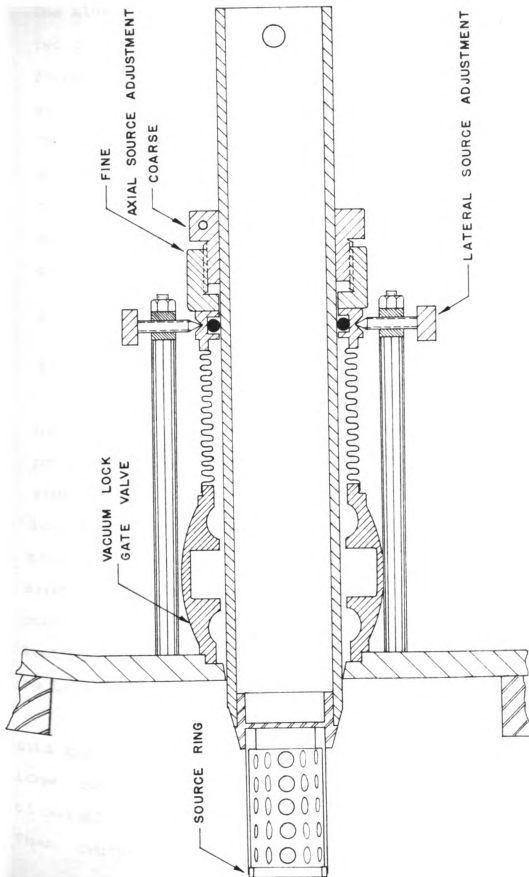


FIGURE 10. THE SOURCE END ASSEMBLY.

The aluminum section is threaded into a closed end of a two inch diameter brass tube, about 18 inches long, which forms the bulk of the source holder and provides vacuum seal via the internal O ring in the collar described above. The insertion depth of the source is fixed roughly by an adjustable tight fitting collar that can be clamped tightly to the tube. A second collar, threaded onto the first, provides fine adjustment. Figure 11 gives the overall view of the source end.

#### 4.5 The Counter System

##### (a) Introduction

There are three types of detectors in most frequent use with beta ray spectrometers: Scintillation counters, proportional counters and Geiger-Mueller counters. Of these three the scintillation counter is the least suitable for low energy work, due to its sensitivity to magnetic fields and its inherent residual noise level that fills the low end of the energy spectrum response of the counter and masks pulses from slow electrons. The efficiency of the scintillation counter in this energy region is difficult to ascertain.

The proportional counter can be designed so it is suitable for this type of work. It has the advantage of low dead-time, making rapid counting possible. The proportionality feature, however, is not necessary in most cases. The output pulses of the proportional counter are rather



Figure 11. The source end assembly.



small, millivolts in size, and thus high amplification is needed.

The Geiger-Mueller counter is the simplest of the three. It provides large output pulses of essentially constant amplitude, its efficiency for electrons is near 100 percent and it can be designed to operate with very low counting gas pressure. On the other hand, it is by far the slowest of the three detectors mentioned. Nevertheless, in high resolution work we do not expect to encounter very high counting rates; this one drawback becomes relatively minor, and the Geiger-Mueller counter is the natural choice for the spectrometer detector.

#### (b) The Side Window G-M Counter

The basic counter was designed by R. A. Parker at Vanderbilt University and a detailed account of its design and construction can be found in Mr. Parker's thesis.<sup>31</sup> Only a brief description is included here for the sake of completeness.

Figure 12 shows that the counter has the form of a right circular cylinder, one-half inch diameter and four inches long, bored in a piece of 2.5 inch diameter brass stock. Part of the counter body is milled away to provide an opening for entering particles, and also to allow space for mounting windows and placing O rings for vacuum seals. The inside bore of the counter is polished free of tool marks and forms the cathode. The anode is a 0.001 inch diameter stainless steel wire, which can be exposed to the

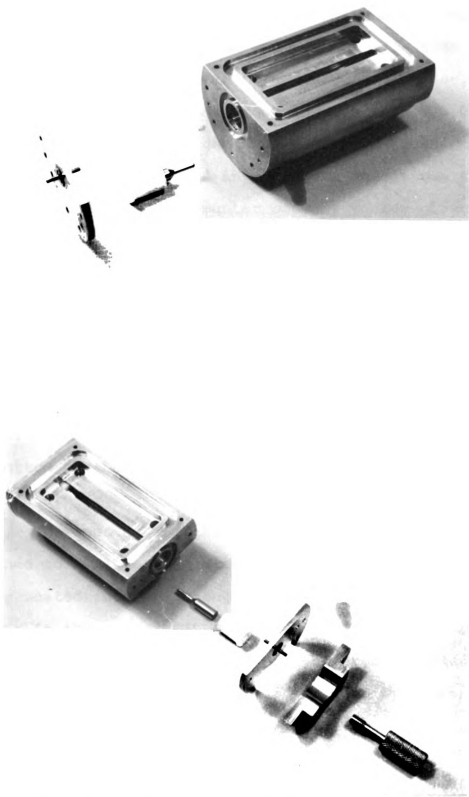


Figure 12. The Side Window G-M Counter.

counter volume in variable length from about 1/4 to 1 1/2 inches, thus allowing an adjustment in the active volume of the counter. The wire is supported at both ends by hollow brass fingers, some 1/16 of an inch in diameter, which are highly polished and have rounded ends with a 0.005 inch diameter hole in them aligned with the axis of the counter. The brass fingers are held in alignment and at the same time insulated from the counter body by teflon plugs. A vacuum seal and the electrical connection to the outside is provided on each end by means of a glass to metal seals that are soldered to detachable end-plates. The end-plates seal against O rings.

The body of the counter is drilled to provide a path for the continuous flow of counter gas and for evacuation. An O ring fitted gas connection is provided at the bottom of the counter along with a high voltage coaxial connector.

The counter and its window supporting plate are attached to a flat end-plate which in turn fits against an O ring seated in a brass end-plate covering the counter end opening in the spectrometer vacuum tank. A proper position of the counter is ensured by a pair of brass locating pins. Attachment to the spectrometer is provided by means of two thumb-screws.

Figure 13a shows the assembled counter. Figure 13b shows the counter positioned on the spectrometer end-plate.

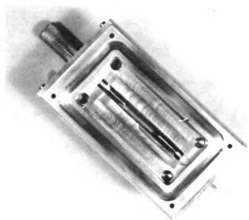


Figure 13 (a). The Assembled Counter .

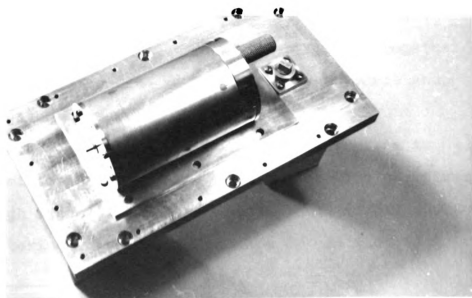


Figure 13 (b). Counter Positioned on Spectrometer End Plate .

The vacuum side of the spectrometer end-plate is provided with a vacuum lock to enable the operator to change windows or to clean the counter without breaking the main vacuum. The gate assembly can be seen in Figure 14. The gate itself is a "C" shaped piece of flat brass stock, one-quarter inch thick, that slides against an O ring seated in the end-plate. The lock is guided by two rack and pinion gears, which in turn are driven by a right angle worm gear drive. The shaft of the worm is brought outside through a rotating vacuum seal. A connection is provided to an external vacuum line allowing the counter and the gate to be evacuated simultaneously, to reduce pressure stresses on the counter windows.

(c) The Counter Gas Flow System

As the spectrometer counter is of the self-quenching type, it is necessary to provide a continuous supply of counter gas to maintain stable operating conditions. Figure 15 shows a diagram of the gas flow system, together with lines provided for the evacuation of the source and the counter gate volumes.

The counting gas,  $2/3$  argon and  $1/3$  ethylene is supplied premixed in a compressed gas tank.\* The gas first passes through a pressure reducer on the tank itself and then to a metering valve V-1. The rate of gas flow is

---

\*The counting gas was obtained from the Matheson Company, Joliet, Illinois.

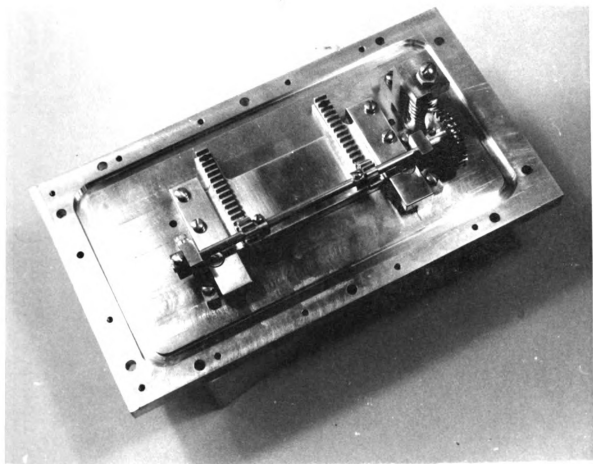


Figure 14. Counter Gate System.

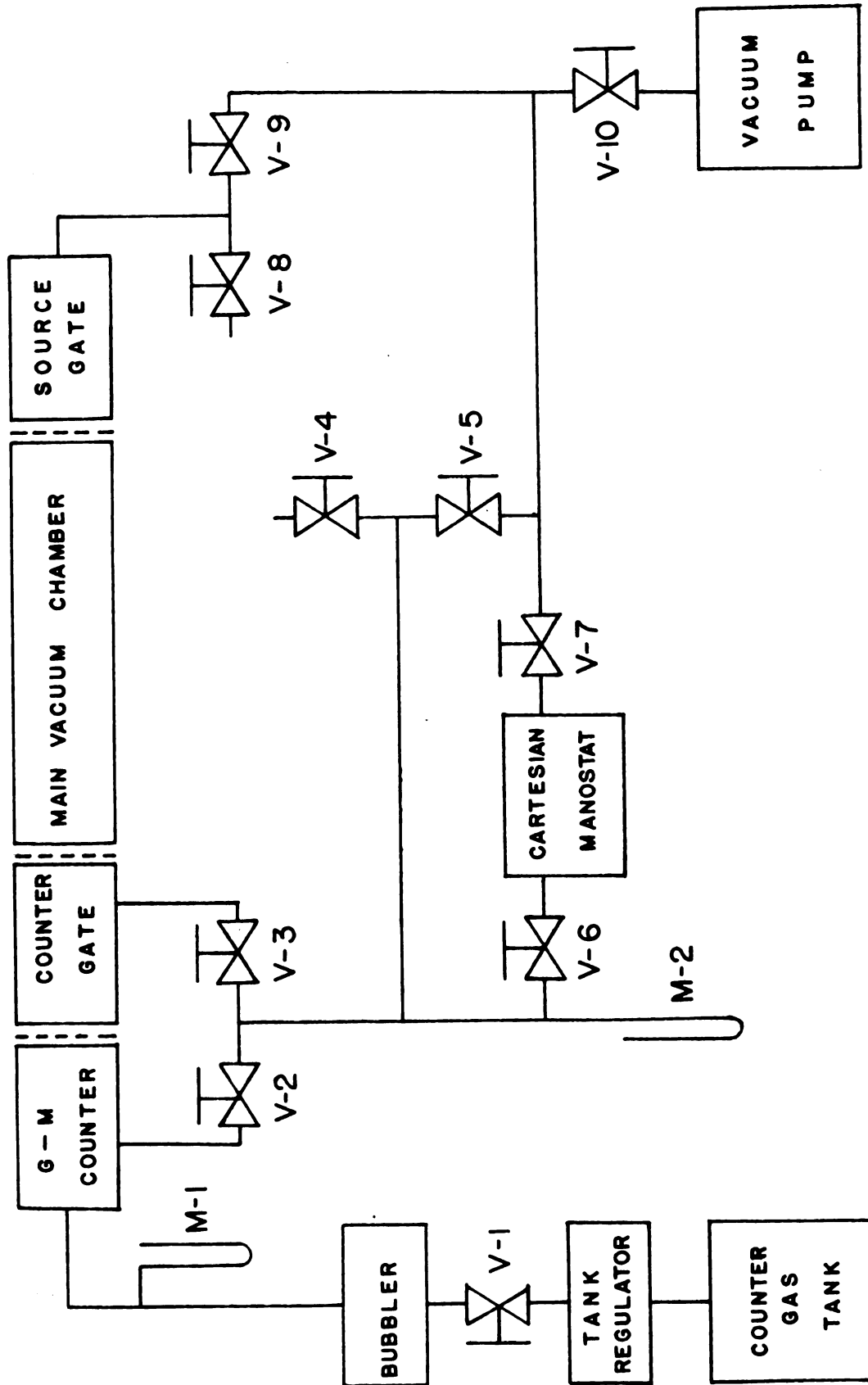


FIGURE 15. COUNTER GAS FLOW SYSTEM.

1



adjusted by valve V-1 and is observed in the bubbler. The bubbler is a device made out of a glass washing bottle, partially filled with silocone vacuum pump fluid. The gas enters the bottle through a vertical tube whose end has been drawn out to a capillary and bent in a slightly more than a ninety degree angle. The opening of the capillary is just below the surface of the liquid. The entering gas thus blows surface bubbles. The rate of gas flow is easily observable and as the capillary is very near the surface of the fluid, the back-pressure in the bubbler is negligible.

The pressure of the counter gas is monitored by a glass tube mercury manometer M-1, placed in the line between the bubbler and the counter. The exhaust lines leading from the counter and the counter gate are connected to a three-way valve whose two halves can be operated independently. On the diagram this valve is shown as V-2 and V-3. During the process of counter evacuation both V-2 and V-3 are opened, relieving pressure on the counter window. During normal counter operation V-2 is open and V-3 is closed. The exhaust line now passes to the fine pressure regulator, a Cartesian Manostat,\* which can hold the pressure constant to a fraction of a millimeter of mercury. Another mercury manometer, M-2, monitors the pressure near the manostat. A three-way valve V-4 and V-5 provides a bypass of the manostat as well as atmosphere shutoff for the purpose

---

\*Manufactured by the Manostat Corporation, New York 13, New York.

of evacuation. Valves V-6 and V-7 are toggle type shutoff valves used to isolate the manostat during pumpdown to preserve its pressure setting. The counter gas then moves down an exhaust line to a mechanical vacuum pump. The source gate, described above, is also connected to this pump via the three way valve V-8 and V-9. Figure 16 shows the actual gas handling system panel.

#### (d) The Data Acquisition System

The remainder of the counting system consists of a regulated high voltage power supply capable of providing 600 to 1500 volts for the operation of the counter, two amplifiers and a scaler. Pulses from the counter are fed through a six foot length of a high voltage coaxial cable to a transistor emitter follower, which drives them through a sixty foot long cable to the control desk. There the signal is amplified further by a two stage transistor amplifier having a gain of about ten and then fed to a seven decade printing scaler. The scaler uses an electromechanical timer and is operated in a preset time mode.

#### 4.6 The Baffle System

To maintain high resolution in a double focusing spectrometer, it is necessary to limit the electron orbits to a relatively narrow cone in the neighborhood of the mean orbit, even if the focusing field has an ideal shape. Normally, the region where the magnetic field can be matched to the desired shape is limited by the inherent errors in

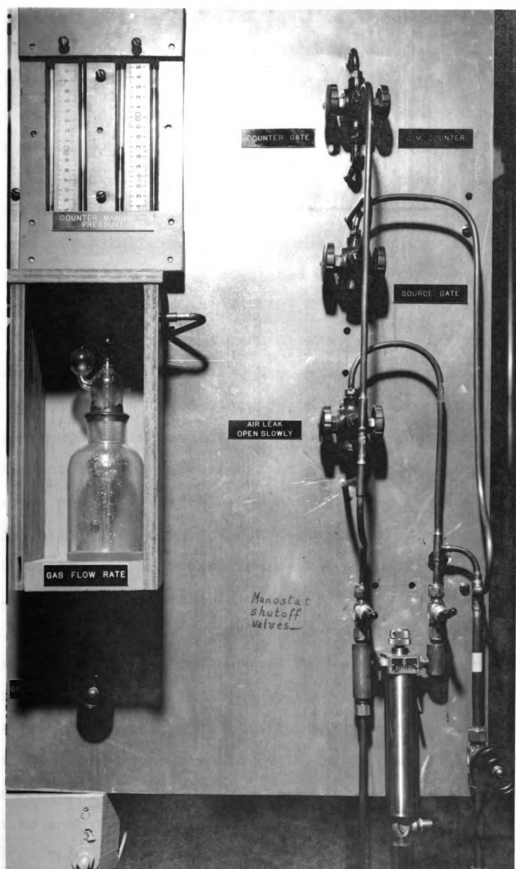


Figure 16. Counter Gas Flow System Panel.

the determination of the mean radii of the focusing coils and by the precision to which the coils can be positioned with respect to the plane of symmetry of the instrument. This makes the confinement of the accepted electron beam even more important.

A system of baffles and diaphragms thus is needed to select a beam of electrons emitted from the source with a known solid angle subtended at the source and to provide some means of preventing scattered electrons from reaching the counter.

Three baffles are used on the present instrument to accomplish this purpose. Midway between the source and the detector is a fixed aperture baffle cut to pass the largest acceptable beam of electrons. The aperture of this baffle corresponds to the maximum permissible emission angles from the source,  $7^{\circ} 40'$  in the radial direction and  $15^{\circ} 30'$  in the axial direction. The acceptance solid angle of the spectrometer can be controlled by two diametrically opposite variable aperture baffles, located  $37^{\circ} 10'$  from the source and the detector. As Figure 17 shows, both of these baffles are formed from two opposed "C" shaped pieces of  $1/8$  inch thick aluminum, arranged so they can be moved together like jaws, enclosing a vertically elongated hexagonal shaped opening. The accepted solid angle is determined by the size of this aperture, which can be varied externally from zero to somewhat over one percent of the total sphere.

The baffles are attached to brass blocks which slide

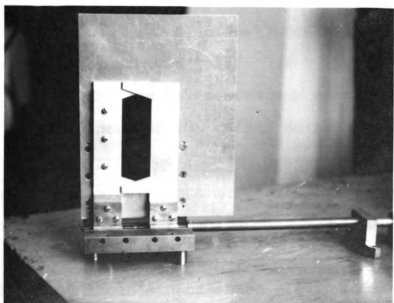
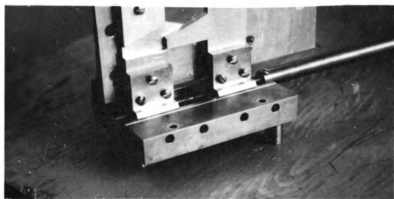
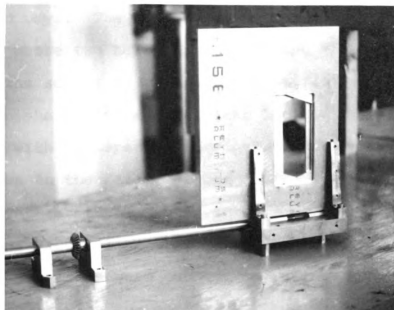


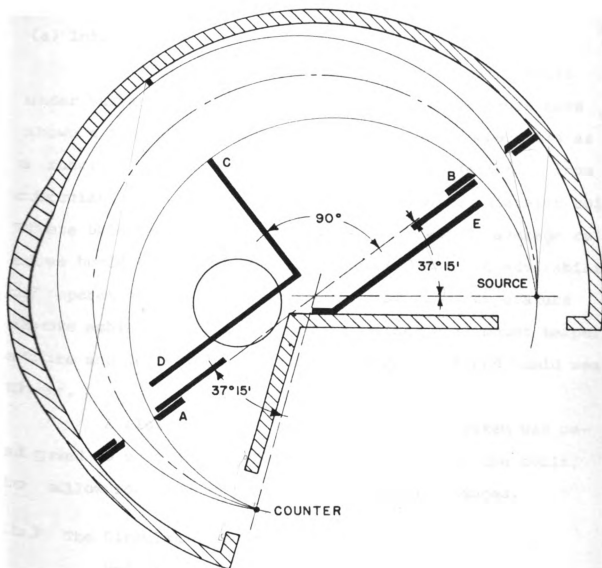
Figure 17 . Beam Defining Baffles.

in machined ways. The motion is provided by means of special screws whose two halves have opposing threads (see Figure 17). The screws of both sets of baffles are attached to a common shaft with a bevel gear located at its center, coincident with the spectrometer axis. A second gear, at right angles to the first, allows a baffle control shaft to be brought out through the center of the bottom of the spectrometer vacuum tank. It is sealed there by an O ring seal. These baffles were constructed in such a way that the axial angle with the baffles fully open to a width of about  $2 \frac{1}{8}$  inches is about fifteen percent larger than its value with the baffles closed.

Subsequently, we have had some second thoughts about this arrangement, particularly as the spectrometer is of the "axial" type, i.e., can accept large axial and small radial deviations from the mean orbit. To take better advantage of this, the baffles may be modified some time in the future.

To reduce the number of scattered electrons reaching the counter, the movable baffles were supplemented by a solid piece of  $\frac{1}{8}$  inch thick aluminum extending to the walls and to the center of the spectrometer tank. A similar extension was provided for the center baffle. With these provisions the only smooth circular trajectories available to the electrons are those permitted by the baffle openings.

Figure 18 shows a horizontal section through the



A, B ADJUSTABLE BEAM DEFINING BAFFLES  
SHOWN IN FULLY OPEN POSITION.

C, D, E ANTISCATTERING BAFFLES.

FIGURE 18. SPECTROMETER BAFFLE POSITIONS.

vacuum tank, showing the baffles and their drive.

#### 4.7 The Focusing Coil Temperature Control System

##### (a) Introduction

Careful measurements made on the focusing coils under varying conditions of current and temperature have shown a fair amount of dimensional change in the coils as a function of both of these factors. Some deviation from circular shape was also observed on the large diameter coils. These observations, and the rather high yearly average relative humidity in Michigan, have pointed out the advisability of operating the coils continuously at some temperature above ambient, both to maintain constant coil mount temperature and to prevent condensation during hot and humid weather.

A closed circuit water circulating system was designed to provide both heating and cooling of the coils, to allow for varying current and seasonal changes.

##### (b) The Circulating System

Referring to Figure 19 below, the closed circuit circulating system consists of a positive displacement pump, Continental EC-22,\* driven by a single phase one-half horsepower motor, a thermostat, a set of heaters and a heat exchanger. Immediately upon discharge from the pump, the

---

\*Continental Pump Company, St. Louis, Missouri.



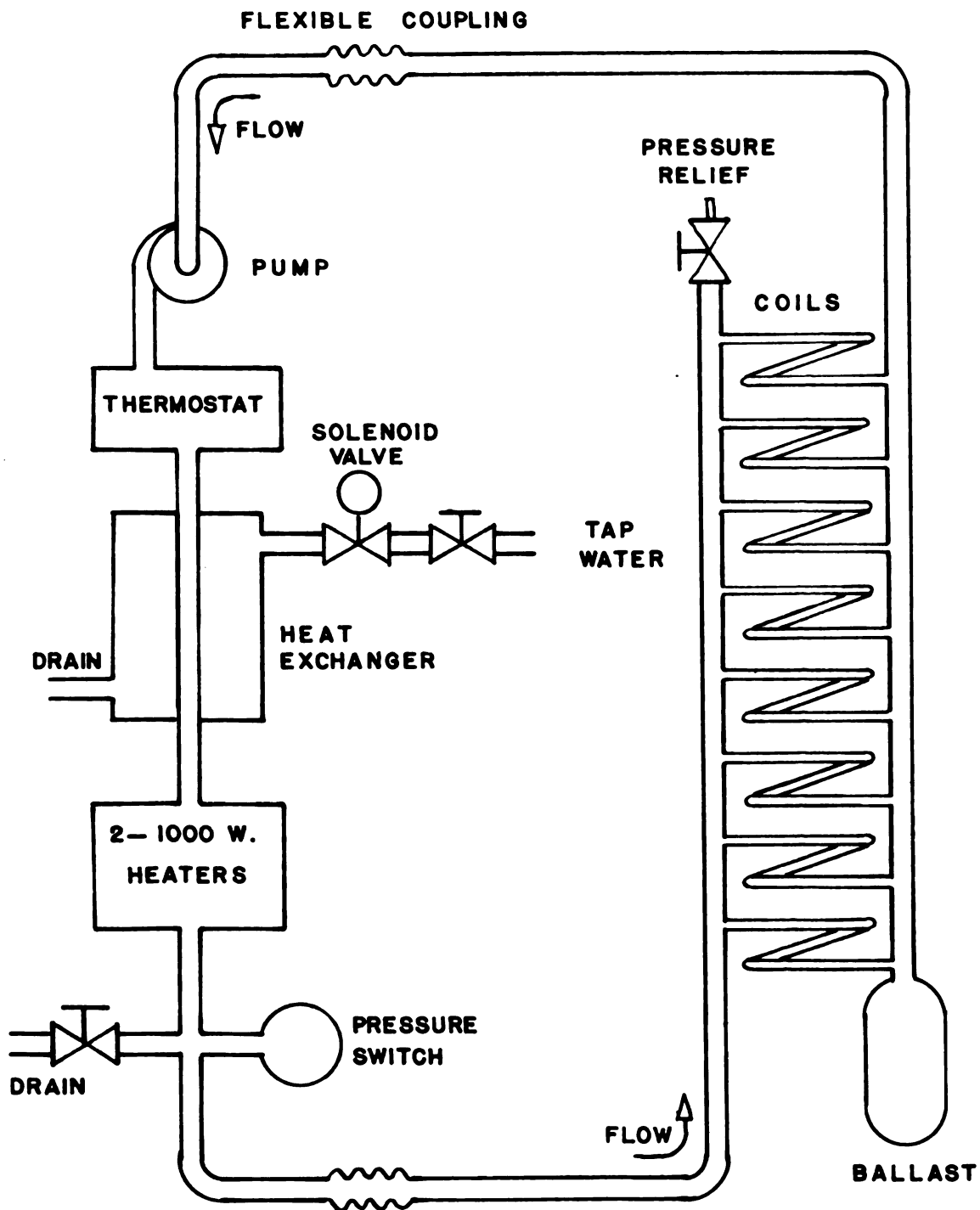


FIGURE 19. FOCUSING COIL TEMPERATURE CONTROL SYSTEM.

water passes over a mercury thermostat, which controls both the heating and the cooling actions of the system. Next, the water passes through a heat exchanger, which consists of a length of 1 1/2 inch diameter copper pipe enclosed in a four inch diameter water jacket. A sheet metal spiral is soldered onto the exterior of the inner pipe to force the cooling water to travel a longer path. The interior of this pipe contains a long copper strip, situated in the manner of the cross bar in the Greek letter theta, which is given a half twist and soldered to the pipe. This forces the fast flowing water to be forced against the walls of the inner pipe, improving the heat transfer. The water jacket is fed by tap water. The rate of flow is controlled by a manual shutoff valve. The demand for cooling is controlled by a solenoid valve which is operated by the thermostat. After the heat exchanger, the water goes through another length of 1 1/2 inch diameter copper pipe containing two 1000 watt immersible cartridge heaters. Power to the heaters is also controlled by the thermostat. At the exit of the heater unit is located a drain valve and a pressure switch which will shut off the pump motor and the power to the heaters in the event of loss of coolant. The supply and drain lines to the spectrometer are one inch diameter copper pipes. The spectrometer coils use 3/8 inch tubing, as was mentioned previously. All eight coils are supplied in parallel. A photograph of the system is shown in Figure 20.



Figure 20. Focusing Coil Temperature Control System.  
The Pump and the Heat Exchangers.

### (c) Thermostatic Control

Considerable difficulty was experienced with the thermostatic control of the coil cooling system. The chief source of the trouble seemed to be the vibration of the pump which caused excessive chattering of the thermostat contacts. The first thermostat tried with this pump was a dual range bimetallic strip type. It proved to be completely unsatisfactory, as settings resulting in a differential of one degree centigrade or less caused almost continuous chattering. Next a home built thermostat was tried. This thermostat used a large reservoir of mercury that was pushed up into a capillary, in the manner of a thermometer, where it could contact tungsten wires set at different heights to give varying differentials. The temperature sensitivity of this unit was excellent, but it too had to be abandoned, for two reasons: Sensitivity to vibration and gradual contamination of the mercury by oxidation due to sparking. After some time of operation, the thermostat would no longer make and break cleanly, causing a several degree shift in the coil temperature.

The last, and finally satisfactory thermostat tried was a commercially built mercury type,\* in the form of a sealed thermometer, with leads entering the bore of the capillary from the side. This thermostat seems to be completely impervious to shock and vibration. Its only possible

---

\*Precision Thermometer and Instrument Company, Southampton, Pennsylvania.

disadvantage is a limited control current that can be passed through it, about one milliampere.

To allow the use of this thermostat, a special circuit was designed and built which could operate the heavy relay needed to switch 2000 watts of power for the heaters. Figure 21 shows the schematic diagram of this control circuit.

In use, the circulating system proved to be reliable over a period of about two and a half years, holding the coils at a temperature of  $41^{\circ}\text{C}$  with a possible deviation of  $1^{\circ}\text{C}$ . The crossover point between heating and cooling occurs in the neighborhood of 25 ampere current through the focusing coils.

#### 4.8 The Vacuum System

##### (a) The Vacuum Pumps

For a high precision spectrometer it is essential to have high enough vacuum in the chamber so that the mean free path of the electrons is several times larger than the characteristic dimensions of the instrument. This means that the pumping speed should be high enough to maintain the pressure below  $10^{-4}$  torr, even for the worst anticipated case of counter window leakage. For this reason a "straight through" system was decided upon, consisting of two oil diffusion pumps placed in series and backed by a fast two stage mechanical pump.

The primary volume to be pumped is approximately

FIGURE 21. FOCUSING COIL TEMPERATURE CONTROL SYSTEM. THE CONTROL CIRCUIT.

five cubic feet, including a twenty percent safety factor. The gas load on this system is essentially unknown, thus as is done in such cases, it is assumed to be five cubic feet per second, or 150 liters per second. Allowances have to be made for outgassing of the system and for any obstructions, such as cooling baffles and traps, placed in the vacuum lines. Outgassing and line impedance account for about a factor of two in pumping speed and the insertion of a water cooled baffle in the line accounts for another factor of two. Thus the main diffusion pump should have a pumping speed of about 600 liters per second or more. Consideration of inlet versus outlet pressures for the main pump led to a selection of a booster diffusion pump with a pumping speed of 100 liters per second and a mechanical pump with a free air displacement of 150 liters per minute.

Some time was spent in searching for a diffusion pump made of nonmagnetic materials to allow its location near the spectrometer. After about six months of negative results or promises of exorbitant cost, Consolidated Electrodynamics Corporation brought to market a six inch stainless steel three stage fractionating diffusion pump, the PMC-721,\* with a pumping speed of 700 liters per second at  $10^{-4}$  torr, using silicone fluid DC-704.\*\* This pump was selected as the main pump for the spectrometer.

---

\*Consolidated Electrodynamics Corporation, Rochester, New York.

\*\*Made by Dow Corning Company, Midland, Michigan.

The booster pump chosen was also made by Consolidated Electrodynamics Corp., type MB-100. This pump is made of ordinary steel and was therefore placed at the end of a ten foot long vacuum line and located outside the sphere enclosed by the compensating coils of the spectrometer. The mechanical pump chosen was the CENCO Hyvac 14.\*

#### (b) The Vacuum System

Figure 22 shows the salient features of the vacuum system. The spectrometer tank is evacuated by a six inch diameter brass pipe, connected to it and to the diffusion pump by bolts and O rings. A water cooled baffle is interposed between the tank and the pump. As commercially made baffles turned out to be either too expensive or made out of magnetic materials, this baffle is home made. Figure 23 depicts a section through the baffle as it was originally designed, with three stages. Later, after about a year of operation it was found that one stage was quite sufficient for our purposes. The upper two stages were removed, yielding a slight increase in pumping speed.

The exhaust of the main diffusion pump passes through a ten foot, three inch diameter line and enters the booster diffusion pump, which is located some twelve feet from the center of the spectrometer. The booster pump is connected to a ballast tank, to reduce the effects of gas surges, and finally exhausts into the mechanical pump.

---

\*Central Scientific Company, Chicago, Illinois.



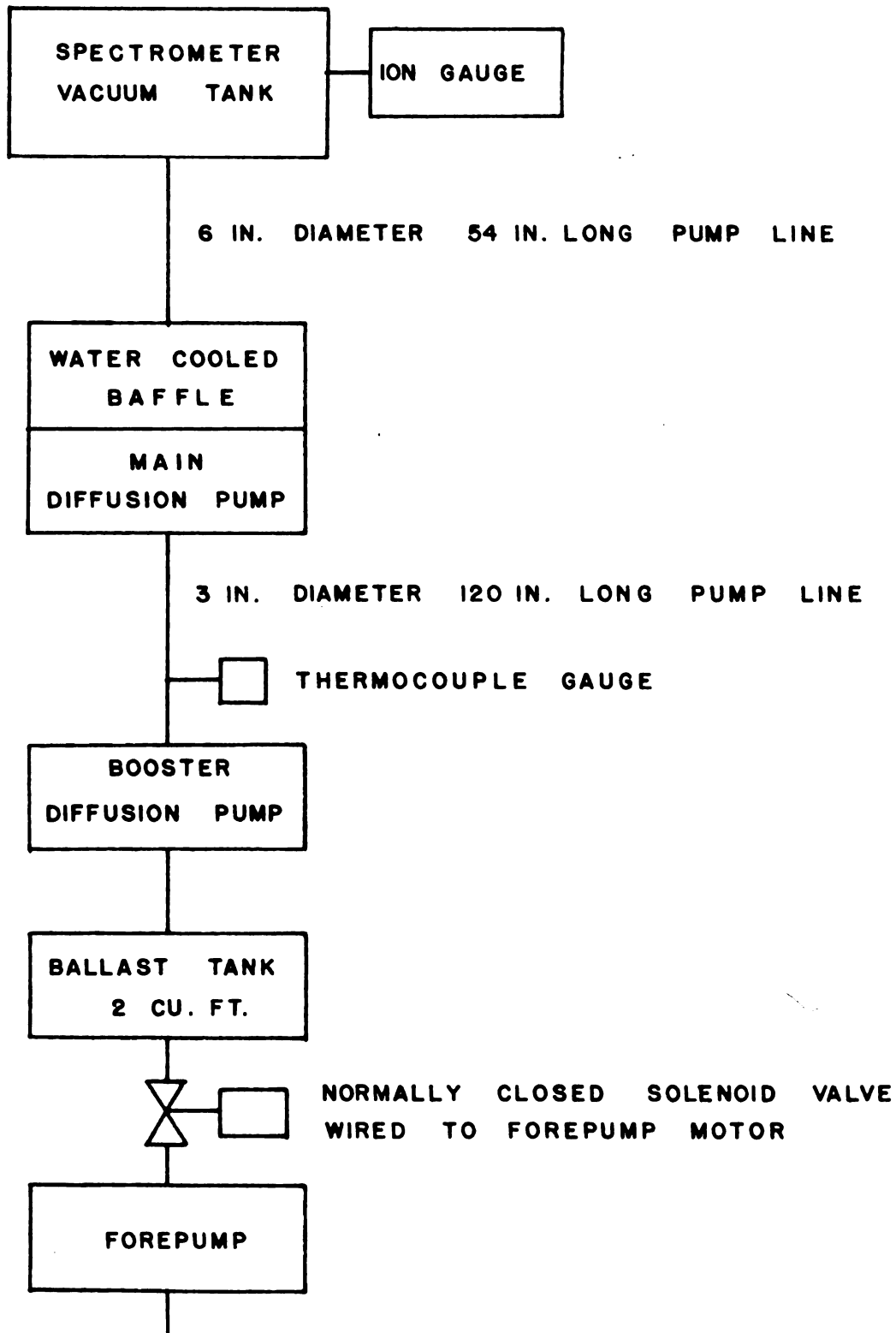


FIGURE 22. BLOCK DIAGRAM OF THE MAIN VACUUM SYSTEM

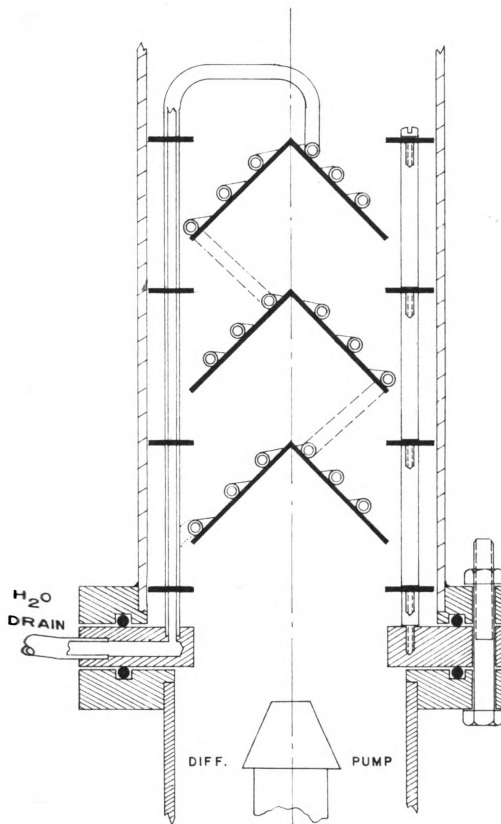


FIGURE 23. HIGH VACUUM WATER COOLED BAFFLE.

Vacuum is protected by a solenoid valve connected to the intake of the mechanical pump and coupled to the motor. The valve closes upon power failure.

During the past three years of operation of the vacuum system it was found that the local water supply contains enough minerals to do extensive damage to the diffusion pumps. Boilerstone was discovered at one point to have completely blocked the water cooling lines of the main diffusion pump, causing severe overheating. The lines could not be cleaned and had to be completely replaced. To ward off similar occurrences in the future when they might interfere with an experimental run, it was decided to place both diffusion pumps on a closed cooling circuit and use distilled water. A large heat exchanger, made entirely of copper and aluminum (found in the University's salvage yard), was immersed in tap water cooled copper tank, its lines were connected to a small rubber impeller circulating pump\* and a pressure switch was provided to shut off the pump and the heaters of the diffusion pumps in case of coolant loss.

#### (c) Electrical Controls and Associated Equipment

The electrical circuit used to control the vacuum pumps is a sequential self-protecting type, shown schematically in Figure 24. The circuit breakers are used as power switches for the mechanical vacuum pumps. The sequence

---

\*Pump made by Sherwood Brass Works, 6331 E. Jefferson Ave., Detroit 7, Michigan.

**FIGURE 24. VACUUM PUMP CONTROL CIRCUIT.**

requires that the spectrometer forepump and the diffusion pump water must be turned on before the heaters of the diffusion pumps can be activated. The heaters are switched on by means of self holding relays and therefore even a temporary malfunction, such as a power failure or water pressure drop, will disconnect the heaters.

Continuous readings of the pressure in the spectrometer tank and in the foreline can be made by means of a combination ionization and thermocouple gauge.\* The ionization gauge tube is located inside the tank, mounted on a glass to metal seal and attached to the source lock end-plate. This location protects the tube from damage and insures a very short connection to the vacuum system.

---

\*Consolidated Electrodynamics Corporation GIC-110  
Ionization and Thermocouple gauge.



## CHAPTER 5

### FOCUSING COIL CURRENT CONTROL SYSTEM

#### 5.1 Introduction

The Michigan State University spectrometer is designed to use focusing coil currents from 0.3 to 60 amperes. This current range corresponds to an energy range from 250 e.v. to nearly 2 Mev. The determination of electron line momenta to within a few parts in  $10^5$ , with the spectrometer adjusted for a resolution of about 0.05% requires a long term stability of the focusing magnetic field of one part in  $10^5$  or better over the entire current range of the instrument. Furthermore, to realize the full high resolution potential of the instrument, line broadening due to short term fluctuations in the focusing current have to be kept low, preferably to one part in  $10^5$  or less. At the time of construction of the spectrometer no power supply meeting these requirements could be obtained from commercial sources at a reasonable price. Its design was therefore undertaken by the author. As transistors were beginning to look attractive in high power applications, the decision was made to abandon the usual configuration of such current sources, namely a regulated d.c. generator supply with vacuum tube noise reduction and regulation circuits, such as those developed by Sommers et al.,<sup>32</sup> in favor of an all transistor

power supply. Other possibilities, such as batteries were discarded as too unwieldy.

The basic design of the current regulator follows quite closely a circuit developed by Garwin and his co-workers at Columbia University.<sup>33</sup> The accessory equipment such as power input and field regulation loops combines original designs with those developed for the Vanderbilt machine.<sup>34</sup>

A block diagram of the entire control circuit is shown in Figure 25. Three phase 440 volt A.C. power is first stepped down to 120 volts and rendered variable by a saturable reactor. The output of the saturable reactor is fed to a three phase full wave rectifier bridge, filtered by a two stage L-C filter and passed through a set of power transistors which serve as the fine current regulator. The current then goes through the focusing coils and finally returns to the power supply. Two main feedback loops maintain current stability. A coarse loop, operating the saturable reactor and activated by error signal derived from the voltage drop across the power transistors and a fine loop, deriving its error signal directly from the field of the spectrometer.

The remainder of the chapter is devoted to the description of the various parts of the current control system.

## 5.2 Design and Construction of the Transistorized Power Supply

### (a) The Input Section

As was mentioned above, the regulator itself was



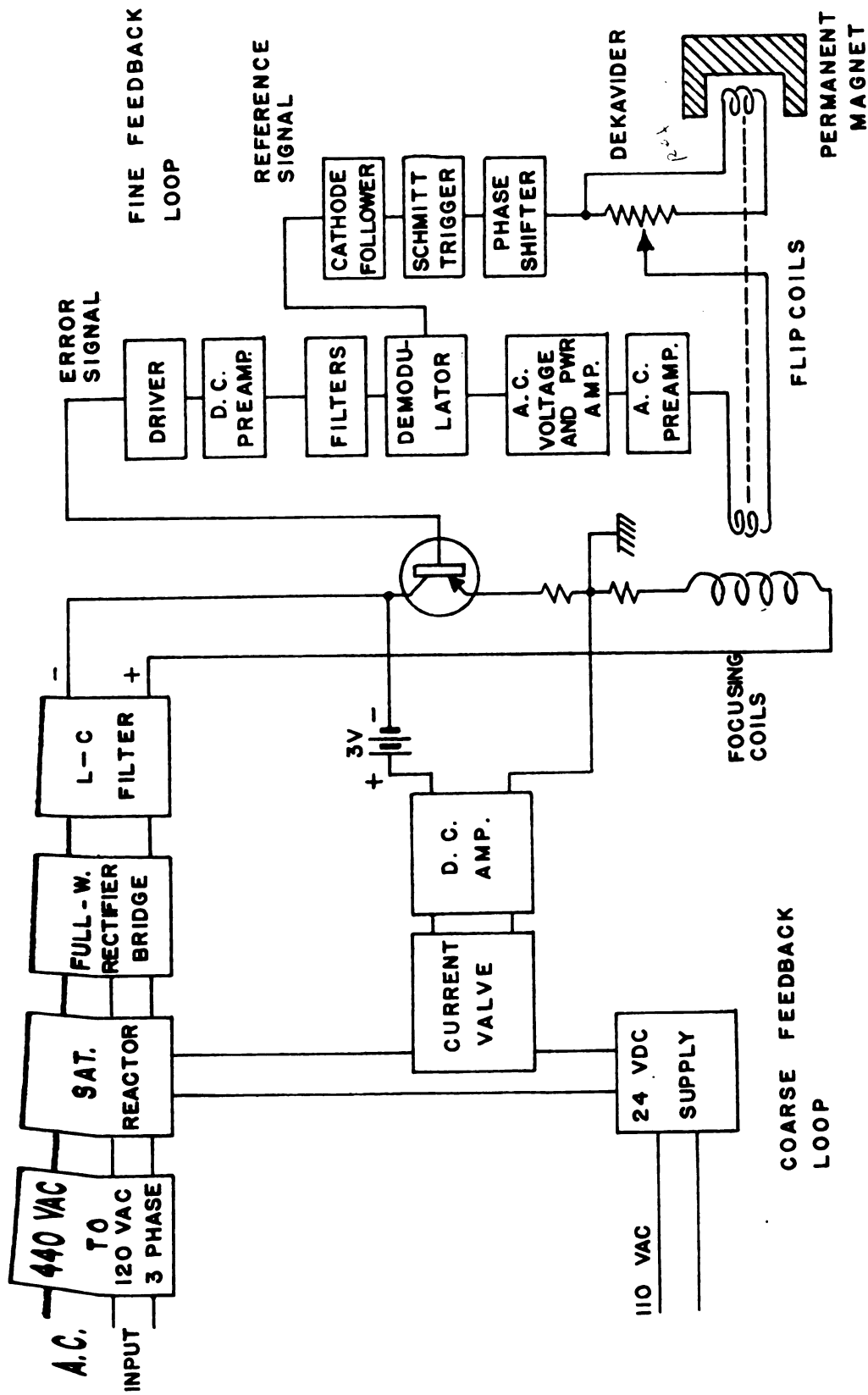


FIGURE 25. BLOCK DIAGRAM OF SPECTROMETER POWER SUPPLY.

patterned after a design by R. L. Garwin.<sup>33</sup> The circuitry was modified somewhat to suit our particular application. The entire power supply will be described in the sequence laid down by the block diagram of Figure 25.

The power supply uses a 440 volt three phase input. The choice is a fairly logical one, for it enables the entire power supply to be built into a rather small package and saves the cost of a 10 KVA motor generator. The 360 cps ripple produced by the rectifiers is not much more difficult to control than generator noise and ripple. The 440 volt input was chosen to insure the use of one of the primary power lines in the physics building, to minimize fluctuations caused by other equipment connected to the same line. The 440 volt input is stepped down to 120 volts by a three phase transformer that serves only the spectrometer. The 120 volt lines are led from the basement of the building to a distribution panel near the control desk where the rest of the power supply is located. The voltage drop in the lines is quite appreciable, about 25 volts, when the power supply is set for maximum current. This limits the focusing coil current to about 58 amperes. Eventually it is hoped to locate the step down transformer at the control desk also, to eliminate these losses. With full 120 volts available, one should be able to obtain about 75 amperes through the focusing coils.

(b) The Rough Regulator

The complete regulator is basically a double loop

servo mechanism. The primary, or rough loop, establishes a small region of current over which the fine regulator operates. The rough regulator has a low gain and is mostly non-dissipative in nature. The fine regulator loop has high gain and performs its function by dissipating some of the available power. It is because of this power dissipation in the fine regulator that the rough loop is needed. Otherwise, the overall efficiency of the regulator would be low and its range would be limited by the power dissipation in the power transistors. In the present power supply which uses 10 power transistors in parallel, the permissible power dissipation is about 250 watts. To keep it from rising above this level, it is necessary to limit the voltage drop across the power transistors to a low value. The figure chosen on the basis of transistor characteristics was 3 volts. The function of the rough regulator is to maintain the voltage drop across the power transistors at approximately this level. The circuit diagram, Figure 26, shows the main features of the rough regulator. The transistor voltage drop is sensed at the power transistors. Long cables or remote grounds should be avoided here, since any additional error signals, caused, for example, by pick-off from the power cable may lead to unstable operation. The sensed voltage drop is added to a three volt battery and amplified by a simple transistor D.C. amplifier which is a modification of the original Garwin circuit.<sup>35</sup> The D.C. amplifier operates three parallel power transistors

Figure 26. Schematic diagram of the spectrometer power supply.



BETA-RAY SPECTROMETER POWER SUPPLY.

## Figure 26

as a current "valve" which controls the output of a 24 volt magnetically regulated power supply and hence the d.c. exciting current through the control windings of the saturable reactor.

The circuit operates as follows: A low voltage drop across the power transistors lowers the current to the base of T15, causing the emitter-collector voltage to increase, thus causing an increase in the base current of the driver transistor T16. Current through T16 rises and thus increases the base current to the "current valve" transistors T17, T18, and T19. The impedance of these power transistors drops, allowing more current to pass from the 24 volt power supply to the control windings of the saturable reactor. The reactor, in turn, supplies more current to the rectifier bridge, more current flows through the pass transistors and the voltage drop across them is restored to the desired level. Three power transistors are used to control the current supplied by the 24 volt power supply, since they must be able to dissipate all the power provided by this supply, about 80 watts. Normally just one power transistor could provide this control alone, as a 2N278 can dissipate about 86 watts. However, the 24 volt supply has very large turn-on transient, thus three transistors are necessary for safety.

#### (c) The Fine Regulator Loop

The fine regulator loop serves to establish the desired magnetic field in the focusing coils and to maintain

it at a predetermined, fixed value. The error signal for this loop is derived directly from the focusing field of the spectrometer. In principle, the fine regulator works as follows: Two separate alternating current signals are developed by two rotating search coils mounted on a common shaft and rotated at the rate of 23 revolutions per second. (This system is described in detail in section 5.3.) One of these coils is located near the electron orbit radius in the spectrometer, and its output is therefore directly proportional to the spectrometer field. The other search coil is rotated in the field of a permanent magnet and thus produces a constant amplitude reference signal. The orientation of the search coil axes is such that the two signals are  $180^\circ$  out of phase. In practice, a known fraction of the reference signal, chosen by the Dekavider, a linear Kelvin Varley voltage divider,\* is matched against the spectrometer coil signal. The difference is filtered and amplified and serves as the error signal. The error signal is then demodulated synchronously with respect to the reference signal. The demodulator output has positive or negative polarity, depending on whether the spectrometer field is higher or lower than the desired value. The output signal is filtered and fed into the transistor D.C. amplifier of the regulator.

---

\*Electro-Measurements, Inc., Portland, Oregon. Model RV-622. Linearity  $\pm 0.001\%$  at 0.5 watt or less, resolution 0.0001%. Input resistance 10,000 ohms.

The raw error signal emerging from the Dekavider contains a great deal of noise and harmonics. While the desired 23 cycle per second sinusoidal signal is small, of the order of microvolts, the undesirable noise may have amplitude equal to an appreciable fraction of a volt. Aside from amplification, the signal must therefore be extensively filtered.

The most obvious and straightforward method of accomplishing this is by use of tuned amplifiers. High gain and very narrow frequency response are relatively easy to achieve. These could not be used, however, for two reasons: First, the rotating shaft does not hold its speed perfectly constant. Small shifts in the flipcoil frequency, when passed through twin-tee or L-C filters, may result in large phase angle changes. The phase detector perceives these changes as bona fide changes in the error signal, causing variations in the focusing field. The second reason is related to the speed of response of these amplifiers. Any amplifier is degraded in stability by introduction of positive feedback. High gain band-pass amplifiers are no exceptions. Their response to a step change in the amplitude of the pass frequency signal is slow and frequently transients will induce ringing. The spectrometer regulator requires that the response speed of the fine loop be faster than the coarse loop, otherwise instability will occur. The rough regulator will cause the power supply to overshoot the balance point before the fine regulator loop can stop



the current from changing.

All the tuned amplifiers that had sufficient gain for our purposes were far too slow. All feedback type filtering had to be abandoned. Instead, we used series filters, in a more or less brute force approach. The efficiency of this method is much lower, as all filtering elements introduce losses into the circuit which have to be compensated by an increased number of amplifying stages. Nevertheless, this system has better stability and higher response speed to amplitude changes in the error signal.

Figure 27 shows the details of the fine regulator loop. After mixing at the Dekavider, the raw error signal is fed to a General Radio transistor preamplifier,\* operated on the "flat" frequency response setting. Output of this amplifier is bridged with a 4 mfd capacitor that shunts the high frequency noise, and then is fed to a voltage amplifier.\*\* A power amplification stage with tuned transformer coupling brings the error signal to the phase sensitive detector. The phase detector, or demodulator has proved to be a critical part of the feedback loop. Initially a design developed at Vanderbilt by Nall<sup>34</sup> was used. In this circuit, the reference signal was passed through a cathode follower for isolation, and then amplified by two parallel 6L6 push pull stages, with transformer input and output.

---

\*General Radio Tuned Amplifier and Null Detector, Type 1232-A.

\*\*General Radio Unit Amplifier Type 1206-B.

Figure 27. Schematic diagram of the error signal amplifiers and the phase sensitive detector.

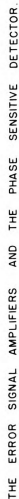
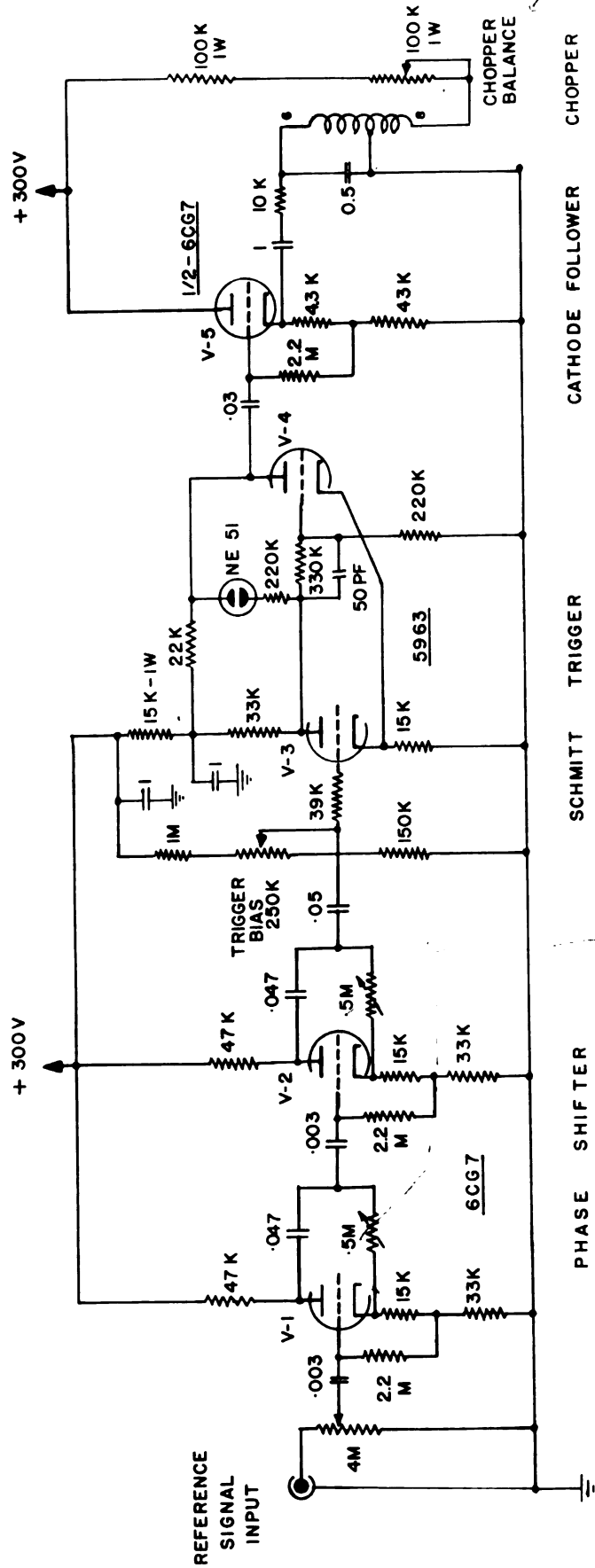


**Figure 27**

Output of the power stages provided, in principle but not in practice, a sinusoidal plate voltage for a pair of demodulator triodes. The error signal was introduced to the grids of the phase detector tubes also by transformer coupling. The difficulties with this unit were, on one hand, an apparent degradation of the transformers with time, due to unknown causes, and on the other hand, very poor fidelity at the 23 cps frequency, leading to grossly distorted waveforms. Drifts were observed in the demodulator stage which tended to change the bias level required by the regulator's transistor preamplifier. Rebalancing the demodulator would produce a change in the magnetic field of the spectrometer. This unit was therefore abandoned in favor of one free of these objections. The new phase detector unit which is presently in operation, uses a mercury wetted contact relay as a synchronous chopper. A chopper operates as a nearly ideal rectifier; its forward resistance is very low, its back resistance essentially infinite. The contact resistance of the relay contacts is of the order of 50 milliohms and stays constant to within 5 milliohms. Dissipative losses are therefore almost eliminated. Furthermore, during the conduction half cycle when the relay contacts are closed, the chopper does not introduce any waveform distortion into the error signal. Figure 28 shows the circuit diagram of the chopper and its driving circuit. The reference signal first goes through a phase shifter. Two triode phase mixing stages are used, V1 and V2, giving a total phase shift

Figure 28. Schematic diagram of the chopper driving circuit.



23 CPS CHOPPER DRIVE.

Figure 28

of about  $270^\circ$ . After the phase shifters, the signal goes to a Schmitt trigger, where the sinusoidal reference signal is converted to a square wave (V3 and V4). A neon lamp is included for visual check of trigger operation. Square driving voltage is needed for proper operation of the chopper, insuring prompt closure of the contacts. For maximum output, the chopper must be synchronized with the zeros of the error signal sine wave. With a sine wave drive a normal mercury wetted contact relay will not pull in at a precisely constant phase angle, causing a jitter in the output waveform.

The output of the Schmitt trigger is power amplified by a cathode follower V5 and fed through a suitable network to the coil of the chopper. The chopper has a two section coil; a d-c current, passed through one section of this coil, can be used to bias a magnetized core of the relay armature and hence to change the dwell time of the two switching positions. The 100K variable resistor is used to vary this d-c bias current and hence the chopper balance. The d-c signal developed by the demodulator is an average of a full wave rectified 23 cps signal and hence is basically a 46 cps signal. Virtually all of the 46 cps component is removed right after the demodulator by a twin tee network tuned to this frequency. The remaining ripple is further minimized by a 3000 mfd capacitor placed across the input terminals of the transistor preamplifier that serves as the fine regulator input.

(d) The A.C. Feedback Loops

Although the fine regulator loop has a very high gain, of the order of  $10^7$ , it has a rather poor frequency response. In fact, due to the long time constant of the filters situated after the demodulator, the response of the loop is poor for any signal with a period appreciably shorter than 0.25 seconds. Such conditions render the regulator incapable of removing noise and ripple from the system and almost always lead to instability. Moreover, in a two loop servo-system such as this one, slow response in the fine loop combined with relatively fast response of the rough regulator causes overshoot of the error signal balance point. If the response mismatch is bad, we will get low frequency, large amplitude oscillation. As the time constants of the loops are brought together the oscillations will diminish in amplitude and may increase in frequency by a factor of two or so. Finally, with the fine loop faster than the coarse one, we can get stable operation.

To aid in stabilizing the regulator and to restore its frequency response, two parallel a-c feedback loops were added. As can be seen from Figure 26, these bypass the fine regulator entirely. They derive their signal from the positive terminal of the power supply and provide high a-c degenerative feedback for the system.

The choice of component values for these feedback loops proved to be rather critical. Considerable length



of time was spent in the effort of securing stability against transients over the entire current range of the power supply. To match the time constants, 4000 and 2000 mfd capacitors were needed, connecting the positive end of the supply output to the input of the preamplifier through a 500 ohm rheostat. In parallel with this loop is another, consisting of two 10 mfd oil filled capacitors in series, also connected to the positive terminal of the power supply and entering the preamplifier through a 50 K variable resistor. This loop is chiefly responsible for high frequency noise feedback. This combination gives a nearly critically damped response to the power supply.

#### (e) Fine Regulator Construction Notes

The regulator is constructed in two basic parts: the power handling section and the preamplifier. The main power transistor section with its drivers, and the power transistors belonging to the rough regulator are placed on copper fins suspended in a bath of transformer oil. A 1/4 inch copper tube circulates tap water in the oil tank to remove excess heat developed by the power section. Current equalizing resistors are soldered directly to the emitters of the power transistors and connected to a common bus bar, also immersed in the oil bath. Although each of the power transistors can carry a collector current of 14 amperes, it is only required to pass 6 amperes or less. This gives a better than 100 per cent safety overload factor and, in addition, operates the transistors in a region

where their gain is higher. (The 2N278 beta begins to fall off at high currents.) The preamplifiers for the main supply and for the rough regulator are built on separate terminal boards and connected to the front of the oil tank by a multiterminal Amphenol connector. The preamplifier section is detachable for ease of servicing.

#### (f) Regulator Operation

The regulator works as follows: when the spectrometer field is smaller than required, the net error signal is in phase with the reference signal, and the output of the demodulator swings negative. Current flows through the filter described above and then through the 1000 ohm input resistor of the transistor preamplifier and then to the base of T1 (refer to Figure 26). This turns T1 to a more conducting state. The collector current of T1 increases, decreasing the base current of T2. This action decreases the collector current of T2 and causes the base of T3 to go more negative with respect to the emitter of T3. This change of potential in T3, the first driver, causes an increased current to flow between the collector and the emitter of T3. This current is amplified in T4, the main driver transistor. T4 causes higher base current to flow to the bases of the pass transistors T5 through T14. This biases the power transistors to a more conducting state and consequently the voltage across the transistors drops.

The rough regulator senses the voltage drop across the power transistors as being insufficient, and in a manner

already described above, begins to turn on the 24 volt power supply and hence the control current through the saturable reactor. The saturable reactor begins to drive upward increasing the a-c input to the rectifiers, and increasing the current output of the power supply. As the balance point is approached, less current flows to T1, more current flows in T2, the driver bias decreases, causing a decrease of base current in the pass transistors. The voltage across the power transistors increases causing the rough regulator to slow down and stop its power increase. The desired value of field in the spectrometer is thus reached. Any further increase of the current will cause an opposite shift in the error signal, which in turn would demand a decrease in the current. Thus the error signal tends to monitor the current.

Frequently, during large downward changes of current, the error signal amplifier circuits overload and cut off the preamplifier. In such instances the voltage across the power transistors will tend to rise (the transistors are biased to cut off) and the power dissipation of the transistors may be exceeded. To prevent this, a Zener diode is connected from collector to base of T3, which will conduct whenever the voltage across the transistors exceeds 6-8 volts. The diode acts as a base to collector clamp. As soon as the signal to the preamplifier reaches a lower level, i.e., when proper operating information is restored and the voltage across the pass transistors drops, the diode stops conducting and the regulator functions normally.

The regulator is connected to building ground at the emitters of the power transistors. This means that the cable leading from the power supply to the spectrometer is floating above ground by the amount of voltage drop in the auxiliary shunts. Likewise, it should be noted that the "common" of the preamplifier floats approximately three volts above ground and therefore the output of the demodulator must likewise be floated.

The regulator is interlocked to the water flow for oil tank cooling and to the switches that control the rotation of the shaft, the B+ supplies and the 24 volt supply of the rough regulator. Failure of any of these will cause an immediate shutdown.

### 5.3 The Rotating Coil System

#### (a) Introduction

The heart of the fine regulation feedback loop is the rotating coil system. This system is comprised of the field sensing coils, the rotating shaft and its drive, the permanent magnet which provides a reference magnetic field, and, finally, the temperature control of the magnet and the rotating coils. At first a modified copy of the Vanderbilt rotating shaft system was built, similar to the one described by Nall.<sup>34</sup> This shaft was still in place when the first overall spectrometer photograph was taken. It can be seen in Figure 5. A number of difficulties finally led to a complete redesign of virtually all of the elements

of the system. First, the Vanderbilt system used a Vee belt drive which proved to be too rough for us, and had to be replaced with a flat endless nylon belt. Second, perhaps due to bad luck in obtaining material for the shaft, our shaft suffered from excessive vibration. The six foot long shaft sections had to be shortened and two extra bearings added. One of these had to be made non-magnetic as it was located too near the spectrometer. This bearing never was completely satisfactory. Third, the spectrometer coil was originally held between two porous bronze, self aligning sleeve bearings which could not hold it in a fixed position with respect to the spectrometer. A simple calculation shows that a radial motion of the spectrometer coil of 0.0025 inches will shift the spectrometer field by one part in  $10^4$ , i.e., ten times the allowable amount. At one point we did manage to find a pair of stainless steel ball bearings and replaced the bronze sleeves by these bearings. Although the quality of the bearings was low, the performance of the shaft improved somewhat. Finally, detailed examination of the system found the shaft torsionally so flexible as to show an appreciable deflection when the lubrication properties of the bearing changed (as would happen, for example, with a temperature change). This made it impossible to hold a fixed phase relationship between the two rotating coils and made the entire system nearly useless. Thus after several months of tests and modifications, in an attempt to save the time and funds invested, this shaft

had to be abandoned and the design of a new shaft was undertaken by the author. Its design and construction features are found below.

#### (b) The Field Sensing Coils

Quite frequently, when one is dealing with nonuniform magnetic fields, the objection leveled against the use of a rotating coil as field measuring device is that it measures the average field over the area of the coil, and its output is therefore rather rich in harmonics. Special coils have been developed, however, that yield an output signal corresponding to the value of the magnetic field at the geometric center of the coil. Such are, for example, the "fluxballs."<sup>36,37</sup> The fluxball is a spherically wound coil with a variable density winding. It is rather difficult to make. A similar behavior in a nonuniform magnetic field can be obtained by using a cylindrical coil of carefully chosen dimensions.<sup>38</sup> If the length to diameter ratio  $L/D$  is equal to 0.72, the coil will behave very nearly as a fluxball. The inner diameter does not affect the performance appreciably as long as it is less than half of the outer diameter, a condition which is easily satisfied. This type of coil is used with the spectrometer.

As was mentioned above, the error signal is generated by matching a known fraction of a signal developed by a coil in a permanent magnet field to the signal developed by a second coil in the spectrometer field. This requires a choice of design parameters, namely, the dimensions of

the coils, the optimum wire size and its resistance and the value of the permanent magnet field strength. The following calculations show how these parameters may be determined: Considering a general case, the E.M.F. generated by a search coil is:

$$\mathcal{E}_{\max} = \omega \bar{\Phi}_{\max} \quad \text{where} \quad (84)$$

$\omega$  = angular frequency of the coil

$\bar{\Phi}_{\max}$  = maximum flux linked by the coil.

Considering the coil to be built up of cylindrical windings of radius  $\rho$ , having  $n$  turns each, then for each layer:

$$\bar{\Phi}'_{\max} = \pi \rho^2 n B \quad ; \quad n = \frac{L}{d} \quad (85)$$

where  $B$  is the strength of the magnetic field,  $L$  is the length of the coil layer and  $d$  is the diameter of the wire and insulation.

For a coil of inner radius  $R_0$  and outer radius  $R$ , the number of layers will be

$$N_L = \frac{R - R_0}{d + t} \quad (86)$$

where  $t$  is the thickness of the insulation between successive layers. The number of turns on the coil is

$$N_t = n N_L = \frac{L (R - R_0)}{d (d + t)} \quad (87)$$

To calculate  $\bar{\Phi}_{\max} = \sum_k \bar{\Phi}'_{k \max}$  consider the radius of the  $k^{\text{th}}$  layer:

$$\rho_k = R_0 + (2k-1)r + (k-1)t, \quad r = \frac{d}{2}$$

$$\Phi_{\max} = \sum_{k=1}^{k=\frac{R-R_0}{d+t}} \pi \rho_k^2 \frac{L}{2r} B \Delta k, \quad (\Delta k = 1) \quad (88)$$

By use of (88)

$$\begin{aligned} \Phi_{\max} &= \frac{\pi L B}{2r} \sum_{k=1}^{k=\frac{R-R_0}{d+t}} \left[ R_0 + (2k-1)r + (k-1)t \right]^2 \Delta k \\ &\simeq \frac{\pi L B}{2r} \int_{k=\frac{1}{2}}^{k=\frac{R-R_0}{d+t} - \frac{1}{2}} \left[ k(2r+t) + (R_0 - r - t) \right]^2 dk \end{aligned} \quad (89)$$

Call  $2r + t = T$  and note that  $T$  is small.

$$\begin{aligned} \Phi_{\max} \simeq \frac{\pi L B}{2r} \left[ \frac{(R-R_0)^3}{3T} + \frac{R^2 R_0 - R R_0^2}{T} + R R_0 - R^2 + R_0^2 + \right. \\ \left. + \frac{RT}{4} - \frac{R_0 T}{4} - \frac{T}{12} \right] \end{aligned}$$

Since  $(R_0 - r - t) \approx R_0$ .

Only the first two terms are significant, since  $T$  is a small number.

$$\begin{aligned} \Phi_{\max} &\simeq \frac{\pi L B}{2r} \left( \frac{R^3}{3T} - \frac{R_0^3}{3T} \right) \\ &\simeq \frac{\pi L B}{3d(d+t)} (R^3 - R_0^3). \end{aligned} \quad (90)$$

The E.M.F. generated by this coil is

$$\mathcal{E}_{\max} = \frac{\pi L B \omega}{3d(d+t)} (R^3 - R_0^3) \quad (91)$$



The length of wire contained in this coil is

$$L_w = \sum_{K=1}^{K=\frac{R-R_0}{2r+t}} l_K \Delta K \quad \text{where} \quad (92)$$

$l_K = 2\pi \rho_K \frac{L}{2r}$  is the length of wire in each layer.

With the help of (88),

$$\begin{aligned} L_w &= \frac{\pi L}{r} \sum_{K=1}^{K=\frac{R-R_0}{2r+t}} (R_0 + [2K-1]r + [K-1]t) \Delta K \\ &\approx \frac{\pi L}{r} \int_{K=\frac{1}{2}}^{K=\frac{R-R_0}{2r+t} - \frac{1}{2}} [K(2r+t) + (R_0 - r - t)] dK \quad (93) \end{aligned}$$

Keeping only the dominant terms we have

$$L_w \approx \frac{\pi L}{d(d+t)} (R^2 - R_0^2) \quad (94)$$

If the radius of the bare wire is  $r'$  and the resistivity of the wire is  $\rho'$ , the resistance of the coil is

$$R_c = \rho' \frac{L_w}{A_w} = \frac{\rho' L}{r'^2 d(d+t)} (R^2 - R_0^2) \quad (95)$$

In our coils  $t = 0$ , and  $L = 1.44R$ ,  $R_0 = R/4$ .

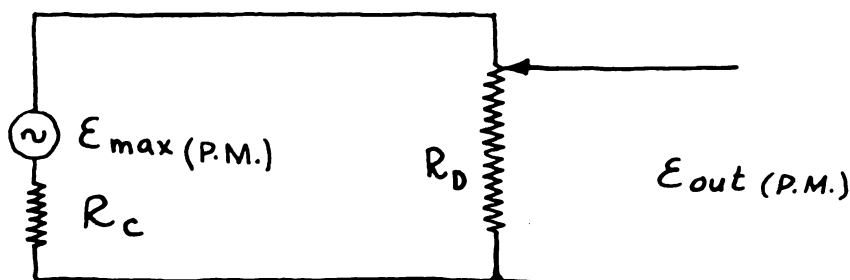
Summarizing we have:

$$\mathcal{E}_{max} \approx 1.484 \frac{R^4}{d^2} B \omega \quad (96)$$

$$L_w \approx 4.241 \frac{R^3}{d^2} \quad (97)$$

$$R_c \approx 1.350 \frac{R^3}{r'^2 d^2} \rho' \quad (98)$$

So far the calculations refer to a general case. In particular, considering the spectrometer feedback loop, it should be remembered that the permanent magnet coil is connected across a 10,000 ohm load, the precision voltage divider. Therefore it draws current and its resistance must be included in calculating the net output voltage available out of the divider. The spectrometer coil, on the other hand, does not draw any current at the balance point, and its resistance is therefore immaterial. Consider the diagram:



$R_c$  stands for the resistance of the coil and  $R_D$  is the resistance of the voltage divider.

$$E_{out(P.M.)} = \frac{R_D}{R_c + R_D} E_{max(P.M.)}$$

$E_{out(P.M.)}$  should be equal to the E.M.F. of the spectrometer coil, when the spectrometer is operating at maximum current, thus

$$E_{max(SP.)} = E_{out(P.M.)}$$

$$1.484 \frac{R_{sp}^4}{d_{sp}^2} B_{sp} \omega = \frac{R_D}{R_D + 1.35 \frac{R_{P.M.}^3}{r'^2 d_{P.M.}^2}} \left[ 1.484 \frac{R_{P.M.}^4}{d_{P.M.}^2} B_{P.M.} \omega \right]$$

It is also possible to maximize  $E_{out}$ , with respect to  $R$  to obtain the best coil diameter. This calculation leads to the equation:

$$\frac{d E_{out(P.M.)}}{d R} = 0 \quad ; \quad R = 2.56 \times 10^3 (r'd)^{2/3} \quad (99)$$

Numerical calculations show that this maximized type of coil can be realized only with some difficulty. For the available magnet gap of 2 1/4 inches, allowing for the housing which must hold the coil in place, the maximum possible  $R$  is about 1.4 cm. The optimum wire size for this coil would be number 44 which is rather difficult to handle. Also, the coil resistance would then be about 40 K ohms and the coil would therefore be very heavily loaded by the voltage divider. Internal heating of the coil may be appreciable in this case, for several milliamperes would be drawn from it. Any changes in resistance would produce errors in the size of the standard signal. Furthermore, the signal change arising from area and resistance changes due to temperature is more pronounced as the coil resistance is increased, thus requiring a closer control of the temperature of the wire in the coil.

For ease of manufacture and the reasons mentioned above, a compromise solution was used. The wire was chosen to be number 40 for both coils, one coil being slightly larger than the other. The spectrometer coil, as it operates in a nonuniform field was made with  $L = 1.44 R$  as closely as possible. The permanent magnet coil was

dimensionally similar to the spectrometer coil, except for having a larger number of turns. The L/R ratio does not have to be adhered to too closely here, for the field of the permanent magnet is relatively uniform.

The following values were used:

$$\rho' = 1.72 \times 10^{-6} \text{ ohm}\cdot\text{cm},$$

$$r' = 5.05 \times 10^{-3} \text{ cm},$$

$$d = 11.2 \times 10^{-3} \text{ cm},$$

$$\text{Max. Spectrometer field} = 260 \text{ oersteds} = 260 \times 10^{-8} \text{ webers/cm}^2.$$

$$\text{Permanent Magnet field} = 360 \text{ oersteds} = 360 \times 10^{-8} \text{ webers/cm}^2.$$

(This was the field of the permanent magnet when it was delivered to us.)

$$\omega = 145 \text{ rad./sec.}$$

$$R_D = 10,000 \text{ ohms}$$

$$R_s = 1.4 \text{ cm.}$$

The calculated radius of the permanent magnet coil is  $R_p = 1.45 \text{ cm.}$

The coils were wound by Abrams Instrument Co. of Lansing. During the winding it was not possible to keep perfectly even layers with such small wire. Thus for the calculated lengths of wire, 5600 feet and 6550 feet for the spectrometer and permanent magnet coils respectively, the radii came out to be nearer 1.5 cm. As field measurements at a point were not an absolute necessity, the coils were allowed to pass. The resistances of the coils are 6870 ohms for the permanent magnet coil and 5900 ohms for the spectrometer coil. The voltage developed by the

spectrometer coil is  $E_{\max \text{ sp}} \approx 31$  volts and that developed across the divider by the permanent magnet coil is  $E_{\text{out P.M.}} \approx 32.5$  volts. The coils thus nearly satisfy the  $E_{\text{out P.M.}} = E_{\max \text{ Sp.}}$  requirement for maximum setting of the spectrometer current.

### (c) The Rotating Shaft System

#### (i) The rotating shaft, its drive and supports

After the rather unfortunate experience with the rotating shaft made of aluminum tubing, a solid, carefully machined one was designed and built, using precision ball bearings wherever possible to insure smoothness. The shaft is built in two sections each six feet long, and is carried by three main bearing supports, one self aligning ball bearing at the permanent magnet end, two ball bearings straddling the drive pulley which is located at the center, and a double beryllium copper ball bearing located at the spectrometer end.

The two shaft sections are made of Alcoa 7075 aluminum alloy in the T 651 temper.\* This means that the original bar stock pieces received heat treatment, and were subsequently straightened and stress relieved. This is an important consideration, when a considerable amount of machining is to be done. This alloy is a special high tensile strength aluminum alloy, having an ultimate strength of 77,000 psi, the highest obtainable. It is quite free

---

\*Aluminum Company of America, Pittsburgh 19, Pennsylvania.

machining, and takes an excellent finish.

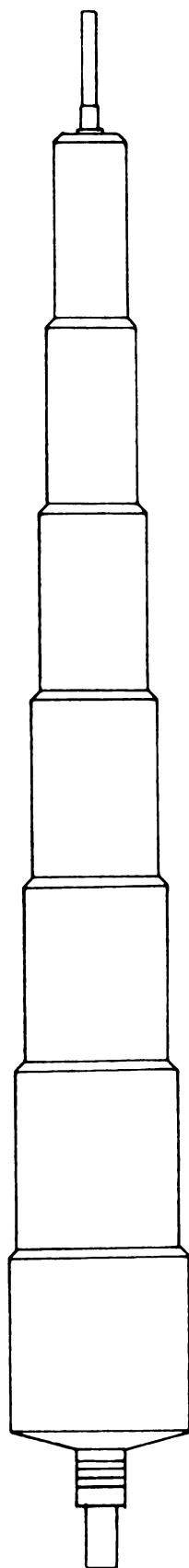
During the original design period, cast shaft sections were considered, since it was reasoned that they would provide good rigidity to shear; however, none of the local foundries were able to cast a blow-hole free specimen and so the idea was abandoned.

After some concessions to the limitations of the physics department's machine shop facilities, the shaft sections were designed in tapered form, using a stepped taper. Each section consists of 18 straight sections of successively smaller diameters, as shown in Figure 29. The reason for tapering the sections is to remove weight at the ends near the search coils, especially at the spectrometer end where limited load bearing capacity bearings have to be used, and to prevent uniform-shaft transverse vibrations as much as possible. Analytically the shaft sections were treated as smooth tapers.

As the search coils must be kept in a fixed angular position with respect to each other within a few seconds of arc, it is of some interest to find the torsional deflection of the shaft as a function of torque. For a uniform cross-section shaft we can write

$$\theta = \frac{\theta_n L}{R}$$

where  $\theta$  is the torsional deflection of the shaft in radians,  $\theta_n$  is the specific torsional deflection,  $R$  is the shaft radius in inches and  $L$  is the shaft length in inches.  $\theta_n$  is defined as follows:



( NOT TO SCALE - SCHEMATIC ONLY )

FIGURE 29. SECTION OF THE ROTATING SHAFT.

$$\theta_n = \frac{TR}{GJ} \quad (100)$$

where  $T$  is the torque in lb-in,  $J$  is the polar moment of inertia, an engineering term defined as  $J = \frac{\pi}{2} R^4$  for a circular cross section,\* and  $G$  is the shear modulus of the material. Thus

$$\theta = \frac{TL}{GJ} \quad (101)$$

Between two cross sections of a shaft a distance  $dx$  apart, the angle of twist  $d\theta$  is:

$$d\theta = \frac{T}{GJ} dx \quad , \text{ so between ends A and B,}$$

$$\theta_{AB} = \int_A^B \frac{T}{GJ} dx \quad (102)$$

This expression may be used to calculate  $\theta$  for shaft of variable radius.  $R$  is implicit in  $J$  since  $J = \frac{\pi}{2} R^4$  for circular cross section. Thus for a tapered shaft as shown in Figure 30:

$$R_x = R_o + x \tan \alpha \quad (103)$$

$$\tan \alpha = \frac{R_L - R_o}{L} \quad (104)$$

$$\theta = \frac{T}{G} \int_0^L \frac{dx}{J} = \frac{2T}{\pi G} \int_0^L \frac{dx}{R^4} \quad (105)$$

---

\* $J$  is the moment of inertia per unit mass, multiplied by the cross sectional area of the cylinder.



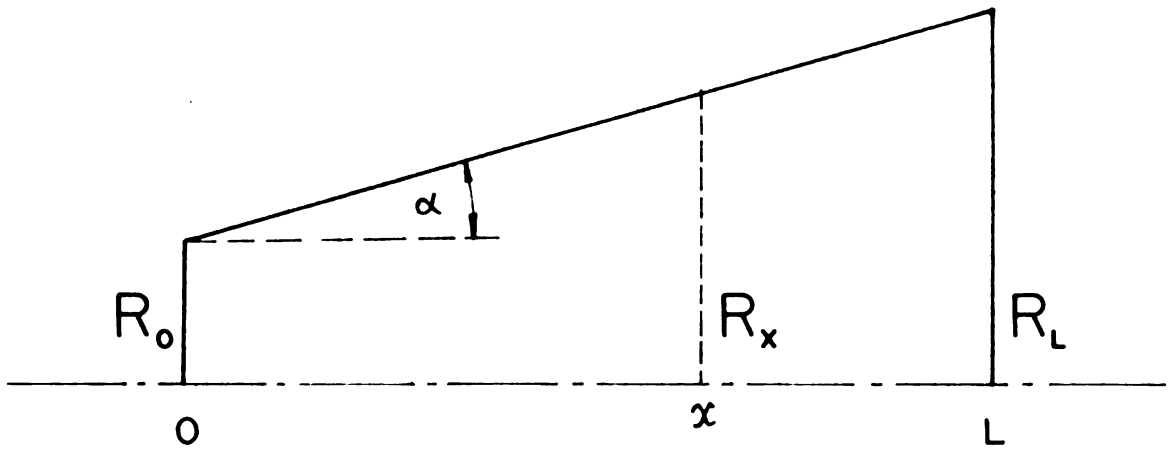


FIGURE 30. SCHEMATIC DIAGRAM OF A SHAFT SECTION.

$$\theta = \frac{2T}{\pi G} \int_0^L \frac{dx}{(R_o + x \tan \alpha)^4}$$

$$= \frac{2}{3} \frac{TL}{\pi G (R_L - R_o)} \left[ \frac{1}{R_o^3} - \frac{1}{R_L^3} \right] \quad (106)$$

For our case

$$G \approx 3.5 \times 10^6 \text{ lbs/in}^2$$

$$L = 72 \text{ in}$$

$$R_o = 0.875 \text{ in}$$

$$R_L = 1.938 \text{ in}$$

$$\theta \cong 5.6 \times 10^{-6} T \text{ radians}$$

$$= 1.15 T \text{ seconds of arc} \quad (107)$$

T is the numerical value of torque in units of lb-in. This is the torsional deflection of each half of shaft. Each half is driven by a three inch section of one inch diameter tool steel shaft whose torsion adds to that of the shaft and is:

$$\theta = \frac{2TL}{\pi G R^4} = 2.54 \times 10^{-6} T \text{ radians} \quad (108)$$

$$\theta \approx 0.525 T \text{ seconds of arc.}$$

The total torsional deflection is

$$\theta \approx 1.675 T \text{ seconds of arc.} \quad (109)$$

This is about two times smaller than the allowable design limit. Furthermore, as the shaft is driven from the center,

torsional deflections should have the same sense and hence will subtract. The only possible net deflection would result from different rolling properties of the two end bearings.

Aside from torsional deflections we are also interested in estimating the so-called critical speeds of the shaft. These are speeds of rotation at which resonances occur. For smooth operation it is desirable that the first critical speed (fundamental frequency of transverse vibrations) be at least twice the operational speed of 23 rps. Treating the shaft as a uniform solid shaft three inches in diameter with rigidly supported bearings, the first critical speed is given by<sup>39</sup>

$$\omega_1 = \left( \frac{\pi}{L} \right)^2 \left( \frac{g E I}{A \rho} \right)^{1/2} \quad (110)$$

where  $L$  = distance between bearings (in inches)

$g$  = gravitational acceleration (in./sec<sup>2</sup>)

$E$  = elastic modulus (p.s.i.)

$I$  = moment of inertia (area), (in.<sup>4</sup>) ( $I = \int r^2 dA$ )

$A$  = cross sectional area (in.<sup>2</sup>)

$\rho$  = density (lb/in<sup>3</sup>)

Numerically

$$\omega_1 \approx 292 \text{ radians/sec}$$

$$\text{or } f_1 \approx 46.5 \text{ cps.}$$

For the actual shaft, the stiffness to mass ratio is higher due to the taper and consequently its first critical speed is also higher. The fundamental frequency of transverse

vibrations for a finished shaft section supported by its ends is near 60 cps which is amply higher than the operational frequency.

(ii) The rotating shaft construction notes

The shaft sections were made as follows: First, the rod stock was located between centers on a large lathe and the shape of the shaft was roughed out to within 1/8 of an inch of the desired diameter. A follow-rest and adequate cooling were used to prevent chattering and distortions. Very light cuts were then taken to reach the desired dimensions, with careful measurements taken frequently to check concentricity. This procedure yielded finished shaft sections that run true to within 0.002 inches along their entire length. The ends of the shaft sections were counter-bored to receive small diameter shaft sections that form connections to the driving pulley and the search coils. These smaller shafts were shrink fitted into the prepared holes. At the search coil ends the inserts are made of bronze, to prevent magnetic field distortions. The driven ends have the inserts made of tool steel.

The search coils are held in position inside two inch diameter plastic holders, shown in Figure 31. Linen containing phenolic was used because of its machinability and superior retention of screw threads. Transverse holes were bored into the coil holders, forming a slip fit for the search coils. The coils are held in position by closing these transverse holes by machined end caps, secured

Figure 31. Cross-section of the spectrometer end of the rotating shaft.

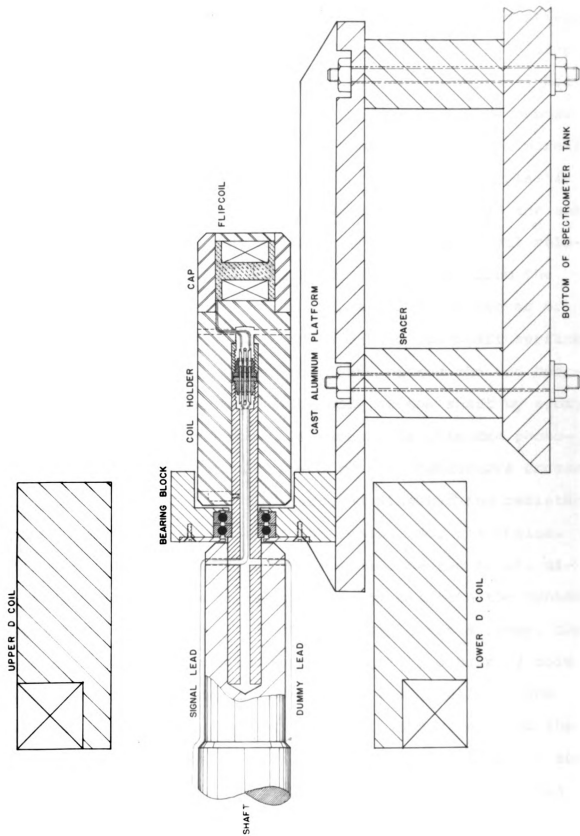


Figure 31

by nylon screws. The leads from the search coils are brought down to the axis of the holders and soldered to a multi-pin male connector, which is glued to the bottom of a 3" deep axially slotted hole; bored into the body of the coil holders. The holes are of slip fit dimensions for the bronze shaft inserts and are secured to them by tightening screws placed transverse to the slot, thus squeezing the plastic holder onto the shaft. A locating pin attached to the shaft ensures a proper angular attitude of the search coil relative to the shaft. The coil leads are brought from the connector at the tip of the shaft, through the center of the bronze shaft ends and then go out to the shaft surface through radial holes, after they have passed the end bearings. They are cemented to the body of the shaft by epoxy glue. The cable used for this purpose is shielded phonograph pickup cable which has two twisted conductors encased in a braid shield. Its low mass and diameter and resistance to pickup of 60 cps hum were the reasons for its choice. Each half of the shaft has two cables cemented to it, diametrically opposite to each other, to maintain the dynamic balance of the shaft. One of these cables is a dummy, the other carries the coil generated signal to a pair of coin silver slip rings located near the driving pulley. The slip rings are press fitted onto a plastic sleeve and the coil leads are soldered to their edges. The signal is then picked off by metallized carbon brushes.\* Three brushes

---

\*Graphite Metallizing Corp., 1050 Nepperhan Ave., Yonkers, N.Y.

per slip ring are used to minimize noise. Figure 32 shows the central pulley assembly, showing the brush holders and the drive.

The shaft is attached to the driving pulley through a flexible diaphragm joint which permits approximately 1/8 inch axial travel and is used to accommodate the thermal expansion of the shaft. The brass diaphragm of the flexible joint was taken from a discarded bellows steam pressure regulator. It is well suited for this purpose, for it is quite stiff to distortions in its plane, and yet its circular corrugations make it quite flexible for axial motion. Near the center, the diaphragm is silver soldered to a brass collar which in turn is firmly attached to the steel extension of the shaft by six steel set screws, that are seated into matching indentations in the shaft. The outer perimeter of the diaphragm is attached to a recessed brass plate by 12 screws. The plate is fixed onto the ends of the driving pulley, by steel pins and screws. The weight of the shaft does not actually rest on the flexible joint but is carried by lubricant impregnated nylon sleeve bearings fitted to the inside bore of the driving pulley. No rotation takes place at these bearings. They serve only to bear the weight of the shaft and to allow axial motions of the shaft.

The driving pulley is made of bronze. It is driven by five O rings that fit into grooves machined in it. O ring drive was chosen for its smoothness, for the tolerances



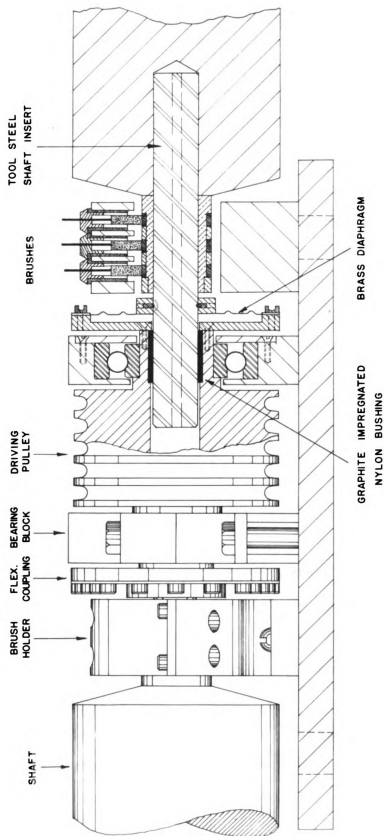


FIGURE 32. CROSS-SECTION OF THE CENTRAL DRIVING PULLEY.

on O rings are kept within narrow limits, they are uniform in composition and are seamless. The pulley is counterbored to accommodate the shaft ends and the nylon sleeve bearings, and has extensions on both sides of it that carry two precision ball bearings, and form the connection to the flexible joints.

The assembly consisting of the brush holders, pulley and its bearing blocks is mounted on a cast aluminum plate machined flat and attached to the uppermost part of a concrete pylon that is used as an inertia platform. The driving motor, a 1/3 HP electric induction motor, is located on the same pylon at a somewhat lower level and is mechanically insulated from it by mounts made of rubber stoppers. Figure 33 shows the overall view of the driving section of the shaft. The concrete pillar holding the drive is visible in Figure 5.

The spectrometer support for the shaft is a U shaped cross-section platform of cast aluminum, which is attached to the bottom flange of the spectrometer tank by four 3/8 inch rods and nuts threaded through two large aluminum blocks serving as spacers. This platform assembly is quite rigid. Figure 31 shows a section through the spectrometer end of the shaft. Supporting the shaft on this end are two beryllium copper ball bearings of 0.625 inches inner bore and 1.375 inches outer diameter. These bearings were located with great difficulty and at great expense in time, from Industrial Tectonics, Inc., Compton, California, as an

Figure 33. Photograph of the shaft drive.



Figure 33

overrun of a production run for a large contract. They cost \$40 apiece and their tolerances are somewhat open to discussion. Two have to be used with their inner races slightly preloaded by a thin brass shim ring 0.003 inches thick to remove all end play. This is necessary, for axial motion of the spectrometer search coil must be minimized at all costs, since due to the nonuniformity of the spectrometer field an axial motion of 0.0025 inches produces a magnetic field shift of  $1 : 10^4$ . Thus the maximum tolerable end play is only 0.00025 inches. Keeping the spectrometer search coil fixed has proved to be the major problem of this instrument, which in fact, has yet to be completely solved. It may be necessary to redesign this end of the shaft, or to place the entire shaft on an aluminum substructure, fixed at the spectrometer and free to move everywhere else.

(d) The Permanent Magnet Assembly

The permanent magnet assembly, located some fourteen feet from the center of the spectrometer and fixed to the top of a second concrete pylon, consists of the following main parts: the magnet and its shielding box, a mechanical arrangement for tilting the magnet about an axis which is coincident with the axis of the shaft, an insulated and thermostatted enclosure, and a platform for mounting the end bearing of the shaft.

The permanent magnet consists of a soft iron yoke, which was built from Vanderbilt designs by our machine shop,

and two Alnico V ring magnets supplied by the Indiana Steel Products Company in Valparaiso, Indiana. The entire assembly was magnetized and stabilized by this company. The temperature coefficient of the magnet is approximately  $-0.016\%/C^{\circ}$ . The pole pieces are 5 inches in diameter and the gap width is 2.25 inches. The magnet is enclosed completely in a shielding box to reduce the effects of the fringing field of the spectrometer. The shield is made of three layers of NETIC and CO-NETIC (trade names) shielding materials.\* A 2 1/4 inch hole was bored into the shielding box to admit the search coil. The magnet and its shield rest on a 1/2 inch aluminum plate to whose sides are attached two steel "skids," Figure 34. The bottom sides of the skids are machined to conform to a circle whose center lies on the axis of rotation of the shaft. Matching pieces, attached to a stationary base plate, fixed to the pylon, form the magnet support. The magnet can thus be tilted through an arc of about  $45^{\circ}$ . Teflon strips attached to the adjacent surfaces of the skids insure smooth operation. The angle of tilt is controlled by a screw and spring arrangement and can be controlled from the control desk by means of a slow speed reversible motor. The angular resolution is about  $10^{-5}$  radians. This arrangement is necessary to permit a fine phase adjustment of the two search coil signals, thus relaxing the accuracy

---

\*Manufactured by the Perfection Mica Company, Chicago, Illinois. This shielding material is insensitive to shock. It can be machined without loss of shielding properties.

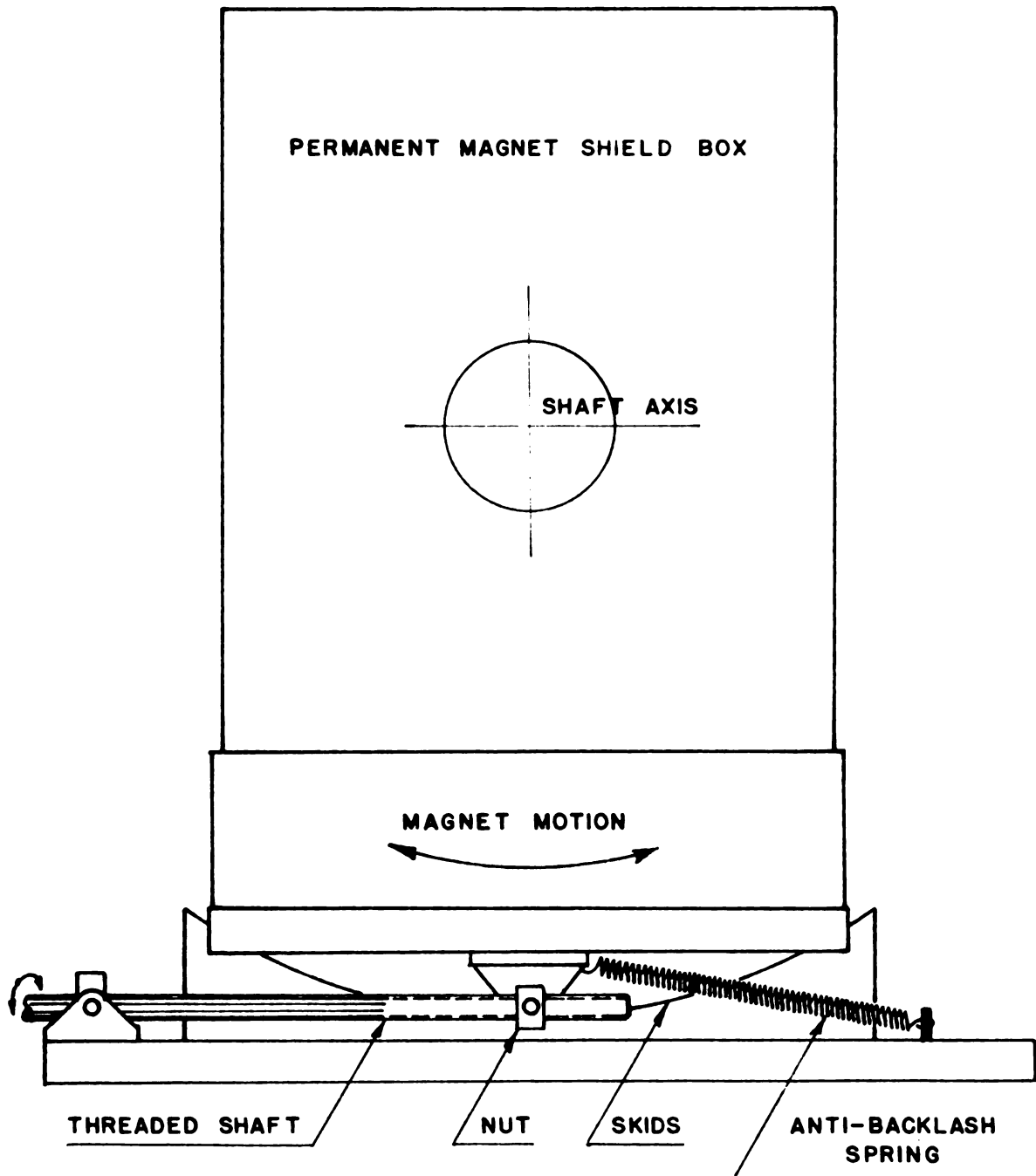


FIGURE 34. PERMANENT MAGNET ASSEMBLY.  
MECHANICAL PHASE CONTROL.

to which the coils have to be aligned on the shaft. Phase misadjustment of  $5 \times 10^{-5}$  radians is easily detectable. The rotating shaft is held in position at this end by a plate fixed to the pylon at a level slightly below the "equatorial" plane of the magnet. The plate is in the shape of a rectangular O, with an opening large enough to admit the magnet and to permit it to be tilted. A commercial self aligning ball bearing holds the shaft in position. The search coil is cantilevered into the gap of the magnet.

Since the permanent magnet search coil is loaded by the potential divider and therefore draws current, it is necessary to maintain the coil at a constant temperature to prevent drifts stemming from its resistance change with temperature. Such drifts would manifest themselves as slow changes in the calibration of the spectrometer. Similar drifts would also appear due to the temperature coefficient of the magnet itself. To hold the assembly at constant temperature the shield box is covered on the inside by a layer of felt, and on the outside by a half inch of styrofoam. The entire permanent magnet assembly is enclosed in a box about two feet on a side, made of plywood and styrofoam with an outer covering of felt. The air enclosed in the outer box is kept well mixed by a small fan, heated by two 100 watt light bulbs and held at a temperature of about  $40^{\circ} \text{C}$  by a thermistor control unit\* with an uncertainty of  $\pm 0.1^{\circ} \text{C}$ . It is reasonable to expect

---

\*Made by the Yellow Springs Instrument Co., Yellow Springs, Ohio.



therefore that in the magnet cavity itself the regulation would be as much as 10 times better.

Bäckström and co-workers<sup>40</sup> have shown recently that use can be made of a cancellation effect of the resistance and area temperature coefficients of the search coil by a proper choice of the coil and divider resistances. However, in our case this does not result in a practical design. The ratio of resistances of the divider  $R$  and the coil  $R_c$ ,  $R/R_c$  should be equal to 120 for the cancellation to take place. With a divider resistance of 10,000 ohms this leads to a coil resistance of 83 ohms. This would require a very large permanent magnet field for a reasonably high voltage output. Furthermore, the temperature coefficient of the magnet is not taken into consideration here, and in order to avoid errors from this source one would have to regulate the magnet temperature anyway.

After manufacture, the rotating shaft was aligned as follows: at first only the bearings were mounted in their respective positions, and machined plugs containing small axial holes were inserted in all bearings. A point source of light was mounted at one end and all bearing supports were aligned until maximum light intensity could be obtained at the other end. The two shaft halves were then inserted into the driving pulley and their ends placed in bearings, but left unfastened to the supports. A fine adjustment could now be made in the elevation of the three platforms by testing the freedom of axial motion at the

driving pulley as the shaft was slowly rotated by hand. Finally similar fine adjustments were made in the horizontal plane and the bearing blocks were fastened down.

In actual running, the shaft has shown to be quite vibration free and phase stable. In fact, some of the residual phase shifts that are still observed can be attributed to the thermal stress distortions of the floor of the room.

#### 5.4 The Performance of the Current Control System

The current to the spectrometer can be regulated in two ranges, the low range, which regulates from approximately 300 ma to 10 amperes, and an overlapping high range, extending from 5 amperes to the maximum of about 60 amperes. The range of the focusing field of the spectrometer is thus 1.5 to 270 gauss. The large negative a-c feedback necessitated by the inherent low response speed of the fine regulator feedback loop makes the supply rather slow to large current changes. The present rate of change is about 5 amperes per minute. The response speed, however, accelerates when only small changes of current are demanded. Thus a one per cent change introduced into the potential divider is accomplished in 3-4 seconds. The supply can be speeded up only at the expense of underdamped operation. This is highly undesirable, since any transient entering the supply from the mains will produce a wobble in the magnetic field of the spectrometer, causing line broadening. Field stability measurements made over long periods of time by counting with the spectrometer on the upper sideband of the

$\text{Ba}^{137}\text{K}$  conversion line, using a resolution of about 0.1% (full width at half maximum) show that when the environment is completely stable the magnetic field can be held to about 2 parts in  $10^6$  over a period of a few hours. Considerably larger variations, however, do occur due to the interaction of the spectrometer and its environment. Extensive study of these variations was made, over a period of more than two years, resulting in a number of modifications designed to reduce these interactions. One of the early chief contributors to long range drifts was an insufficiently precise control of the temperature inside the permanent magnet cavity. Replacement of the original bimetallic thermostat by a thermistor controlled unit improved the operation by almost an order of magnitude. Nevertheless, drifts of 2-3 parts in  $10^4$ , having an approximate periodicity of 24 hours, remained pointing most clearly to daily temperature variations in the machine room. Tests have shown that a slow temperature change of a few degrees had more effect than fast change of higher amplitude. The drifts were especially noticeable at times when the building heating and ventilating system was in operation. During the cooler parts of the year, the heat would be turned off at approximately midnight and would come back on about 6 a.m. The field drift would change direction at about these times. We could show experimentally that the spectrometer was quite sensitive to air circulation. Fans directed at various sections of the machine showed that the thermal expansion of the

spectrometer vacuum tank relative to the focusing coils was at least partly responsible for the drifts. Closing off all air supply vents in the machine room resulted in somewhat smaller drifts with much improved smoothness. Furthermore, there were indications that uniform outdoor temperature would bring about improved operation of the machine. Slight improvement was secured by covering of the two large windows in the machine room with three inch layer of styrofoam, and the insulation of parts of the spectrometer. Nevertheless, the 24 hour period variations were still in evidence, even after the installation of an air conditioning system to control the long range temperature drifts in the room. Further investigations, carried out by Mr. R. Krisciokaitis, have shown that the influence of the building heating system was of greater importance than we at first realized. The space under the floor of the spectrometer room serves as a plenum. Changes of temperature there and even just the presence or absence of air flow would affect the stability of the spectrometer. The plenum space was therefore blocked off.

Subsequent stability runs showed that these measures have reduced the drifts to about  $\pm 5$  parts in  $10^5$ . The remaining drifts still have a fairly clear 24 hour period, especially during days when the outdoor temperature has wide fluctuations. On especially cloudy days when temperature variations are low and smooth the machine does work considerably better. There is a several hour phase lag

between the magnetic field drift and the outdoor temperature. The overall drifts also seem to follow long range changes in the outdoor temperature. The 24 hour periodic character is superimposed on these longer drifts.

It is my opinion that the remaining drifts are still caused by the interaction of the machine with thermal motions of the building, such as buckling and expansion of the floor, which slightly alters the positions of the shaft bearings in the process. As far as the present configuration of the machine is concerned, they are almost irreducible, unless means can be found to isolate the entire machine from the building. I believe that the basic cause can still be traced to motion of the spectrometer field sensing coil relative to the spectrometer field. Buckling of the spectrometer structure itself, the distortions of the supporting table or thermal motions of the vacuum tank, to which the search coil is attached, may all contribute to this motion. Keep in mind that only  $2.4 \times 10^{-4}$  inch axial motion of the search coil relative to the spectrometer field produces, by feedback, a  $1:10^5$  field variation! Therefore, to be able to eliminate the search coil motion as a primary cause of field drifts, its position should be fixed at least to within 50 microinches. This, of course, is quite difficult, even if high precision non-magnetic ball bearings were available. Without them the difficulty becomes extreme. Spectrometers using a rotating shaft system for field regulation and capable of high resolution will probably find such interactions

as these to be the limiting factors to their usefulness. Quite possibly, had the machine been located on the ground floor of the building on a concrete slab platform, these problems would have been much less severe.

## CHAPTER 6

### EXTERNAL FIELD COMPENSATION

#### 6.1 Introduction

The present spectrometer is designed primarily for observations of conversion electrons and electron lines arising from the Auger effect. A considerable part of its operating time will be spent in measurements dealing with very low energy electrons, requiring focusing fields of only a few gauss. In such circumstances, the magnetic field of the Earth, about 0.6 gauss, would be an appreciable fraction of the focusing field, and as it does not have the proper shape it should be limited as much as possible. The spectrometer axis is vertical. It therefore makes an angle of about  $20^\circ$  with the earth's magnetic field. The vertical component of the earth's field is thus of major importance, for it is parallel to the focusing field and will therefore add to the radial aberrations of the spectrometer. The horizontal components, i.e., the north-south and east-west components, of the earth's magnetic field are not as prominent; however, they can cause a loss in transmission by deflecting the electron beam vertically so part of it misses the counter slit.

Three pairs of mutually orthogonal coils are used to compensate separately the three components of the earth's magnetic field.

## 6.2 The Compensating Coils

The coil forms are made of U-shaped aluminum extrusions bent into circular shape. The pair that compensates the vertical component of the field, hereafter referred to as the vertical coils, have a radius of 74.5 inches and are wound with 1395 turns of wire each. They are spaced symmetrically above and below the symmetry plane of the spectrometer, 73 inches apart. This spacing gives a slightly better slope of the compensating field near the electron orbit than pure Helmholtz spacing.

The coil pair which compensates the north-south component of the field, the N-S coils, have a radius of 68.5 inches and carry 600 turns of wire each. Their spacing is 69.5 inches. Finally, the east-west, or E-W, pair has likewise a radius of 68.5 inches. Each coil contains 200 turns of wire and the coil spacing is 80 inches.

The spacing of the compensating coils is arrived at in a semi-empirical fashion, the field non-uniformities of the individual location of the spectrometer determining the requirements.

The set of six coils is mounted about the spectrometer on a framework of aluminum tubing and braces, a part of which is visible in Figure 5, the photograph of the spectrometer. Cables leading from the control room enable the three pairs to be powered separately. The members of each pair are connected in series.



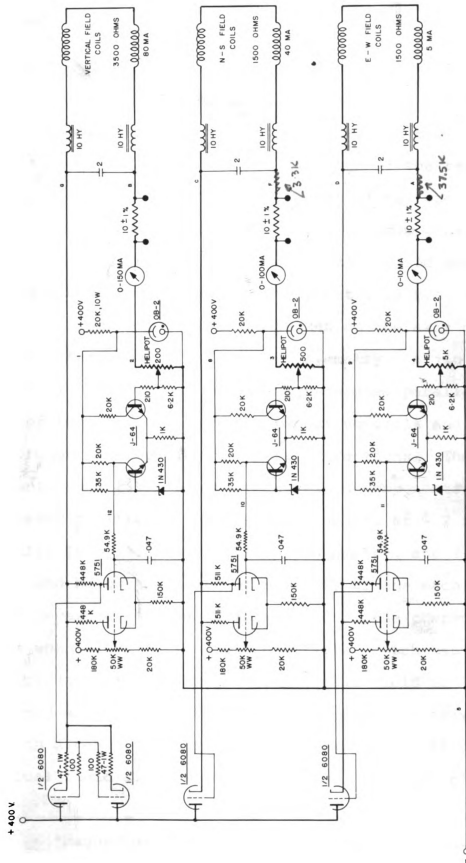
### 6.3 The Compensating Coil Power Supply

The power supply is a hybrid transistor and tube three channel supply, designed and built in the departmental electronics shop by Mr. William Harder. It uses a basic power supply module, Calmag model 5VT47,\* which can provide 375-425 volts d-c at 400 ma with a line and load regulation of 0.05 percent. Figure 35 shows the remainder of the regulator of the supply. Currents from the coils are detected across helipot controls. The potentials thus developed are compared with reference diode elements 1N430, and the resulting error signals are amplified by three transistor differential amplifiers. This entire assembly is contained in a temperature controlled box. The output of the transistor preamplifiers is led to three separate tube differential amplifiers using 5751 tubes. The output of these second amplifiers provides the grid bias for 6080 pass tubes that control the current to the coils. Two sections of a 6080 are used for the vertical coils which normally run at 80 ma. One section each is used for the N-S and the E-W coils which use 40 and 5 ma respectively. Precision 10 ohm resistors are included in series with each coil pair and their terminals are led to the panel of the power supply. These connections can be used to monitor the compensating coil currents by means of a potentiometer. This power supply regulates the compensating coil current to

---

\*California Magnetic Control Corporation, North Hollywood, California.

**Figure 35. Schematic diagram of the compensating coil current regulators.**



COMPENSATING COILS CURRENT REGULATORS.  
Figure 35

0.01% and has proved itself to be stable over long periods of time.

#### 6.4 Performance

After completion of the compensating coils, measurements were made in the vicinity of the mean orbit of the spectrometer to determine the magnitude of the residual fields. A saturable strip magnetometer\* was used for these measurements. This instrument has a maximum sensitivity of 1 millioersted full scale. Near zero field measurements can be made with a resolution of about 0.03 mOe.

First, a position was chosen on the axis of the spectrometer and in its plane of symmetry. A jig was used to position the probes of the magnetometer parallel to the axes of the three pairs of compensating coils and the field was brought to zero for the three directions. Then, measurements were taken of the three field components at nine different positions: At the mean radius, at  $\pm 2$  inches radially from it, in the plane of symmetry, and 2 inches above and below the plane of symmetry of the machine. As could be expected, the uniform field of the compensating coils when added to the external field, which has a gradient, produces a sine wave like residual field as the probe is moved around the spectrometer. A representative sample of such a measurement for the vertical component of the residual field is shown in Figure 36. The data collected

---

\*Magnaflux Corporation, Chicago, Illinois.

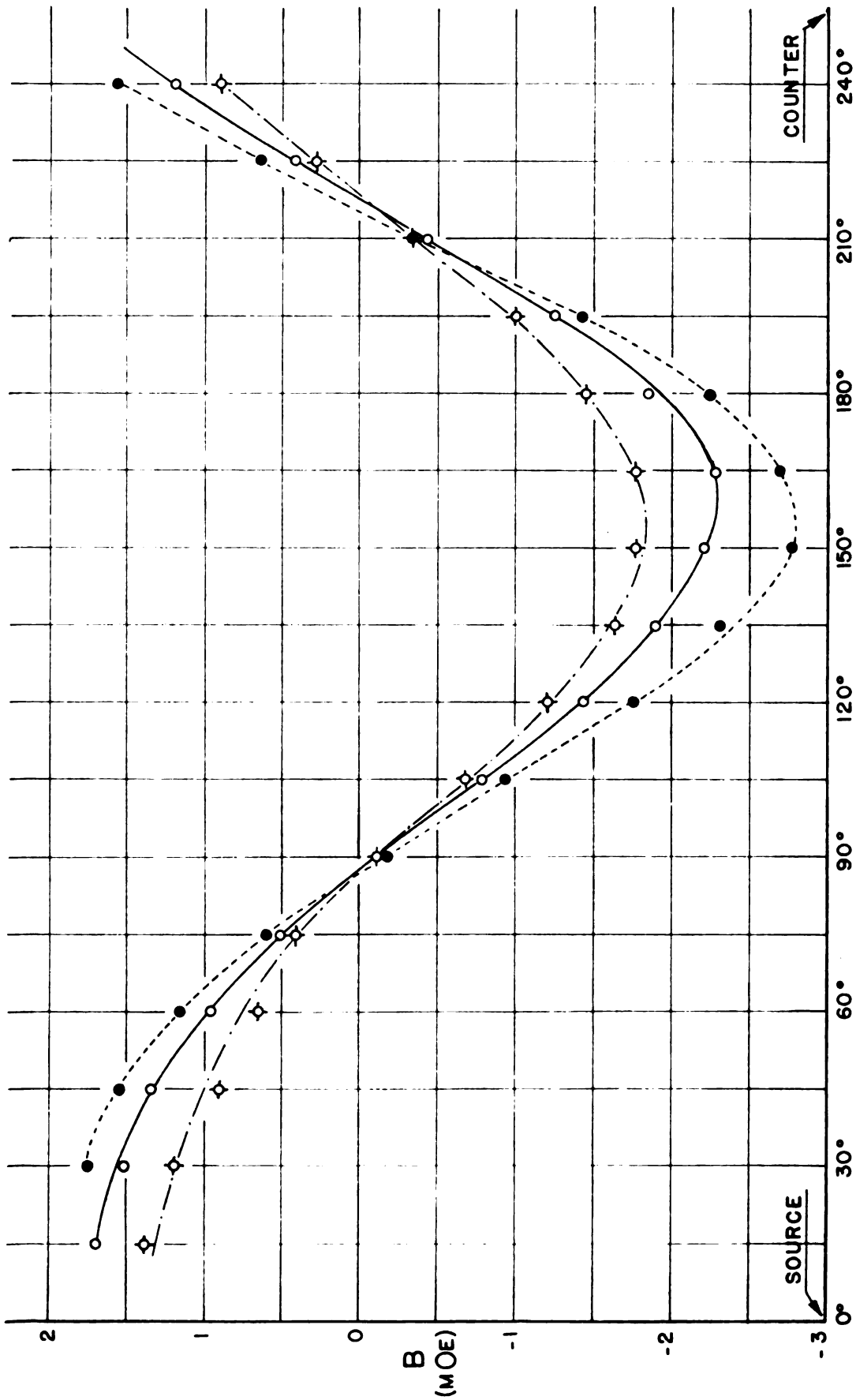


FIGURE 36. RESIDUAL VERTICAL FIELD.  $Z = 0$  PLANE, RADII:  $\bullet R_O + 2''$ ,  $\circ R_O - 2''$ ,  $\diamond R_O$ .

from these measurements were used to calculate the amount of bias field needed to obtain a zero net deviation for low energy electrons traveling along the mean orbit of the spectrometer. Note that a small residual field applied to the electron near the source may result in an appreciable deflection by the time the electron reaches the counter. The calculation solves for a net field that has to be introduced, such that all the deflections will cancel.

For simplicity the residual field is assumed to have a pure sinusoidal shape. It can therefore be written as

$$B_{\text{res.}} = B_{\text{res. max}} \cos \theta' \quad (111)$$

Considering a zero focusing field, this case can be resolved into a straight line of flight perturbed by  $B_{\text{res.}}$  according to

$$\vec{F} = -e \vec{v} \times (\vec{B}_{\text{res.}}) \quad (112)$$

A uniform biasing field  $B_b$  is to be added to  $B_{\text{res.}}$  such that  $z = 0$  at the end of the trajectory. In one dimension:

$$m \ddot{z} = -e v (B_b + B_{\text{res.}}) \quad (113)$$

$v$  is a constant velocity along the x-axis,  $B$  is directed along the y-axis.

$$\ddot{z} + \frac{e}{m} v B_b + \frac{e}{m} v B_{\text{res. max}} \cos \theta' = 0 \quad (114)$$

As the  $\theta'$  measurements start  $30^\circ$  away from maximum  $B_r$  we must write

$$\cos \Theta' \rightarrow \cos \left( \Theta + \frac{\pi}{6} \right) \quad (115)$$

$\Theta$  now has range 0 to  $\pi\sqrt{2}$  radians. For an electron with momentum  $p = mv$  the time of flight is  $\tau = \frac{d}{v}$  where  $d = \pi\sqrt{2} R_0$ . Time at position  $\Theta$  is

$$t_{\Theta} = \frac{\Theta}{\pi\sqrt{2}} \tau = \frac{\Theta}{\pi\sqrt{2}} \frac{\pi\sqrt{2} R_0}{v} = \frac{\Theta R_0}{v} \quad (116)$$

The equation of motion becomes:

$$\frac{d^2 z}{d\Theta^2} + \frac{e R_0^2}{p} B_b + \frac{e R_0^2}{p} B_{\text{res. max}} \cos \left( \Theta + \frac{\pi}{6} \right) = 0 \quad (117)$$

with the boundary values:

$$\frac{dz}{d\Theta} = 0 \quad \text{at} \quad \Theta = 0 \quad \text{and} \quad z = 0 \quad \text{at} \quad \Theta = 0. \quad (118)$$

The solution is

$$z = \frac{e R_0^2}{p} B_{\text{res. max}} \left[ \cos \left( \Theta + \frac{\pi}{6} \right) + \Theta \sin \frac{\pi}{6} - \cos \frac{\pi}{6} \right] - \frac{e R_0^2}{2p} B_b \Theta^2. \quad (119)$$

Condition for solution is  $z = 0$  at  $\Theta = \pi\sqrt{2}$ .

$$0 = \frac{e R_0^2}{p} B_{\text{res. max}} \left[ \cos \left( \pi\sqrt{2} + \frac{\pi}{6} \right) + \pi\sqrt{2} \sin \frac{\pi}{6} - \cos \frac{\pi}{6} \right] - \frac{e R_0^2}{2p} 2\pi^2 B_b \quad (120)$$

$$B_b = 0.163 B_{\text{res. max}}$$

$$B_{\text{res. max}} \approx 2.3 \text{ mOe} \quad \text{hence}$$

$$B_b \approx 0.37 \text{ mOe} \quad (121)$$

Similar calculations performed for the North-South field

and the East-West field yield

$$B_b \text{ N-S} \approx 0.4 \text{ mOe} \quad (122)$$

$$B_b \text{ E-W} \approx 0.28 \text{ mOe} \quad (123)$$

The current supplies were set at these bias field values at the center of the spectrometer. As the center of the spectrometer is inaccessible during operation, the reference positions of the magnetometer probes were transferred to the outside of the tank. This is always possible to do, since the residual field passes through at least two zero field positions as one moves the probes around the circumference of the spectrometer, and so any value from zero to a few millioersteds can be obtained just by changing the positions of the probes. Three such external positions were determined for the three components of the field.

During runs with the spectrometer, the field is compensated at convenient intervals, a few hours or so. Aside from drifts in the compensating power supplies, the variations in the earth's field are not very large, a few tenths of a millioersted in any given day. These are caused chiefly by causes beyond experimenter's control, such as parked cars in the neighboring parking lot, internal building changes, magnetic storms and the like. To first order these disturbances (for the vertical field component) are ignorable, as the field control system of the spectrometer tends to compensate for them.



## CHAPTER 7

### ALIGNMENT OF THE SPECTROMETER

#### 7.1 Coil Measurements

After completion of the focusing coils, careful measurements were made of the cross-section dimensions of each winding and thereby, of the mean radii of the coils. The measurements were carried out both at room temperature and near the anticipated operating temperature of the coils. The data were then used to compute the optimum spacing of the coils about the symmetry plane of the spectrometer.

In order to perform calculations of an off-axis magnetic field produced by a number of circular coils it is necessary to determine the electrical equivalents of the coils, that is, the coils must be reduced to equivalent current filaments. Lyle<sup>30</sup> has shown that a rectangular cross section winding can, in general, be reduced to two equivalent current filaments as follows. Referring to Figure 37,

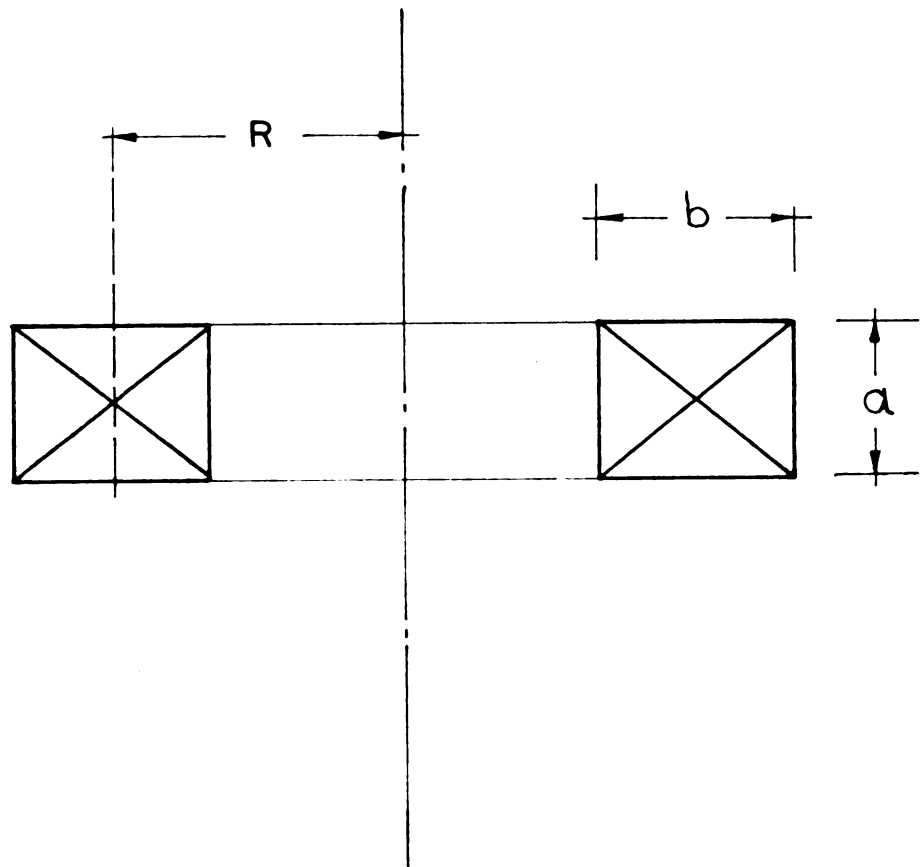
#### Case 1. $a > b$

Coil is replaced by two filaments at radius

$$r = R \left( 1 + \frac{b^2}{24 R^2} \right) \quad (124)$$

Spaced a distance  $p$  above and below the median plane of the coil.

$$p^2 = \frac{a^2 - b^2}{12} \quad (125)$$



$R$  = MEAN RADIUS

$a$  = AXIAL BREADTH

$b$  = RADIAL DEPTH

FIGURE 37. DECOMPOSITION OF A RECTANGULAR  
CROSS - SECTION COIL INTO  
EQUIVALENT CURRENT FILAMENTS.

Case 2.  $b > a$ 

Coil is replaced by two filaments of radii  $r' \pm q$  lying in the median plane of the coil.

$$r' = R \left( 1 + \frac{a^2}{24 R^2} \right) \quad (126)$$

$$q^2 = \frac{b^2 - a^2}{12} \quad (127)$$

Table II shows the cold and hot  $a$  and  $b$  dimensions of the spectrometer coils. The A and B coils conform to Case 2 and the C and D coils to Case 1. The last figures of the radii in the table are not particularly significant, but were carried for purposes of computations and rounded off later. The equivalent radii were computed from these figures as were also the values of  $p$  and  $q$ . Table III shows the results. All dimensions in Table III were converted to centimeters for future calculations.

As the M.S.U. spectrometer is based on the Moussa-Bellicard design, using essentially the same design parameters, except for its larger size and low voltage, high current focusing coils, the Moussa parameters for Z positions of the focusing coils were used as a departure point for subsequent more refined calculations.

The axial positions of the coils are determined from:

$$Z = R_{eq} \cdot \xi \quad (128)$$

where  $\xi$  has four different values for the four coil pairs.

Particularly,  $\xi_A = 1.2$ ,  $\xi_B = 0.9$ ,  $\xi_C = 0.25$ ,  $\xi_D = 0.2$ .

TABLE II. Coil Winding Cross Sections

Coil	a cold	a hot	b cold	b hot	R <sub>m</sub> cold	R <sub>m</sub> hot
A <sub>u</sub>	2.0000	2.0009	2.0605	2.0614	10.7618	10.7665
B <sub>u</sub>	2.0000	2.0009	2.0758	2.0767	11.2694	11.2743
C <sub>u</sub>	1.4000	1.4006	1.3360	1.3366	23.1810	23.1911
D <sub>u</sub>	1.4000	1.4006	1.3670	1.3676	19.7415	19.7500
A <sub>l</sub>	2.0000	2.0009	2.0665	2.0674	10.7618	10.7665
B <sub>l</sub>	2.0000	2.0009	2.0745	2.0754	11.2688	11.2737
C <sub>l</sub>	1.4000	1.4006	1.3285	1.3291	23.1728	23.1828
D <sub>l</sub>	1.4000	1.4006	1.3787	1.3793	19.7526	19.7611

All dimensions in inches.

TABLE III. Equivalent Radii and the Spacing of Current Filaments for the Focusing Coils

Coil	R <sub>eq</sub>	p	q
A <sub>u</sub>	27.3862	---	0.0364
B <sub>u</sub>	28.6742	---	0.0408
C <sub>u</sub>	58.9133	0.0307	---
D <sub>u</sub>	50.1751	0.0222	---
A <sub>l</sub>	27.3862	---	0.0382
B <sub>l</sub>	28.6727	---	0.0404
C <sub>l</sub>	58.8924	0.0324	---
D <sub>l</sub>	50.2035	0.0179	---

All dimensions in centimeters.

off  
 10  
 (6.50)

This leads to the following axial positions of the coils (referred to the median plane of spectrometer):

	Z cm		Z cm
A <sub>u</sub>	32.8634	A <sub>l</sub>	32.8634
B <sub>u</sub>	25.8068	B <sub>l</sub>	25.8054
C <sub>u</sub>	14.7283	C <sub>l</sub>	14.7231
D <sub>u</sub>	10.0350	D <sub>l</sub>	10.0407

It is clear that since the focusing coils sometimes depart significantly from the ideal equivalent radii, it would be valuable to calculate the magnetic field produced by the real coils and to optimize its shape by adjustment of their z positions. To this end we have first obtained the shape of a field varying as  $1/\sqrt{r}$ , which incidentally gives a very good match for double focusing, and also the shape of the sixth order focusing field as found from the parameters calculated by Lee-Whiting and Taylor at Chalk River.<sup>20</sup> Both were calculated to see how well they could be matched by positioning of the focusing coils and whether or not we had a choice. The sixth order field is, of course, by far the more desirable as it results in improved transmission. Subsequent computations did show that the sixth order field could be matched quite well near the mean orbit of the spectrometer. Unfortunately the dimensions of the focusing coils were such that a match better than 1 part in  $10^4$  was not possible for radial deviations greater than 2 cm on either side of the mean orbit.

To find the field due to the focusing coils, one

needs to calculate the sum of the fields, off axis, of sixteen circular filaments spaced the appropriate distances from the plane of symmetry. For a single circular current we can write (referring to Figure 38):

$$\vec{A} = \frac{\mu_0 I}{4\pi} \oint \frac{d\vec{s}}{|\vec{r}|} \quad ; \quad \vec{B} = \nabla \times \vec{A} \quad (129)$$

$$r = [L^2 + \rho^2 - 2L\rho \cos \theta + z^2]^{1/2}$$

$$= [(\rho - L \cos \theta)^2 + (L \sin \theta)^2 + z^2]^{1/2}$$

$$\vec{A} = \frac{\mu_0 I}{4\pi} \oint \frac{d\vec{s}}{[(\rho - L \cos \theta)^2 + (L \sin \theta)^2 + z^2]^{1/2}} \quad (130)$$

$$A_\rho = A_z = 0$$

$$A_\theta = \frac{\mu_0 I}{4\pi} 2 \int_0^\pi \frac{L \cos \theta d\theta}{[(\rho - L \cos \theta)^2 + (L \sin \theta)^2 + z^2]^{1/2}} \quad (131)$$

$$\text{let } \theta = \pi + 2\phi$$

$$A_\theta = \frac{\mu_0 L I}{\pi} \int_0^{\pi/2} \frac{(2 \sin^2 \phi - 1) d\phi}{\left\{ [(L + \rho)^2 + z^2] \left[ 1 - \frac{4L\rho \sin^2 \phi}{(L + \rho)^2 + z^2} \right] \right\}^{1/2}} \quad (132)$$

$$\text{Set } \frac{4L\rho}{(L + \rho)^2 + z^2} = k^2$$

$$A_\theta = \frac{\mu_0 I k}{2\pi} \left( \frac{L}{\rho} \right)^{1/2} \int_0^{\pi/2} \left[ \frac{\sin^2 \phi}{(1 - k^2 \sin^2 \phi)^{1/2}} - \frac{1}{(1 - k^2 \sin^2 \phi)^{1/2}} \right] d\phi \quad (133)$$

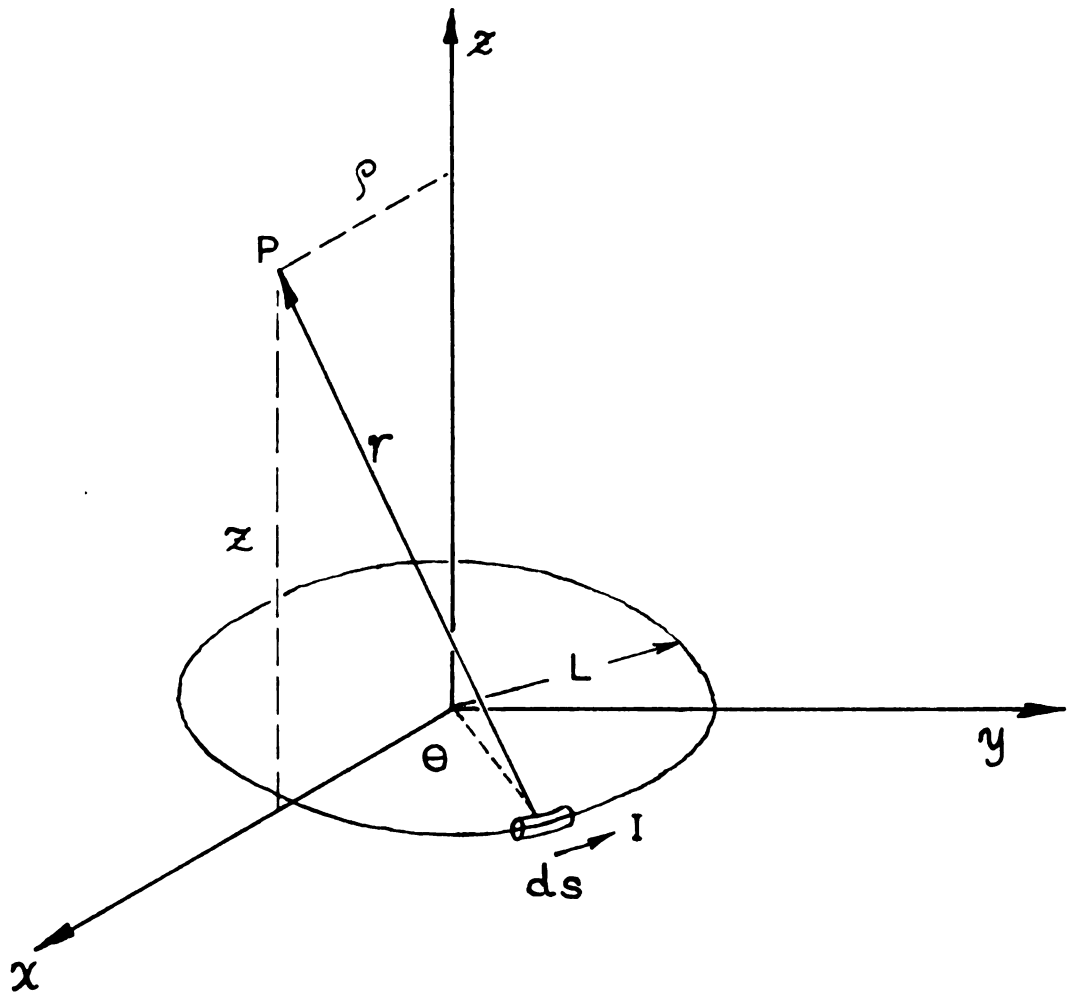


FIGURE 38. MAGNETIC FIELD OF A CIRCULAR CURRENT.  
DEFINITION OF SYMBOLS.

But

$$\frac{\sin^2 \phi}{(1 - k^2 \sin^2 \phi)^{1/2}} = \frac{1}{k^2} \left[ \frac{1}{(1 - k^2 \sin^2 \phi)^{1/2}} - (1 - \sin^2 \phi)^{1/2} \right] \quad (134)$$

whence

$$A_\theta = \frac{\mu_0 I k}{2\pi} \left( \frac{L}{\rho} \right)^{1/2} \left\{ \frac{1}{k^2} \int_0^{\pi/2} \frac{d\phi}{(1 - k^2 \sin^2 \phi)^{1/2}} - \right. \\ \left. - \frac{1}{k^2} \int_0^{\pi/2} (1 - k^2 \sin^2 \phi)^{1/2} d\phi - \int_0^{\pi/2} \frac{d\phi}{(1 - k^2 \sin^2 \phi)^{1/2}} \right\} \quad (135)$$

Recognizing the elliptic integral forms we have

$$A_\theta = \frac{\mu_0 I k}{2\pi} \left( \frac{L}{\rho} \right)^{1/2} \left[ \frac{1}{k^2} K - \frac{1}{k^2} E - K \right]$$

or

$$A_\theta = \frac{\mu_0 I}{\pi k} \left( \frac{L}{\rho} \right)^{1/2} \left[ \left( 1 - \frac{k^2}{2} \right) K - E \right] \quad (136)$$

Since

$$\vec{B} = \nabla \times \vec{A} = - \frac{\vec{\rho}}{\rho} \frac{\partial A_\theta}{\partial z} + \frac{\vec{z}}{\rho z} \frac{\partial (\rho A_\theta)}{\partial \rho}$$

Thus

$$B_\rho = - \frac{\partial A_\theta}{\partial z} \quad (137)$$

and

$$B_z = \frac{1}{\rho} \frac{\partial (\rho A_\theta)}{\partial \rho} \quad (138)$$





Finally, using the explicit value of  $k$

$$B_{\rho} = \frac{\mu_0 I}{2\pi [(L+\rho)^2 + z^2]^{1/2}} \left( \frac{z}{\rho} \right) \left[ \frac{L^2 + \rho^2 + z^2}{(L-\rho)^2 + z^2} E - K \right] \quad (139)$$

$$B_z = \frac{\mu_0 I}{2\pi [(L+\rho)^2 + z^2]^{1/2}} \left[ \frac{L^2 - \rho^2 - z^2}{(L-\rho)^2 + z^2} E + K \right] \quad (140)$$

The calculation is carried out in a straightforward manner using these expressions. Though simple it is quite tedious since it requires the evaluation of thirty-two expressions to find the field at one point. Furthermore, the modulus of the elliptic integrals is not likely to be an even integer in most cases, requiring an interpolation in the tabulated values. It is altogether preferable to perform the entire calculation by a digital computer which can evaluate several field values per minute.

## 7.2 Computer Runs for the Optimization of the Focusing Field

B. T. Smith<sup>41</sup> has prepared a MISTIC program for the computation of the magnetic field of a circular current. This program was used in all subsequent calculations.

Several runs were made in the attempt to accomplish two main objectives: To match the spectrometer field to the sixth order field over as large a span of radius as possible, and to reduce the radial component of the field ( $B_r$ ) in the plane of symmetry. The radial field arises from the fact that the focusing coils are not perfectly

symmetrical pairs. The spacing of the focusing coils as calculated by Moussa, for example, assumes identical members of the coil pairs. If we have asymmetry, then the surface of zero radial field does not coincide with the geometrical median plane. For a pair of circular coils of slightly different radii and spaced distances  $-z$  and  $+(z + \Delta z)$  from the median plane, the surface of zero radial field will cut the median plane in a circle whose radius is, of course, a function of the coil radii and  $z$  values. The objective here is to obtain  $B_r = 0$  on the mean orbit of the spectrometer, i.e., to make the locus of  $B_r = 0$  coincide with the mean orbit. To minimize  $B_r$  analytically for a pair of coils of unequal radii and each containing two equivalent filaments is very tedious and, therefore, a numerical calculation was done by means of the computer to save time. Each of the coil pairs was placed initially at the Moussa setting and the radial ( $B_r$ ) and axial ( $B_z$ ) fields were computed. The coils were then shifted in small increments relative to the median plane of the spectrometer and  $B_r$  and  $B_z$  were recomputed for several values of radius. The calculation leads to a choice of coil pair  $z$  positions which minimize  $B_r$  at the mean orbit of the spectrometer. The results of these calculations are shown in Figures 39, 40 and 41. Examination of the figures reveals that the Moussa indicated values of coil spacing do not give a zero radial field anywhere near the central orbit, though the actual adjustments needed to bring  $B_r$  to zero there are

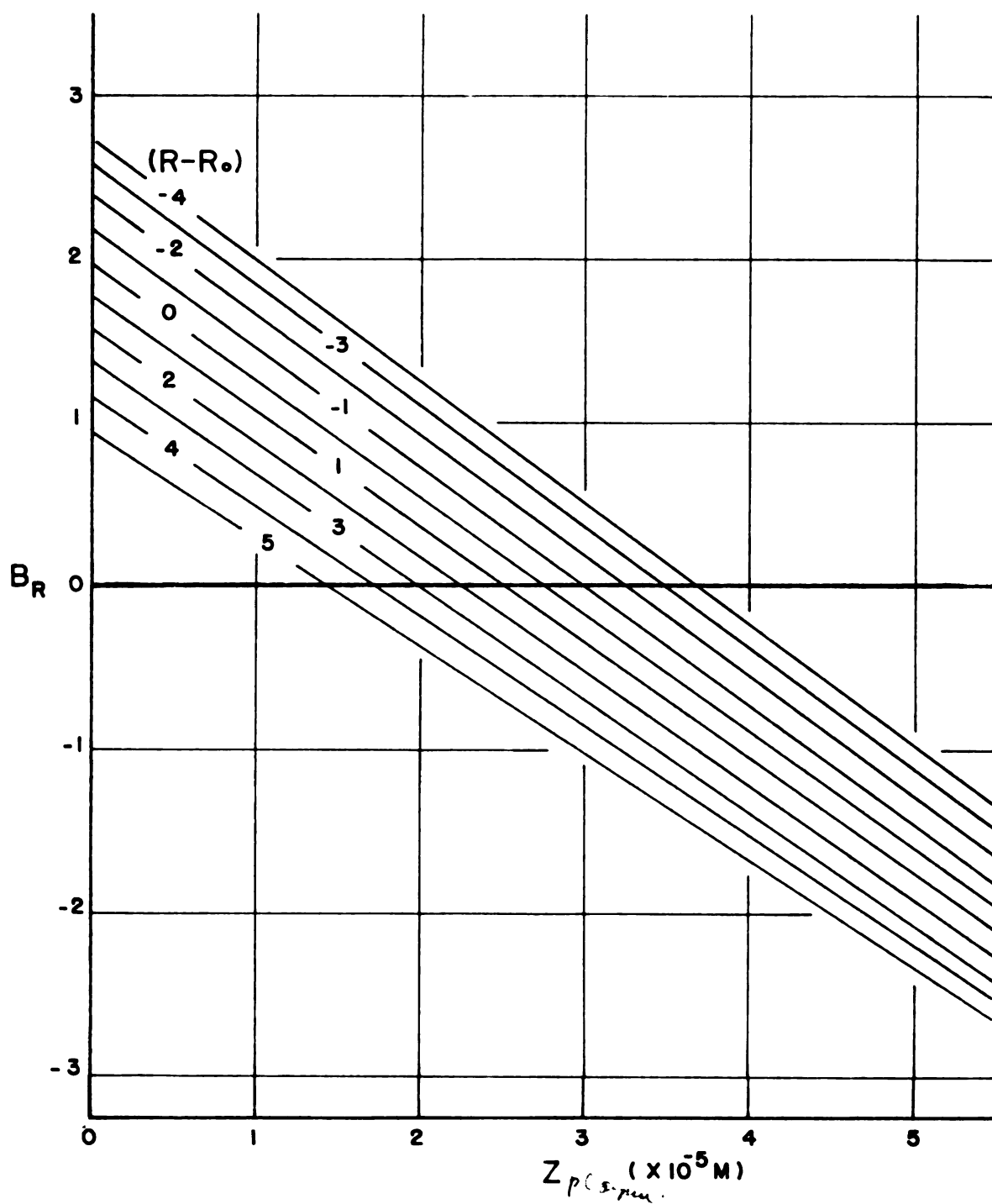


FIGURE 39. RADIAL FIELD OF THE B COIL PAIR AS A FUNCTION OF ITS DISPLACEMENT RELATIVE TO THE MEDIAN PLANE OF THE SPECTROMETER.

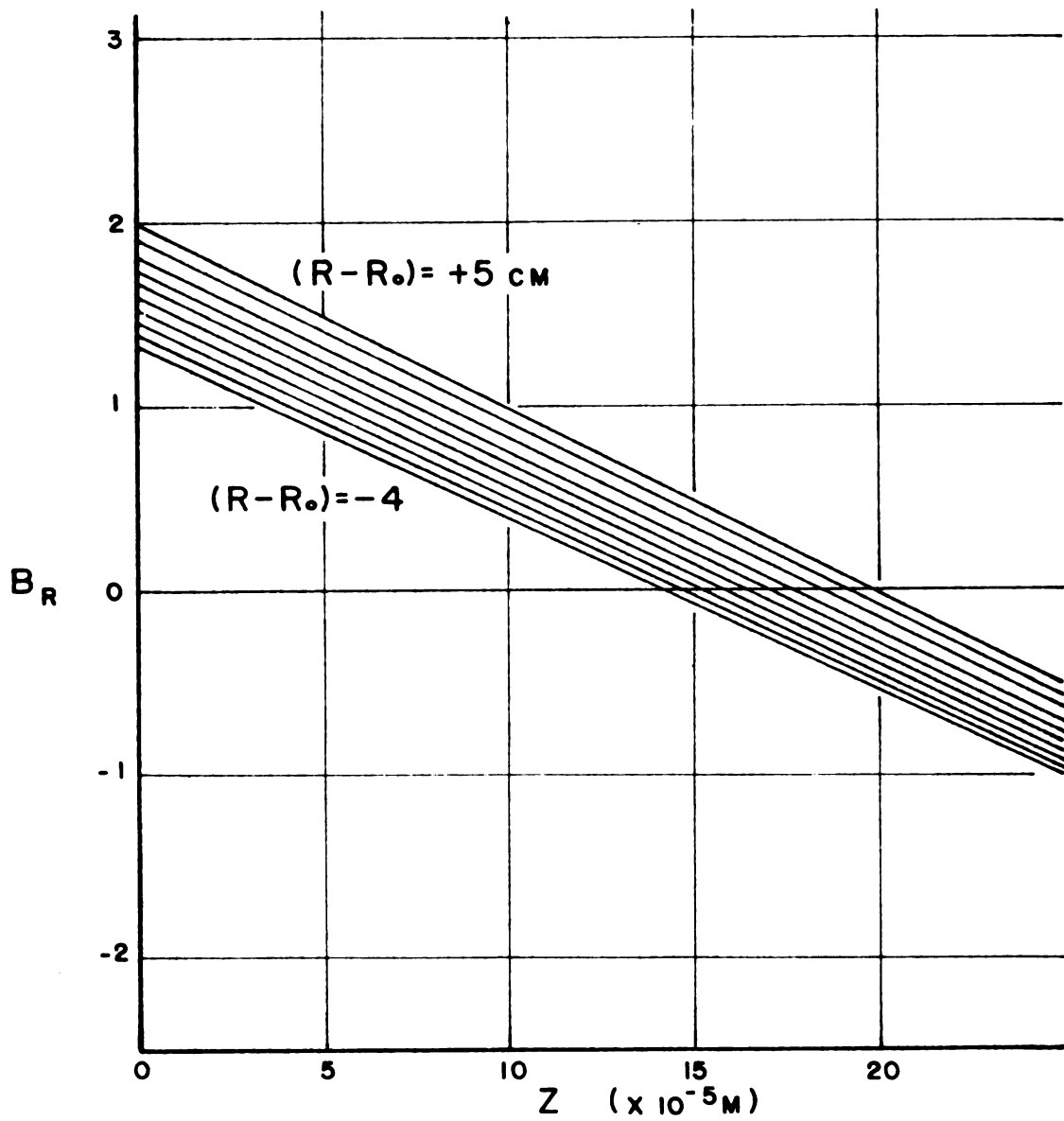


FIGURE 40. RADIAL FIELD OF THE C COIL PAIR AS A FUNCTION OF ITS DISPLACEMENT RELATIVE TO THE MEDIAN PLANE OF THE SPECTROMETER.

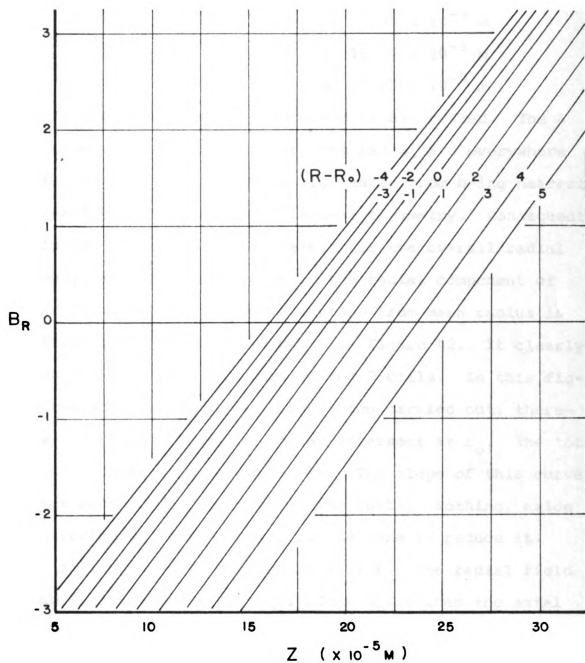


FIGURE 41. RADIAL FIELD OF THE D COIL PAIR AS  
A FUNCTION OF ITS DISPLACEMENT RELATIVE  
TO THE MEDIAN PLANE OF THE SPECTROMETER.

rather small. To obtain  $B_r = 0$  at  $r_0$  the coil pairs had to be shifted as follows:

B coils	down	$2.75 \times 10^{-5}$ m
C coils	up	$16.25 \times 10^{-5}$ m
D coils	down	$19.25 \times 10^{-5}$ m

Only the B, C and D coil pairs had to be treated. The A coils were symmetric and therefore had  $B_r = 0$  everywhere on the  $z = 0$  plane. The D coils, aside from being nearest the central orbit, have the largest asymmetry. Consequently it is the D coil pair that determines the overall radial dependence of  $B_r$ . The value of the radial component of the field as a function of departure from mean radius is plotted for the B, C and D coils in Figure 42. It clearly shows the dominant character of the D coils. In this figure the adjustments have already been carried out; therefore, all three coil pair curves intersect at  $r_0$ . The total field is shown as a dashed curve. The slope of this curve arises from the asymmetries of the coils. Nothing, aside from rewinding of the coils, can be done to reduce it. Even so, for a  $\pm 2$  cm departure from  $r_0$ , the radial field is about five orders of magnitude smaller than the axial field.

The procedure for the optimization of the axial component of the magnetic field,  $B_z$ , of the spectrometer consisted of two parts: First, the fields of individual coil pairs were calculated for different spacings grouped about the Moussa values. The results are given in Figures 43, 44, 45 and 46. The graphs depict the variation of the

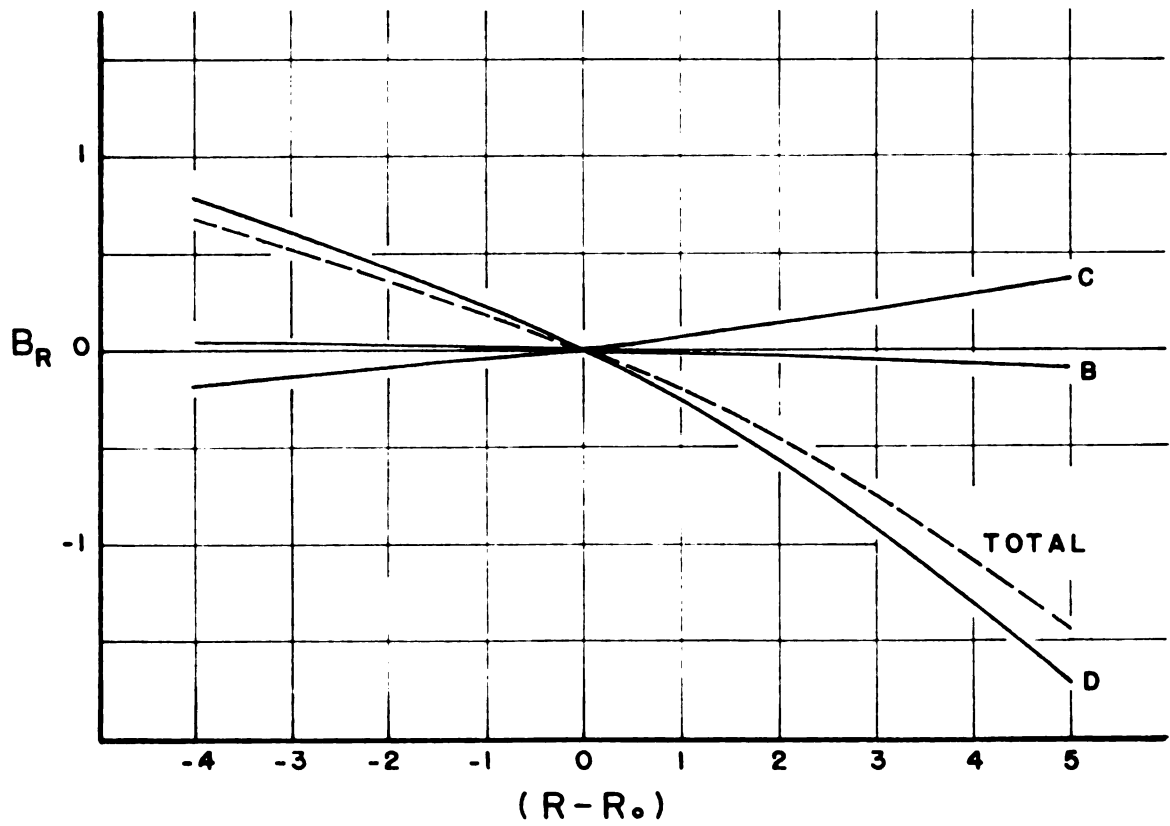
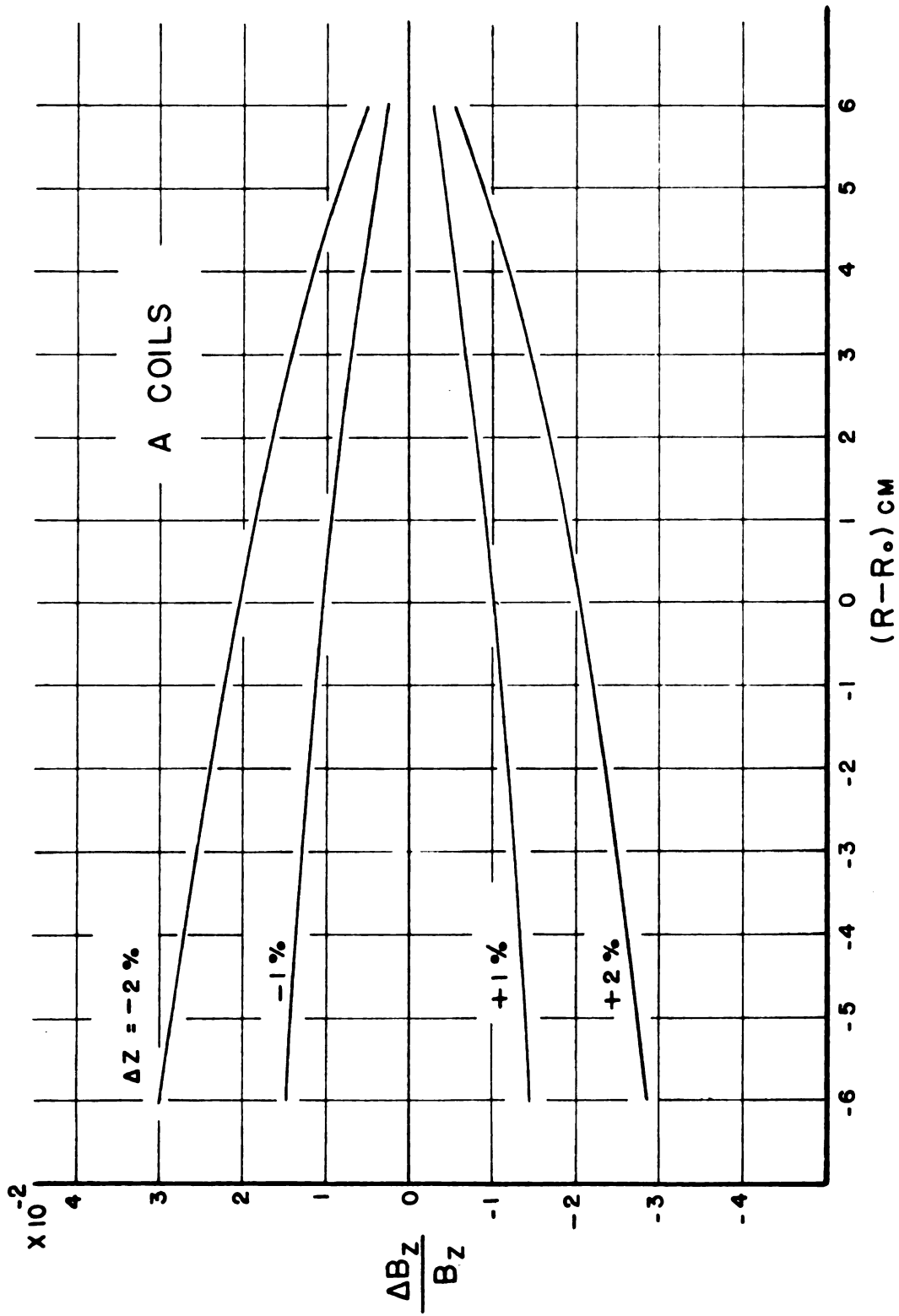


FIGURE 42. RADIAL FIELD AS A FUNCTION OF RADIUS.



FIGURE 43. VARIATION IN  $B_z$  AS A FUNCTION OF RADIUS.

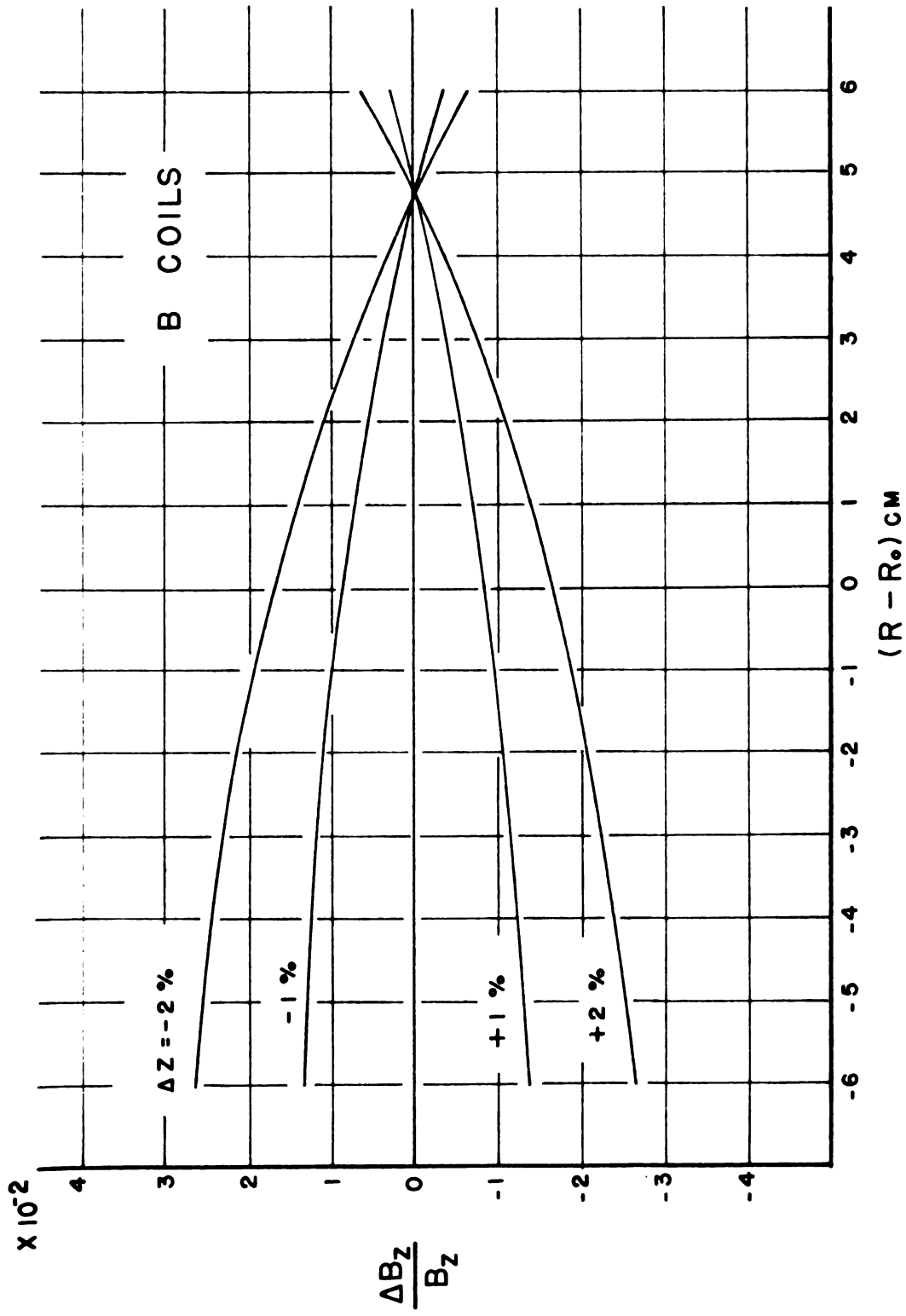
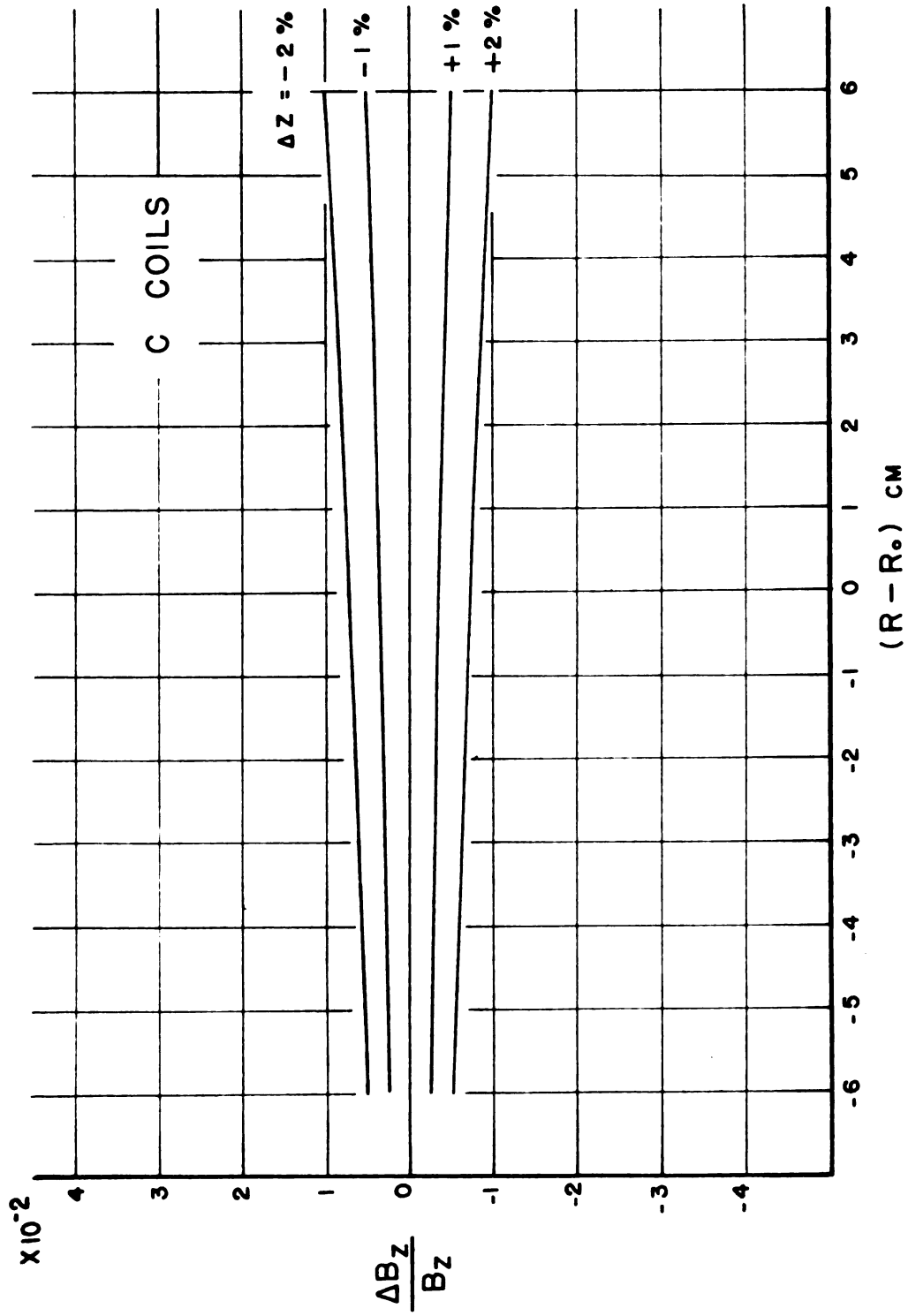
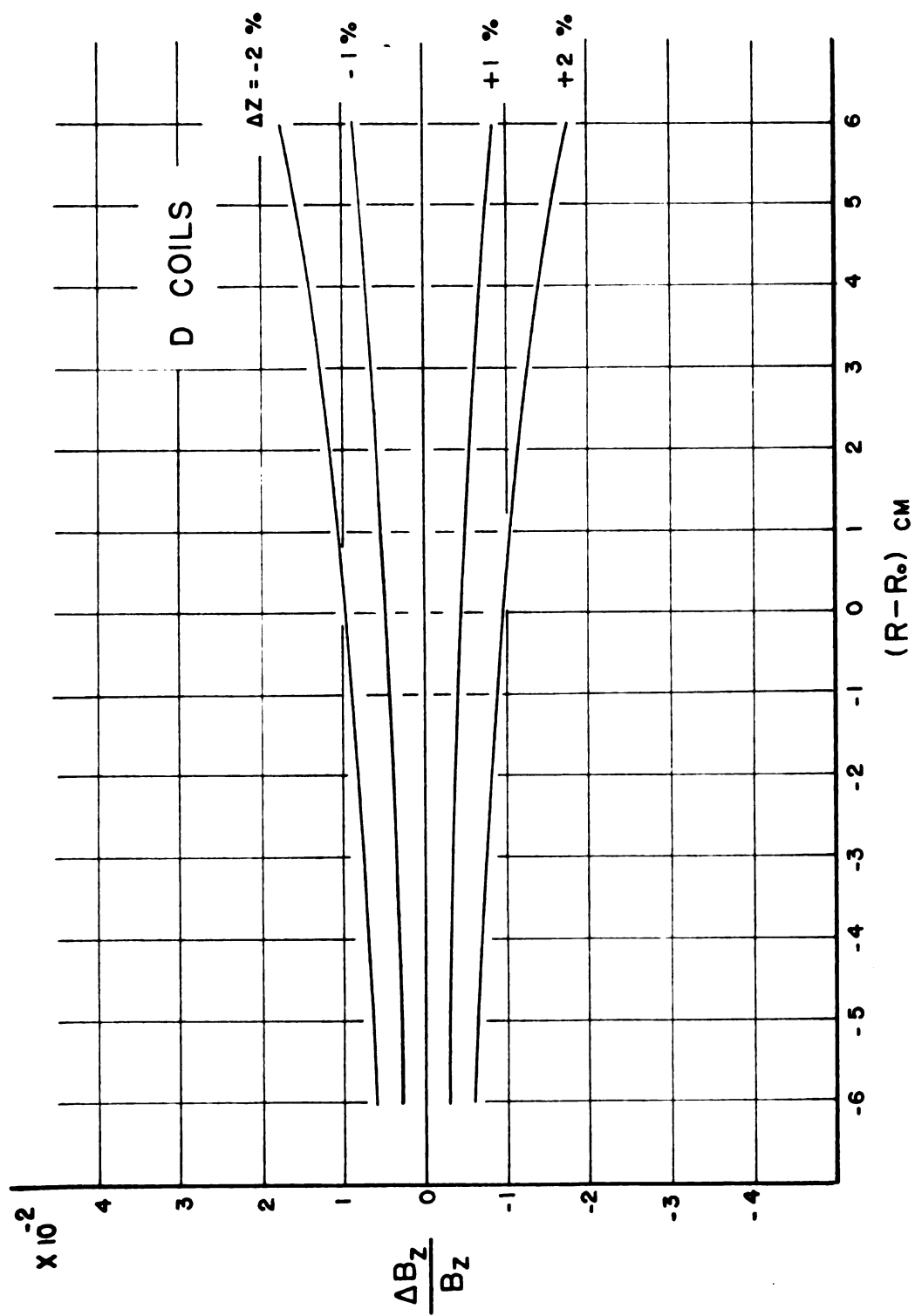


FIGURE 44. VARIATION IN  $B_z$  AS A FUNCTION OF RADIUS.

FIGURE 45. VARIATION IN  $B_z$  AS A FUNCTION OF RADIUS.

FIGURE 46. VARIATION IN  $B_z$  AS A FUNCTION OF RADIUS.

axial field as a function of radius,  $(r - r_0)$ . The spacing change  $(\Delta z)$  is held as a parameter.

The slope and curvature of these curves provides a guide for the alteration of the coil spacing to improve the shape of the focusing field. The curves show that motion of the C coils has the least effect on the total axial field, while the motion of the B pair produces the largest changes in the total field.

Second, the influence of axial spacing of an individual coil pair on the total field was investigated. To evaluate the results of these calculations, the total axial field was subtracted from the sixth order ideal field, normalized at the central orbit radius. The differences thus obtained are plotted against radius,  $(r - r_0)$ . Figures 47, 48, 49 and 50 show the effect of moving the A, B, C and D coils in steps of  $\Delta z = 1\%$ . Clearly as all the curves have the same sense, it is impossible by any combination of coil motions to provide a perfect fit for a large span of radius. The question that must be answered now is, therefore, whether it is better to get a near perfect fit for small radial deviation and suffer a steeper departure from the ideal field farther out, or to try for a "good" fit over as large a span of radius as possible. The desirability of high resolution points to the first of the two choices. It is preferable to have a near perfect fit in a limited region, for then the field shape improves as the machine is baffled down for high resolution running.

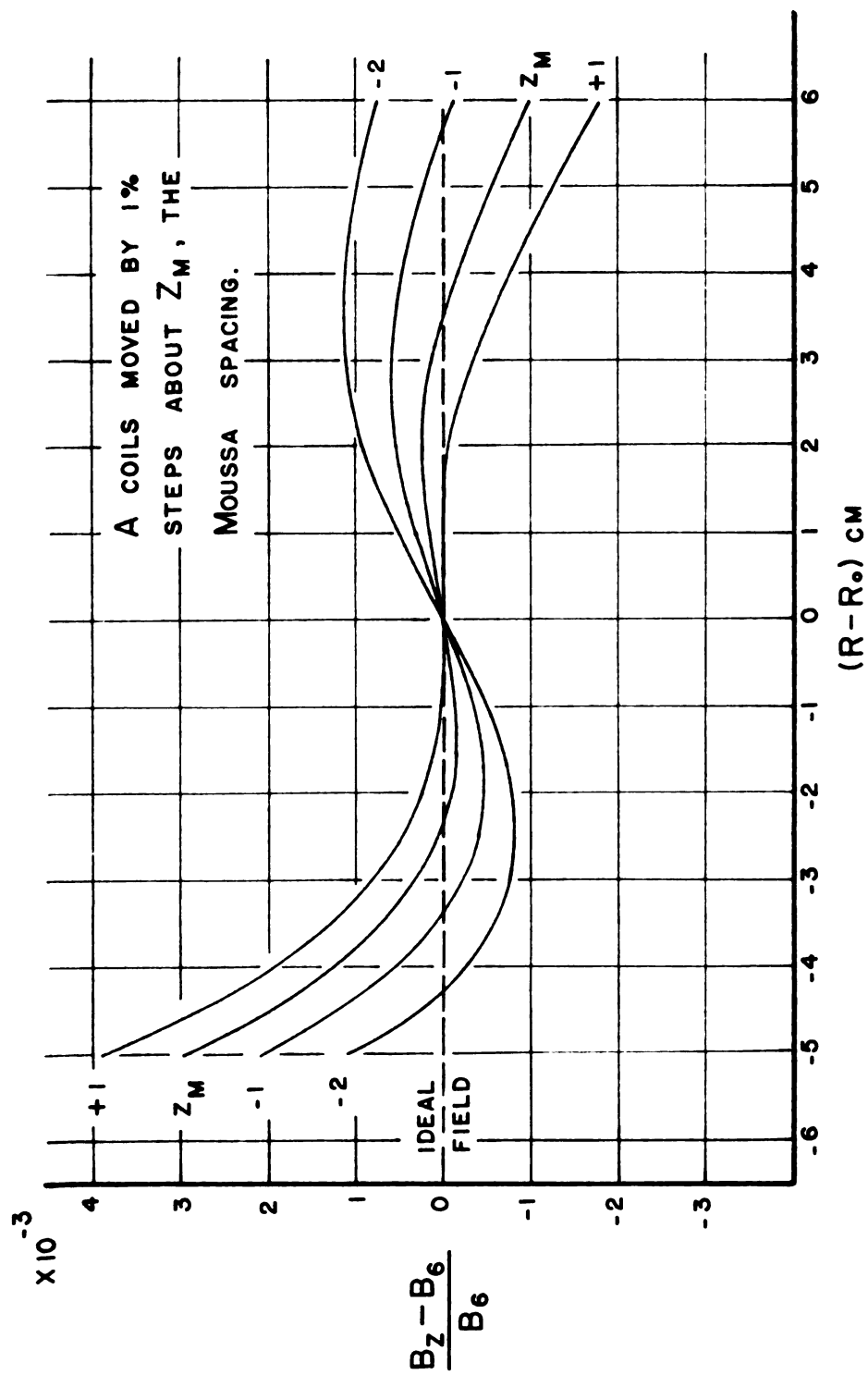


FIGURE 47. DEVIATION OF TOTAL AXIAL FIELD FROM IDEAL SIXTH ORDER FIELD.

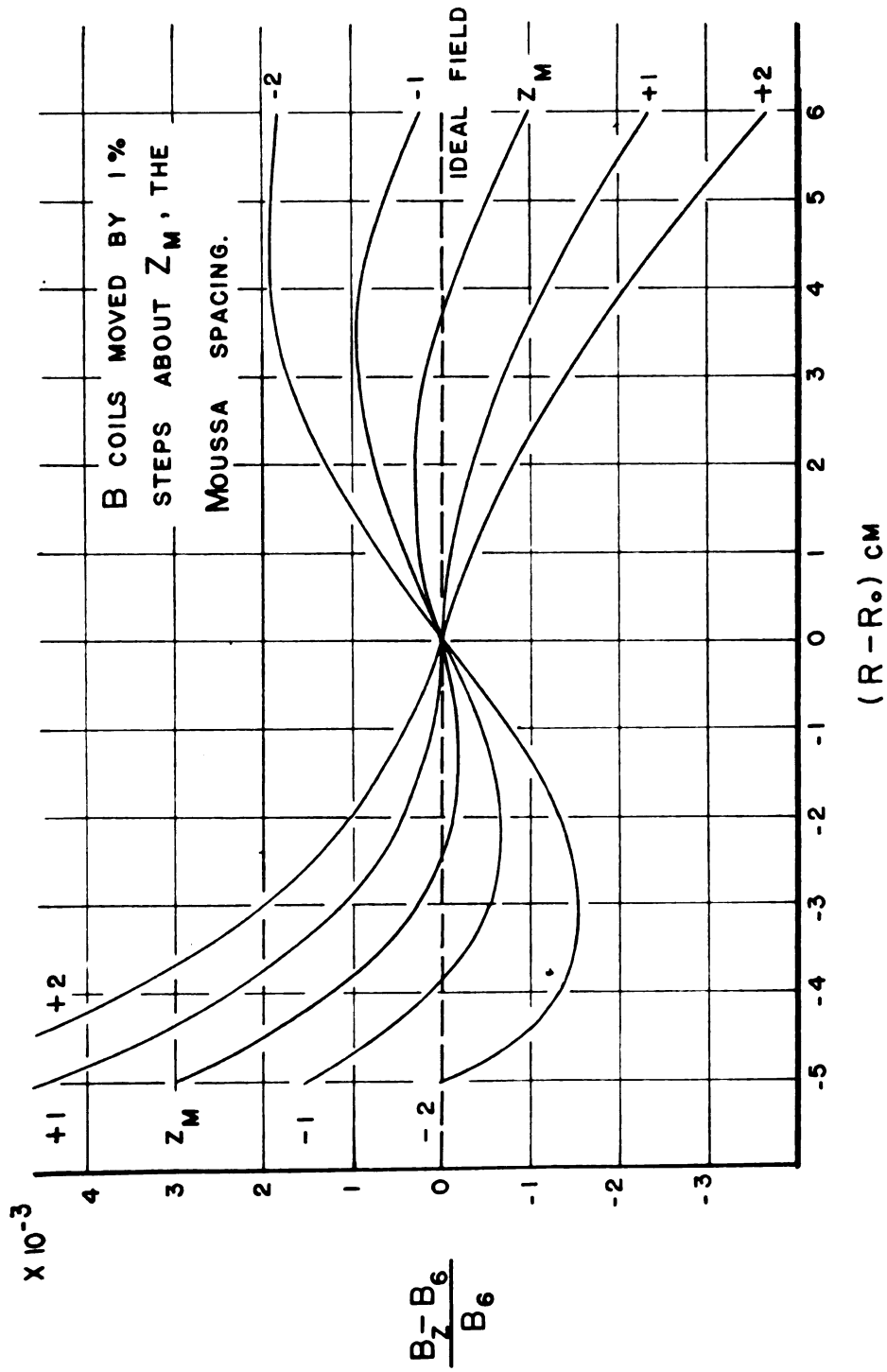


FIGURE 48. DEVIATION OF TOTAL AXIAL FIELD FROM IDEAL SIXTH ORDER FIELD.

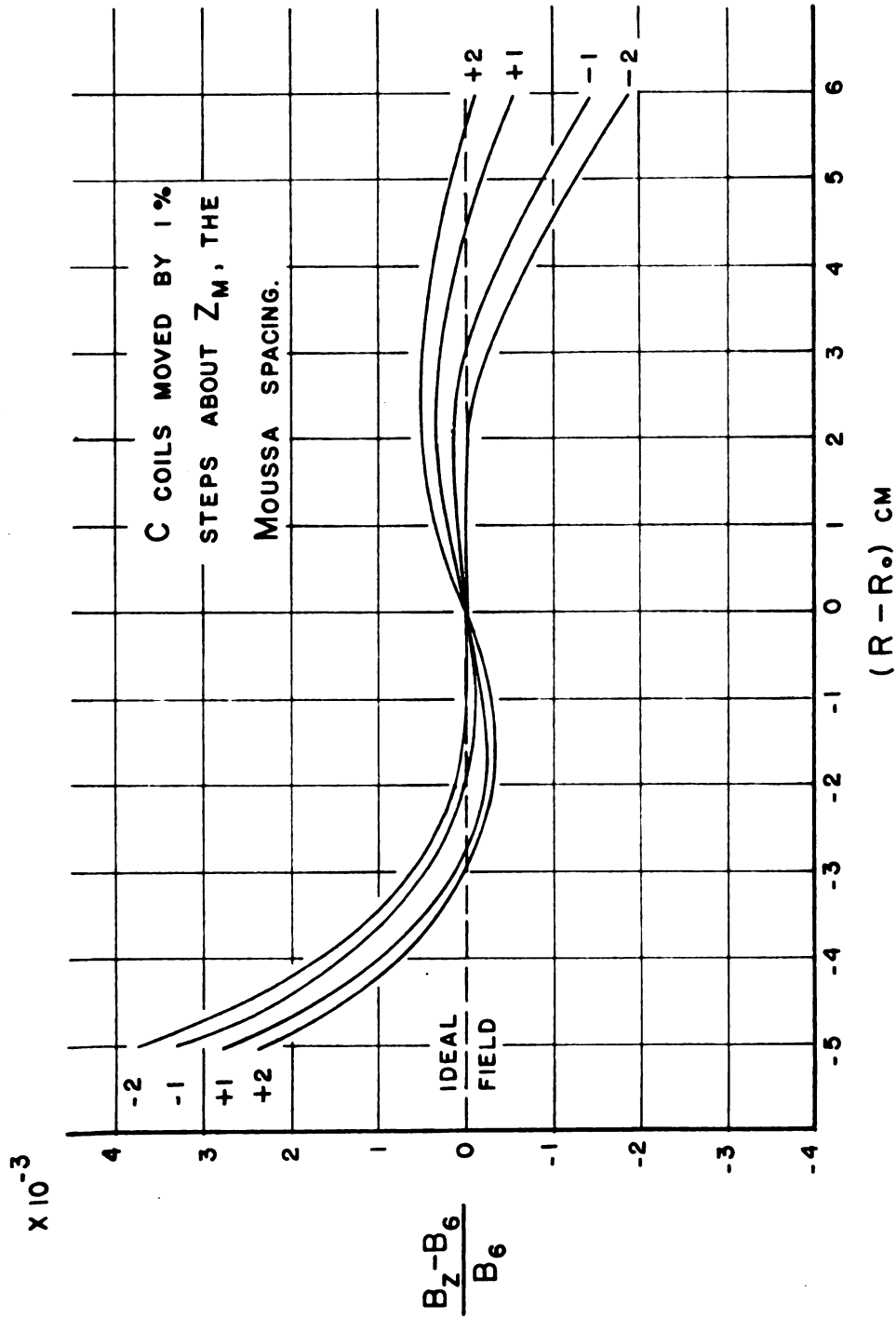


FIGURE 49. DEVIATION OF TOTAL AXIAL FIELD FROM IDEAL SIXTH ORDER FIELD.



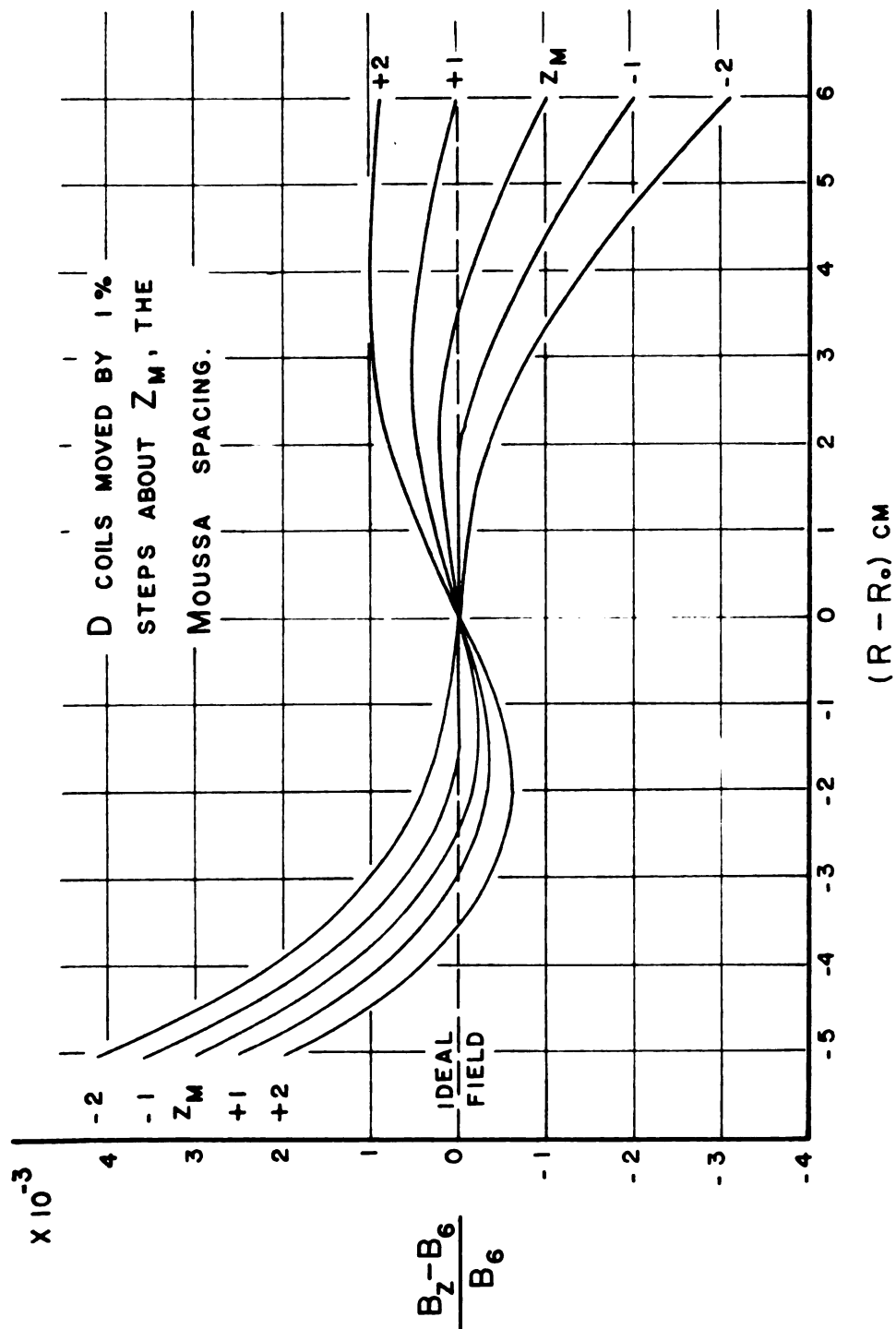


FIGURE 50. DEVIATION OF TOTAL AXIAL FIELD FROM IDEAL SIXTH ORDER FIELD.

We should thus choose a curve that has an inflection point at the mean radius and is most nearly flat in its vicinity. Study of the curves and the numerical data from the computer showed that one of the best curves was obtained when the D coils were moved in (toward the  $z = 0$  plane) by one percent. This position was therefore taken as the second departure point for further computations.

During the second phase of the calculations the radial component of the field was examined and corrected again, and the fitting to a sixth order field was repeated. The calculation did not yield an appreciable difference from the one percent shift of the D coils, or a significant improvement in the radial field.

The final spacing of the median planes of the coils used in the final alignment of the spectrometer is shown in Table IV.

TABLE IV. Axial Spacing of the Focusing Coils

Coil pair	Spacing from $z=0$ plane (cm)
$A_u$	32.863
$A_l$	32.863
$B_u$	25.807
$B_l$	25.806
$C_u$	14.745
$C_l$	14.707
$D_u$	9.917
$D_l$	9.959

### 7.3 Alignment of the Spectrometer

The focusing coils and the spectrometer tank are mounted on three threaded mounting posts. (These can be seen in Figure 5, the photograph of the machine.) Preliminary to the alignment procedure the tank was leveled by use of a high sensitivity spirit level. Measurements were taken around the circumference of the tank mounting flange and the unavoidable undulations allowed for in the leveling process. Micrometer readings of the flange then established the position of the median plane of the instrument.

Measurements previously performed on the focusing coils have established the dimensions of the windings, and thus the distances from the equivalent filaments representing the coils could be transferred to the outside of the coils with a fair degree of precision. The cleaned edge of the outermost turn of copper was used as a measuring position.

A little experimenting has shown that to align the coils by fixing the distances between the mounts at three or more points around the circumference would be folly, as the mounts were somewhat wavy. Any method of using shims of Johannsen blocks also had to be rejected due to the varied diameters of the coils and the inaccessibility of some of the measuring positions. The coils were finally aligned by use of a precision cathetometer capable of 0.01 mm resolution. Some compromise had to be made in the number of positions by which the coils would be set. Finally three

positions were chosen as near as possible to the adjusting screws. Three complete adjustment runs were made for all eight coils. The entire procedure took about two weeks to complete. The coils were adjusted to the nearest 0.01 mm, so it is hoped that the overall setting error of the centers of the coils does not exceed  $\pm 0.05$  mm at the measuring positions.

#### 7.4 Phasing of the Rotating Coils

During manufacture of the rotating coil system, the search coils were mounted nearly at right angles to each other, since the field of the spectrometer is vertical and that of the permanent magnet is horizontal. To bring the output signals of the coils into exact opposition, a fine adjustment is possible by means of tilting the permanent magnet. This adjustment can be made while the shaft is running. The procedure for phasing the coils is as follows. First, the magnetic field of the earth is compensated. Second, a stable current is sent through the focusing coils and the sum signal from the search coils is minimized by using the Dekavider. A better minimum can then be reached by the fine phase adjustment. This process is repeated while the sum signal is being amplified to a higher and higher level until the best minimum is reached for the maximum gain of the error signal amplifiers. The error signal loop is then phased for this particular current through the coils. The phase setting, unfortunately, is not unique for all current settings of the spectrometer. This seems

to be an inherent property of this type of a field measuring system. The inductances of the search coils, the capacitance to ground of the signal carrying cables and the load of the voltage divider form a LCR circuit. The phase of the signal changes with different positions of the divider wiper arm. Therefore slight adjustments of the mechanical phasing are necessary for different currents through the focusing coils. Fortunately, as can be shown by a simple calculation, below, a slight mechanical misphasing results in rather large changes in the phase of the sum signal. These changes are easily observable on an oscilloscope connected just after the demodulator. The normal signal should look approximately as a full-wave rectified waveform. A small phase mismatch will cause the cusps of the wave to move apart until, for signals  $90^\circ$  apart, it will resemble a series of S shapes. Phasing by observation of this waveform can be done to within  $5 \times 10^{-5}$  radians. A reversible motor connected to the magnet tilt mechanism permits this adjustment to be done remotely from the control room.

To examine the character of the error signal, let the output of the Dekavider be

$$E_D = (A + \Delta A) \sin(\omega t + \phi) \quad (141)$$

and the output of the spectrometer coil be

$$E_S = A \sin(\omega t + \pi) = -A \sin \omega t \quad (142)$$

The error signal is the sum signal

$$E_e = E_D + E_s \quad (143)$$

$$E_e = (A + \Delta A) \sin(\omega t + \phi) - A \sin \omega t$$

$$E_e = (A \cos \phi + \Delta A \cos \phi - A) \sin \omega t + \\ + (A \sin \phi + \Delta A \sin \phi) \cos \omega t \quad (144)$$

Since  $\phi$  and  $\Delta A$  are small, the first order terms in  $\phi$  and  $\Delta A$  give:

$$E_e \approx \Delta A \sin \omega t + A \phi \cos \omega t \quad (145)$$

Thus for non-zero values of  $\phi$ , the mechanical phase mismatch, the amplitude  $A\phi$  can become rapidly larger than  $\Delta A$  and a large signal will appear 90° out of phase with the desired error signal. Since, however, the demodulator output is proportional to  $\cos \Theta$ , the electrical phase angle between the error and the reference signals, it will tend to discriminate against the  $A\phi \cos \omega t$  part of the error signal and the power supply will still regulate even if this signal is fairly large. Regulation will begin to deteriorate when the cosine signal starts to saturate the error signal amplifiers, thus reducing their sensitivity to the error signal proper.

Given pure sinewave signals and a perfect adjustment of the relative phases of the reference and error signals, the field output of the supply will be independent

of small mechanical phase shifts. In a real system, however, a small  $\Theta$  always exists. Therefore, the output of the demodulator is slightly sensitive to the  $A\phi \cos \omega t$  part of  $E_e$ . The contribution of this part either adds or subtracts from the real error signal depending on the sign of  $\phi$ , causing focusing field changes dependent on  $\phi$ . One would expect the magnetic field to change fairly rapidly for  $\phi$  large and very slowly in the region where  $\phi$  is near zero. This behavior has been observed.

## CHAPTER 8

### COUNTER WINDOW AND SOURCE PREPARATION

#### 8.1 Counter Window Preparation

The side window Geiger-Mueller counter used on the spectrometer requires windows in the shape of long rectangular slits. The slits are milled in "window plates" that are demountable to facilitate window changes during an experimental run with the spectrometer. The dimensions of the windows vary according to the size of the source used in the spectrometer and the resolution required. As a rule, the width of the window is chosen to be the same as the width of the source. The range of sizes is approximately 0.25 to 4 mm wide by 15 to 30 mm long. The thickness of a counter window, measured in micrograms per square centimeter, will vary according to the energy range of the electrons under observation from about  $5 \text{ ug/cm}^2$  for electron energies of a few kilovolts to several hundred  $\text{ug/cm}^2$  for energies greater than 0.1 Mev. The window thickness is chosen to have nearly 100% transmission for the lowest anticipated electron energy. Usually, a choice is made by following the results of Lane and Zaffarano<sup>42</sup> who treat electron transmission by thin films in some detail.

The counter window is usually made of a thin organic film, and except for the very low energy electrons, is self



supporting under the 6 cm of mercury counter gas pressure. Only windows that are wider than 1 mm and thinner than about  $15 \text{ ug/cm}^2$  need additional support. This is usually provided by soft soldering a fine copper mesh\* over the counter plate window slit. The mesh is electro-formed from copper foil and is available in several sizes from 50 to 1000 lines per inch. The maximum transmission for a mesh of 250 lines per inch is 70%. The material, copper about 0.001 inch thick, is opaque to electrons having energies up to 130 Kev.

We have also successfully supported thin windows by soldering a loose grid of 0.001 inch or 0.002 inch stainless steel wire across the slit of the window.

The technique of preparation of very thin windows has been studied in some detail by Smith<sup>43</sup> and Burford<sup>44</sup> at Vanderbilt University. Their findings indicate that the thinnest windows can most reliably be made of collodion, non-flexible U.S.P. The second best material is Zapon. Success in the actual preparation of thin windows that are free of leaks depends to a large degree on the manual dexterity and luck of the individual experimenter and it is the firm belief of the author that in this field of endeavor experience is indeed the best teacher. Thus only a general outline of the preparation method is presented here.

First, a solution of collodion in amyl acetate is prepared. This can be done in two ways. Either stock (ether

---

\*Buckbee Myers Company, St. Paul, Minnesota.

solution) collodion is directly mixed with amyl acetate, or the collodion can be dried first and then dissolved. There is no conclusive evidence to show one way preferable to the other. The total volume of the prepared solution should be small, say 10 ml. or so, since once prepared the solution will age in the course of a few days, gradually deteriorating to the extent that thin windows can no longer be made. A few dozen drops of the solution are then placed on a weighed microscope slide, dried, and reweighed, giving the weight per drop.

The films are made by allowing a drop of the solution to spread on the surface of water. When the amyl acetate solvent evaporates, the film can be picked up by a wire frame as a double layer and transferred to the window plate. Usually, multiple layers are used for counter windows, the layers being oriented at different directions to reduce possibility of window rupture by strains "frozen" in the individual layers. Normally no special cementing procedure is used to attach the windows to the window plate. The films are laid down wet, in quick succession, and in drying seem to attach themselves to the plate quite effectively. The overall window thickness is estimated by knowing the approximate area over which a single drop of solution will spread and the weight per drop.

Normally, room temperature tap water is used. However, if the hardness of the water is such that sediment stains show on the finished window, one should use distilled

water since the sediment grains will cause rupture of the window as soon as gas pressure is applied to it. The surface of the water must be kept very clean, otherwise the solution will not spread properly resulting in very non-uniform layers. Such films are very susceptible to strains and besides that, non-uniform windows are undesirable. Aside from this, the chief hazards are dust in the atmosphere, excessive humidity and lack of patience.

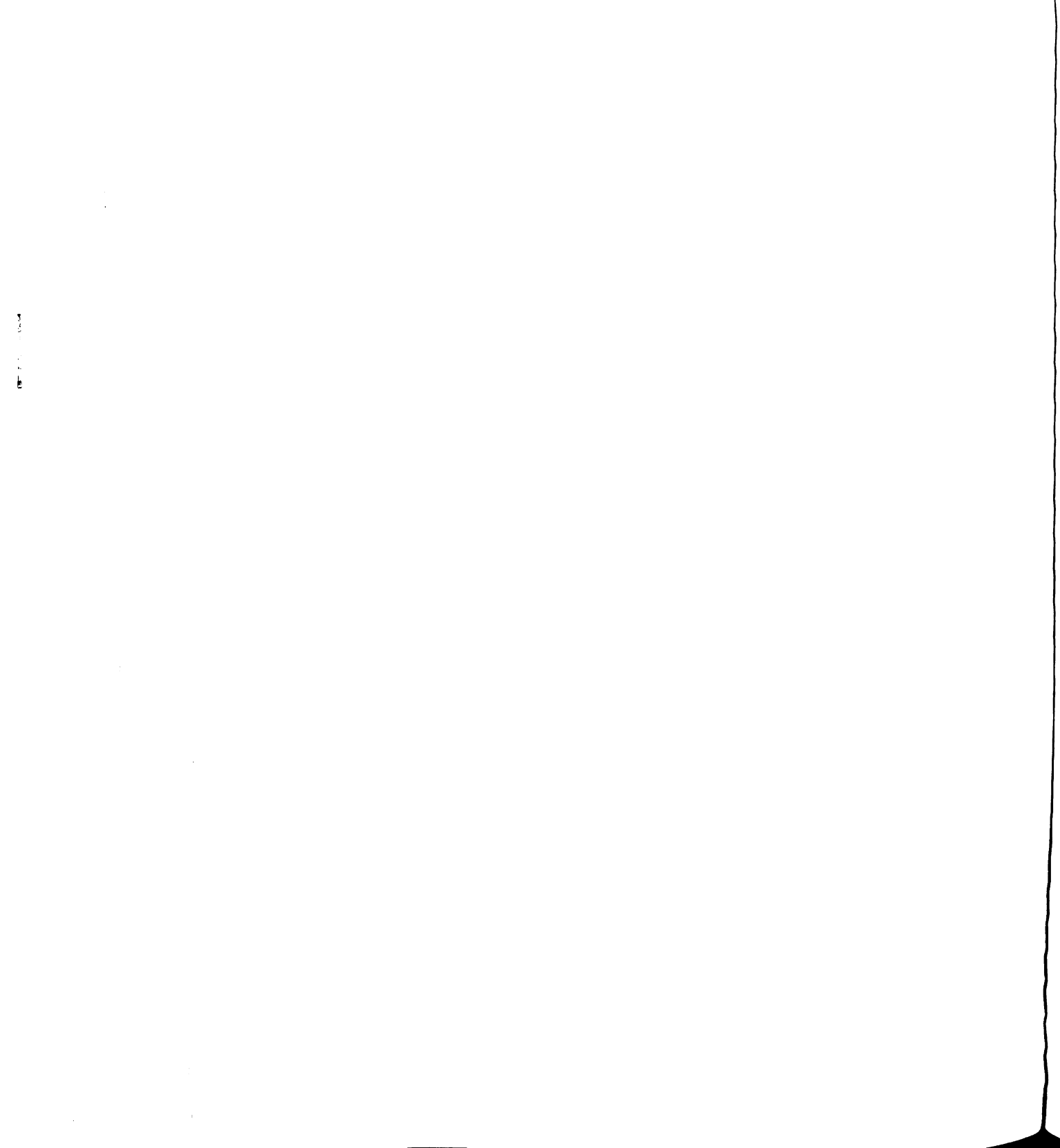
Although thin collodion windows are relatively easy to make, the author feels that there is another avenue of approach to the counter window problem which may give promising results. Many workers<sup>45,46,47,48</sup> have prepared self supporting films of inorganic oxides, such as aluminum oxide, and of pure carbon. Results of these papers show that aluminum oxide films can be prepared down to about  $10-15 \text{ ug/cm}^2$  and if the span of the film is small, can be expected to support counter gas pressure without additional reinforcement. Carbon films, which have the additional advantage of being electrically conducting, have been prepared in varying thicknesses down to  $4 \text{ ug/cm}^2$ .<sup>49,50</sup> So far no reports have been found in literature about use of such films as counter windows.

## 8.2 Source Preparation

For the investigation of very low energy beta spectra the preparation of the source is of major concern since any non-uniformity of the source or its excessive thickness will cause distortions of the spectrum. Self absorption in the

source itself and backscattering caused by the source support both contribute to these distortions.

The requirement of a source support or substrate that would give low backscattering from the source is a difficult one, for it means essentially that only materials of low  $Z$  should be used. A further restriction is imposed by requiring that the material be electrically conducting to avoid charging of the source and the consequent energy shift of the observed spectrum. Light metals are, as a rule, not suitable by themselves as they will not form self supporting films in the thickness range that is necessary for low energy beta spectroscopic work, namely 5 to 50  $\mu\text{g}/\text{cm}^2$ . Organic films are very easy to prepare in this range of thickness but are non-conducting. They require a layer of metal to be evaporated or otherwise deposited on them before a source can be placed on them. Thus part of their initial advantage is lost in the process. Furthermore, they can withstand only moderate temperatures, such as may occur during vacuum evaporation, and tend to break easily. In spite of all these disadvantages, metallized organic films are the most widely used source backings, primarily due to ease of their preparation. The most common of these are films made of formvar with a few micrograms of aluminum evaporated on them. Their total thickness can be as low as 15-20  $\mu\text{g}/\text{cm}^2$ . Most of the sources used in the M.S.U. spectrometer are made on such backings. The most promising material for source backings would be carbon in the form



of self supporting foils. As reported in the preceding section, films as thin as  $4 \text{ ug/cm}^2$  have been made. Their manufacture does, however, present some difficulties. These are being studied at present and it is hoped to use these films in the future. A survey of film making procedures can be found in a paper by Parker et al.<sup>51</sup> and the reader is referred there for description of the experimental techniques.

The preparation of the source itself can be carried out in a variety of ways, the most important and widely used of which are: vacuum evaporation, electro-deposition and ion ejection methods. The use of the isotopic mass separator is becoming more common as more and more institutions are gaining access to these machines. Isotope separated sources are, by and large, of the highest obtainable quality in terms of thickness and uniformity of the active deposit. Source preparation on this project is done almost exclusively by the method of vacuum evaporation. A brief description of the equipment and techniques follows.

(a) The evaporator

For a project that concerns itself with a large variety of radioisotopes and where the purity of the sources under study is important, it is desirable to have some means of preparation of uncontaminated sources. An evaporator was therefore designed and built which is of very simple, almost primitive construction and very inexpensive and therefore disposable. A cross-sectional view of the evaporator, Figure 51, shows its essential features. A brass base plate

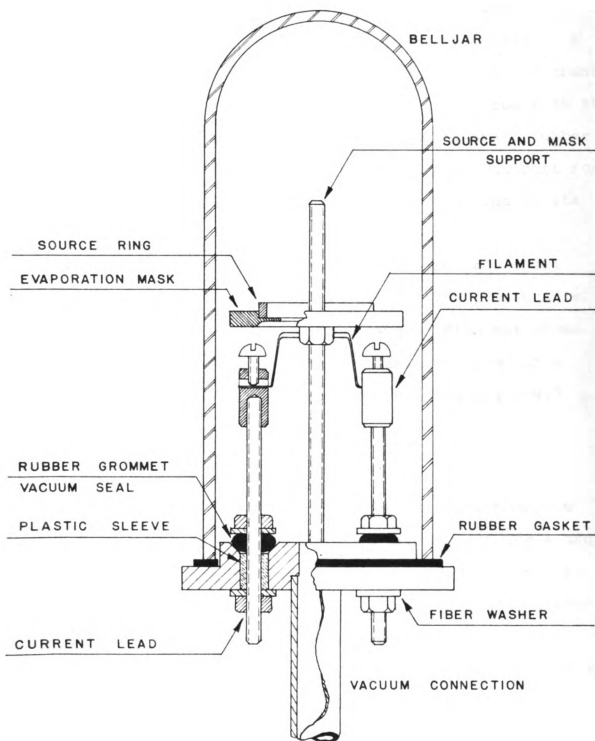


FIGURE 51. SOURCE EVAPORATOR.





forms the main platform. A half inch vacuum pipe is soldered to it. The pipe contains a small quantity of glass wool to trap radioactive materials coming from the evaporator. A sawed off large size test tube forms the bell-jar. Current leads are brought through the base plate, insulated from it by plastic spacers and sealed vacuum tight by small rubber grommets. Two threaded rods with nuts form the support for an evaporating mask which holds the source backing in its mount.

The evaporator is evacuated by means of a small diffusion and a fore pump vacuum system. The pressure is monitored on a thermocouple vacuum gauge. Filament power is provided by a 20 ampere 220 volt variac coupled to a step-down transformer. The outputs available are 0-4.5 volts and 0-46.5 volts.

#### (b) Preparation of source backings

The organic film backings that are in common use on the spectrometer are made of formvar, by allowing a drop of solution\* of known mass per drop to spread on the surface of lukewarm water. The source holding rings are covered by several double layers of this film, left to dry and then covered by a thin layer of vacuum evaporated aluminum to make them conducting. The aluminum evaporation is carried out in a large evaporator, allowing the treatment

---

\*The formvar solution is prepared by dissolving approximately 300 milligrams of formvar in 15 milliliters of ethylene dichloride and then adding 175 drops of methyl alcohol.

of about a dozen source rings at a time.

(c) Preparation of thin sources

The evaporator uses filaments in the shape of 1/8 inch wide ribbon. The filament material most commonly used is platinum, although for some materials, such as tin, tantalum is preferred. The filament is bent into a trough shape to allow a certain amount of "focusing" during evaporation. The open side of the trough is then placed very close to the underside of the source defining mask, which serves also as a holder for the source ring and backing. The efficiency of the evaporator depends on the distance of the filament from the mask and the size of the slit in the mask. Normally the source making procedure is as follows: A quantity of radioactive material is placed on the filament and left to dry if it is in the form of a solution. For some isotopes it may be necessary to dry the filament in an inert atmosphere to prevent the formation of non-volatile oxides. A series of evaporations is then carried out. The active material is deposited on aluminum foils. After each step of the multiple evaporation procedure the foils are counted. The results of such "differential evaporation" yield a curve of evaporation rate versus current through the filament, and also determine the presence of inactive low boiling point contaminants that must be eliminated from the actual source if it is to be kept thin. After this procedure has been completed, the filament is cleaned by flashing it to a high temperature and then

reloaded. After drying, any present contaminants are first boiled off onto a blank foil. Next, the mask and source ring are inserted and the source is made. The final thickness of the source depends chiefly on the evaporator efficiency for that particular isotope and on the amount of material that is loaded onto the filament. Typically the efficiency runs from about one to ten percent.

## CHAPTER 9

### PERFORMANCE OF THE SPECTROMETER

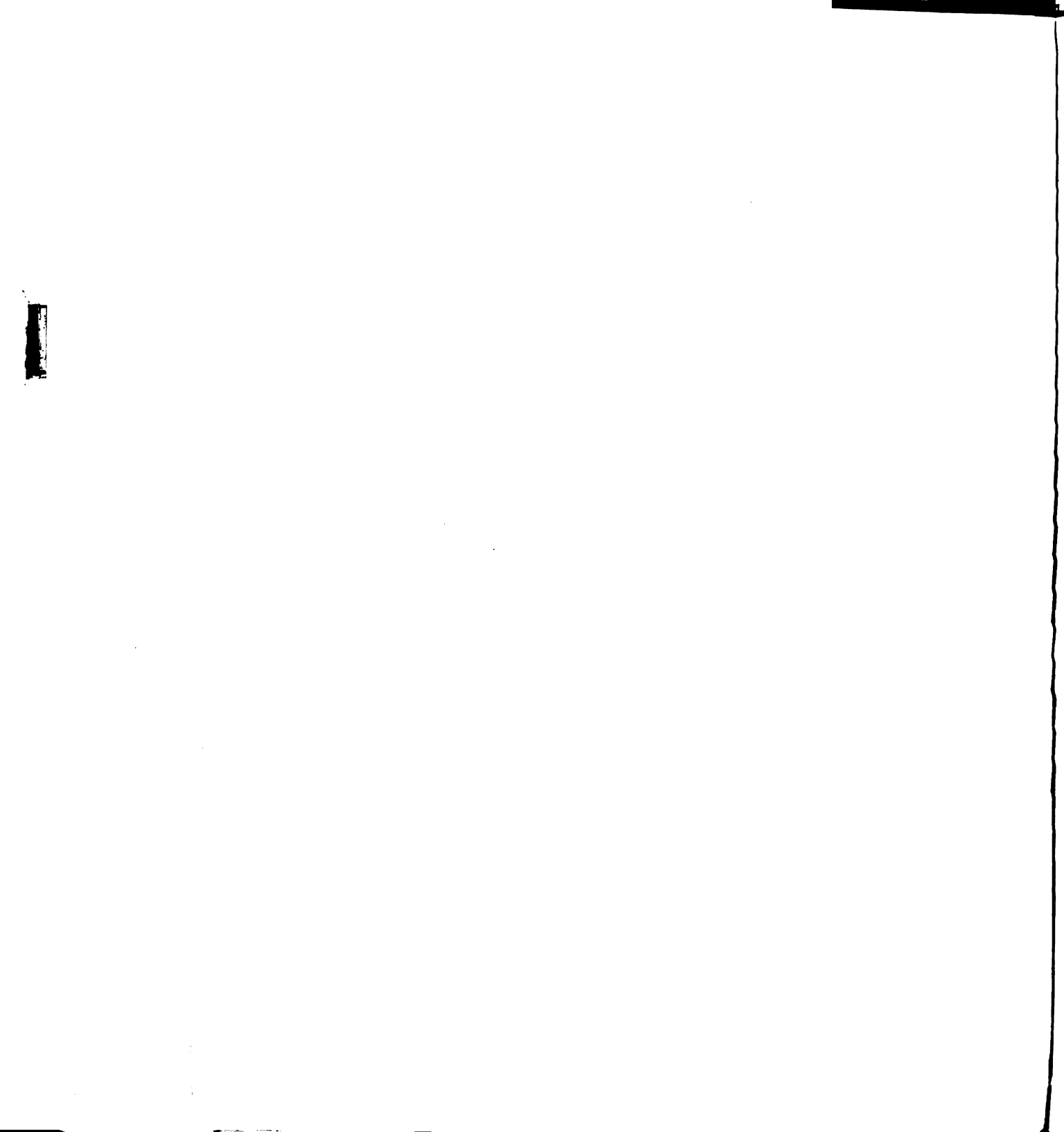
#### THE CONVERSION ELECTRON SPECTRUM OF Cs - Ba 137

##### 9.1 Introduction

Preliminary runs with the spectrometer gave us an indication that the focusing field shape was quite good, particularly near the mean orbit. Resolution for conversion electron lines, measured as the full width at half maximum of the lines, was near the theoretical value.<sup>13</sup> Comparison with the Vanderbilt spectrometer showed that for any given baffle opening we could do better in resolution by approximately a factor of two to four.

Most of the preliminary runs and all of the stability runs were done using the internal conversion electrons from Cs-Ba<sup>137</sup>, which has the advantage of long half-life ( $\sim 30$  years) and is obtainable carrier-free from Oak Ridge National Laboratory. Sources are easily prepared from this material by thermal evaporation in vacuo.

To evaluate the high resolution capability of our spectrometer, we decided to attempt to resolve the L and M subshell lines in the conversion spectrum of this isotope. This experiment does present a severe test of the machine, as the  $L_I$ ,  $L_{II}$ ,  $L_{III}$  lines are spaced only slightly more than 0.04 percent apart in momentum.

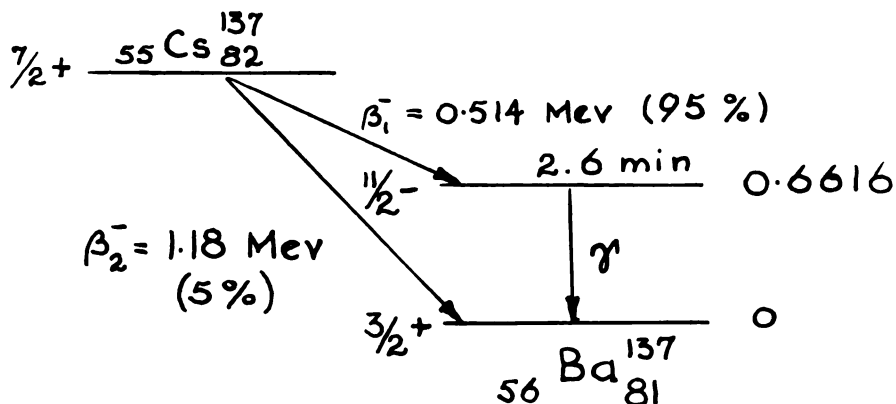


Shortly after the beginning of the experiment we found that Geiger et al.<sup>52</sup> have recently published results of just such a measurement. Their data were obtained on the Chalk River  $\propto \sqrt{2}$  spectrometer, using a momentum resolution of 0.02 percent. We, of course, could not better this resolution figure for any source of reasonable intensity (to do this the source width would have to be less than 0.1 mm). Nevertheless, we were still interested in comparing results and were anxious to find out how well we could do with a spectrometer whose total budget outlay was only 2-3 percent of the Canadian machine. The Chalk River group, by the way, did not report any M subshell results, so we can claim some small measure of originality there.

## 9.2 The Conversion Electron Spectrum of Cs-Ba<sup>137</sup>

A historical sketch of the internal conversion process is presented in the next chapter. The discussion here will be therefore restricted to the decay of Cs<sup>137</sup> and its daughter Ba<sup>137m</sup>.

The decay scheme is well known:



1

The two beta-ray components have been studied by Peacock and Mitchell,<sup>53</sup> Agnew,<sup>54</sup> Langer and Moffat,<sup>55</sup> Yoshizawa,<sup>56</sup> and others. Aside from the energies and intensities indicated on the decay scheme diagram, the results indicate that the 514 Kev beta transition has a unique first forbidden shape, while the 1180 Kev transition has a non-unique second forbidden shape.

The spins and parities of the levels in the  $\text{Ba}^{137\text{m}}$  daughter nucleus are quite well established as  $11/2 (-)$  for the excited state and  $3/2 (+)$  for the ground state. The transition therefore involves a spin change of four and a parity change, indicating a gamma ray of predominantly M4 multipolarity. Past measurements of the K conversion coefficient and of the  $K/\sum L$  conversion line intensity ratio, summarized below in Table V, confirm the transition as an M4, but leave open the question of possible admixture of E5. To resolve this question, we need data regarding the relative intensities of the  $L_I$ ,  $L_{II}$  and  $L_{III}$  conversion lines. The  $L_I/L_{II}$  and the  $L_I/L_{III}$  intensity ratios provide a sensitive test of the multipolarity of the transition. So far, only Geiger et al.<sup>52</sup> and the present work provide any measurements of the barium L subshell intensity ratios. The Canadian results and theoretical values obtained from Rose's<sup>73</sup> and Sliv and Band's<sup>74</sup> tables are shown in Table VI. Note that the experimental results are consistently higher than the theoretical values. The  $K/\sum L$ ,  $L_I/L_{II}$  and  $L_I/L_{III}$  will hence be below Rose's and Sliv's values. Geiger notes



TABLE V. The K Conversion Coefficients and the K/ $\Sigma$  L Line Intensity Ratios for Ba<sup>137m</sup>

K	K/ $\Sigma$ L	Reference
0.081 -----	-----	57
0.118 -----	-----	58
0.097 $\pm$ 0.003	-----	59
0.095 $\pm$ 0.005	-----	60
0.11 $\pm$ 0.01	6.0 $\pm$ 0.1	61
0.096 $\pm$ 0.005	4.6 $\pm$ 0.2	62
0.092 $\pm$ 0.006	5.8 $\pm$ 0.3	63
0.095 $\pm$ 0.008	-----	64
0.093 $\pm$ 0.018	-----	65
0.0976 $\pm$ 0.0055	5.66 $\pm$ 0.04	56
0.093 $\pm$ 0.006	-----	66
0.093 $\pm$ 0.005	-----	67
-----	5.5 ---	68
-----	5.43 $\pm$ 0.05	69
-----	5.2 $\pm$ 0.2	70
-----	5.9 $\pm$ 0.1	71
0.0918	5.66 (Rose, point nucleus) 72	
0.094	5.58 (Rose, finite nuc.) 73	
0.093	5.38 (Sliv) 74	

TABLE VI. Relative Conversion Line Intensities

Line	Geiger	Rose (M4)	Sliv (M4)
K	$1 \pm 0.02$	1	1
$\Sigma L$	$0.192 \pm 0.006$	0.179	0.186
$L_I$	$0.151 \pm 0.004$	0.143	0.148
$L_{II}$	$0.0222 \pm 0.0011$	0.0202	0.0207
$L_{III}$	$0.0189 \pm 0.0010$	0.0165	0.0171

this discrepancy and suggests about three percent admixture of E5 to bring the data into agreement. At the same time, however, he argues that such admixture is not very likely, since it would require an enhancement of the E5 component over the single particle rate (by about a factor of 50). He does not present any other explanation but mentions that presence of systematic errors could not be excluded. Our results, except for the  $K/\Sigma L$  ratio which falls very near the predicted value for pure M4 radiation, confirm Geiger's results. Our errors, however, are considerably larger due to poorer resolution and statistics.

### 9.3 The Experiment

#### (a) Source Preparation

The source was prepared by evaporation in vacuo. The evaporator filament was first thoroughly cleaned by flashing it repeatedly to yellow color for 5-10 second intervals. After cleaning, the filament was loaded with about

two drops of stock solution of carrier free  $\text{Cs}^{137}$  (obtained as  $\text{CsCl}$  in 1 N  $\text{HCl}$  from Oak Ridge National Laboratory) and dried with a heat lamp. A differential evaporation procedure was then carried out (see section 8.2, (c)) to determine low boiling point contaminants.

The preliminaries completed, the filament was cleaned again, reloaded, contaminants boiled off. The source backing ( $15 \text{ ug/cm}^2$  aluminized formvar film) and the source defining mask were placed in the evaporator and an evaporation was carried out. Due to the small size of the source defining slit,  $0.25 \text{ mm} \times 15 \text{ mm}$ , a total of fourteen evaporations had to be done onto a single source backing to obtain a source of usable intensity. Immediately after preparation, the source was barely visible to the naked eye. In the spectrometer no thickness effects could be seen on the  $\text{Ba}^{137} \text{ K}$  conversion line. The resolution obtained with this source was 0.047 percent (full width at half maximum).

#### (b) Data Collection

Several passes were made over the entire conversion spectrum, running both upward and downward in momentum. The spacing between successive points was 25 on the dekadider, corresponding to  $25/403000$  or 0.0062 percent in momentum on the K line. On the average, seven three-minute counts were taken at each point. About a dozen runs were made over the L and the M lines.

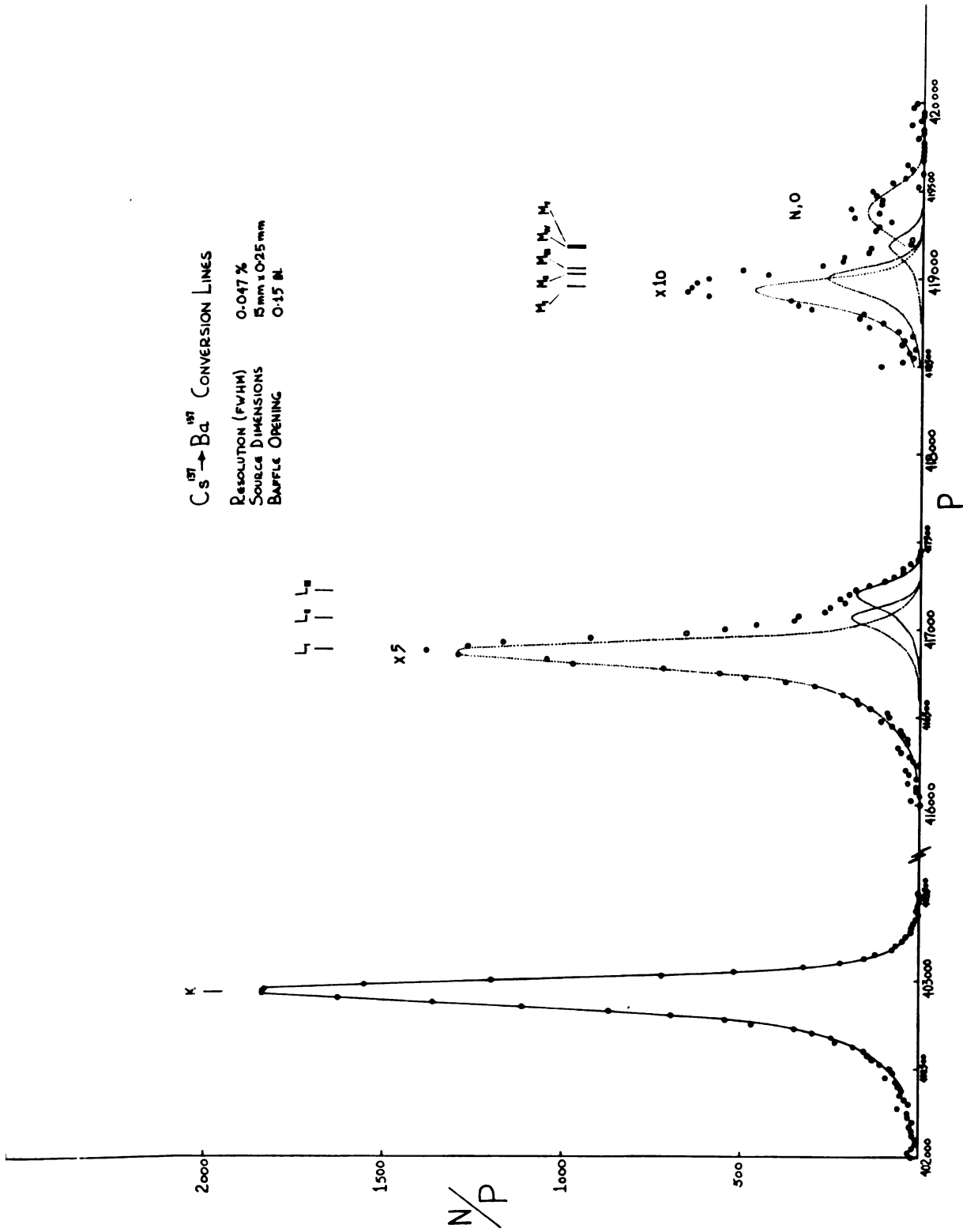
During the data run, which for the most part was

conducted on a 24 hour day basis, background and earth's field compensation readings were taken about once every eight hours. Usually one ten minute background count was taken and the shut-down time of the spectrometer used to reset the compensating field back to zero. In addition, to keep track of the spectrometer drifts, a preselected point on the upper sideband of the K conversion line (called by us the "calibration point") was checked for three 3-minute counts once every two hours.

### (c) Data Analysis

The first step in the treatment of the raw data was the subtraction of the background and the application of drift corrections. The background and the reference point counts were plotted against time, the graphs smoothed out somewhat and the corrections then read off to the nearest integral count, directly from the plots. It should be made clear at this point that the counts taken at the calibration point yield a very sensitive measure of the focusing field drift. In fact, the slope of the upper sideband of the K conversion line is so steep in this case that a change of one part in  $10^5$  in the field is easily detected as a counting rate shift of some ten percent (for a point halfway up the peak).

The drifts were corrected to the nearest 5 units in the last dekadiver place. All the run data were then collected together and all points were averaged around dekadiver settings spaced by 25 units. The plot, Figure 52,

Figure 52. Internal conversion lines of  $^{137}\text{Cs} - ^{137m}\text{Ba}$ .

represents these three minute averages divided by the dekaider setting to make the data suitable for relative intensity measurements.

The shape of the K conversion line was assumed as a standard for fitting the L and M subshell data. The  $L_I$ ,  $L_{II}$  and  $L_{III}$  lines could be fitted unambiguously. In the M group we could fit only  $M_I$ ,  $M_{II,III}$  and  $M_{IV,V}$ . From Figure 52 it can be seen that the second and third, and the fourth and fifth lines of the M shell are far too closely spaced to be resolved. We did, however, manage to separate the N+O shells from the M shell electrons. The fitting is shown in Figure 52 by dotted lines.

The errors in the present data are shown in the next section and are primarily due to statistics. They represent the latitude with which the individual lines may be fitted, while their sum remains within the probable error of the experimental points. It is also possible that the data contain systematic errors unknown to the experimenters.

#### 9.4 Results and Conclusions

The results of this experiment are shown in Figure 53 and in Table VII. The figure shows theoretical values of the conversion line intensity ratios, plotted against the energy of the transition. Both Rose's and Sliv's values are presented. The experimental values of Geiger et al. and of the present work are also indicated on the graph. Table VII summarizes the above information and adds our results for the M shell. It can be seen that our results

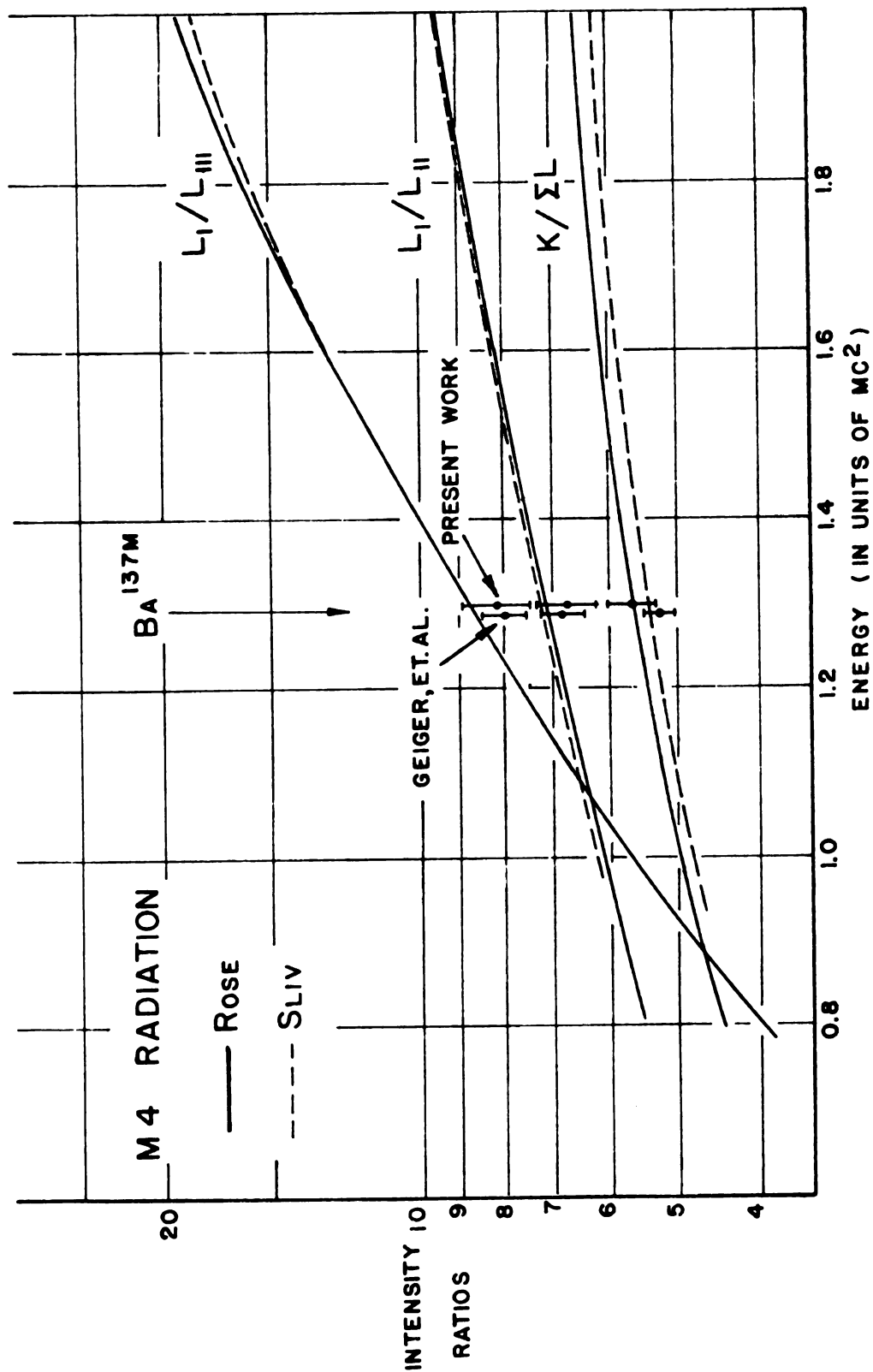


FIGURE 53. CONVERSION LINE INTENSITY RATIOS AS A FUNCTION OF TRANSITION ENERGY.

TABLE VII. Relative Intensities of Ba<sup>137m</sup> Conversion Lines

Line	Theory			Experiment
	Rose	Sliv	Geiger	Present work
K	1	1	$1 \pm 0.02$	$1 \pm 0.04$
L <sup>(a)</sup>	-----	-----	-----	$0.182 \pm 0.010$
$\Sigma L$ <sup>(b)</sup>	0.179	0.186	$0.192 \pm 0.006$	$0.178 \pm 0.010$
L <sub>I</sub>	0.143	0.148	$0.151 \pm 0.004$	$0.140 \pm 0.007$
L <sub>II</sub>	0.0202	0.0207	$0.0222 \pm 0.0011$	$0.0207 \pm 0.0046$
L <sub>III</sub>	0.0165	0.0171	$0.0189 \pm 0.0010$	$0.0171 \pm 0.0041$
M <sup>(a)</sup>	-----	-----	-----	$0.0411 \pm 0.0037$
$\Sigma M$ <sup>(b)</sup>	0.0745*	-----	-----	$0.0425 \pm 0.0040$
M <sub>I</sub>	0.0565*	-----	-----	$0.0233 \pm 0.0030$
M <sub>II,III</sub>	0.0200*	-----	-----	$0.0145 \pm 0.0020$
M <sub>IV,V</sub>	0.0002*	-----	-----	$0.0047 \pm 0.0016$
N + O	-----	-----	-----	$0.0095 \pm 0.0031$
K/L	-----	-----	-----	$5.51 \pm 0.36$
K/ $\Sigma L$	5.58	5.38	$5.21 \pm 0.16$	$5.63 \pm 0.38$
L <sub>I</sub> /L <sub>II</sub>	7.07	7.16	$6.80 \pm 0.38$	$6.75 \pm 0.55$
L <sub>I</sub> /L <sub>III</sub>	8.66	8.66	$7.97 \pm 0.47$	$8.14 \pm 0.74$

\*The theoretical values of the M line intensities were obtained by extrapolation from Z=65 and higher.

(a) Area under the experimental points for the entire shell.

(b) Sum of the areas of the fitted lines.



are in fairly good agreement with those of Geiger, particularly in the case of the L subshell intensity ratios.

In our case, the K/L ratio and the relative intensities of the  $L_I$ ,  $L_{II}$  and  $L_{III}$  lines are closer to the theoretically predicted values for pure M4 radiation. Geiger's values, on the other hand, are consistently high. We cannot draw any definite conclusions from this, however, as our results contain substantially larger errors and a glance at Table VII shows that there is a considerable amount of overlap in the results of the two experiments.

I feel that the agreement in the  $L_I/L_{II}$  and  $L_I/L_{III}$  ratios gives us a greater degree of confidence in saying that a small amount of E5 admixture exists in this decay. We have to qualify this conclusion, however, that it still may not be so in case that both Chalk River and M.S.U. experiments suffer from similar systematic errors. Perhaps the experiment ought to be done on a high resolution machine of different type, such as the uniform field solenoidal spectrometer of Jungerman.<sup>14</sup>

The M shell results are new. Unfortunately the relative line intensities cannot be readily compared with theory, as Rose<sup>73</sup> calculates the M shell and subshell conversion coefficients only for unscreened point nucleus. The theoretical values of the conversion coefficients are therefore likely to be high. Only the total M shell conversion coefficient is available near the desired  $Z = 56$  value. The M subshell coefficients must be obtained by

extrapolation, since the tabulation covers only  $Z \geq 65$ , with  $\Delta Z = 5$ . Such extrapolation has been carried out. The errors in the individual M subshell coefficients may be high, but the general agreement of the total M conversion coefficient with the sum of the extrapolated values indicates that it should be less than a factor of two for the  $M_I$  line and possibly also the  $M_{II,III}$  line. The  $M_{IV,V}$  line is much more uncertain, perhaps as much as an order of magnitude.

Looking at Table VII, it is clear that the theoretical line intensities do not agree with experimental results. It should be noted, however, that the experimental values obtained for the M,  $M_I$  and the  $M_{II,III}$  lines are consistently low by roughly a factor of two. The drastic disagreement in the  $M_{IV,V}$  line can be easily accounted for by assuming a greater overlap of this line with the conversion line group arising from the N + O shells. In this work the group was separated only by an empirical guess--the statistics in this region are very poor.

These results are generally in agreement with the M subshell relative line intensities obtained by Bäckström, Bergman and Burde<sup>75</sup> for the 50 Kev (M1) and the 158 Kev (E2) transitions in  $Hg^{199}$ . The L/M ratios are quite similar:

		Multipolarity	L/M (theory)	L/M (exper.)
$Hg^{199}$	50 Kev	M 1	2.11	3.97
$Hg^{199}$	158 Kev	E 2	2.06	3.85
$Ba^{137m}$	662 Kev	M 4	2.40	4.43

In conclusion, it should be said that the spectrometer drifts proved to be sufficiently smooth that they could be well accounted for by the calibration point checks. At the present time, therefore, there is every reason to believe that with a sufficiently narrow and intense source, the spectrometer resolution could be brought down to the 0.01 percent level.

## CHAPTER 10

### THE CONVERSION ELECTRON SPECTRUM OF RADIUM D

#### 10.1 Introduction

A nucleus may decay from an excited state by the emission of electromagnetic radiation (gamma rays) or by a radiationless transition wherein the transition energy is transferred to one of the extranuclear electrons, ejecting it from the atom. This process is called internal conversion, the ejected electrons being the internal conversion electrons, or more simply but less precisely--conversion electrons. It is this electromagnetic interaction between the nucleus and its atomic electrons that allows zero angular momentum change nuclear transitions to proceed, although such transitions are strictly forbidden by the selection rules governing the emission of electromagnetic radiation.

As internal conversion and gamma ray emission are, in the majority of cases, competing processes, it is useful to define an internal conversion coefficient as the ratio of the number of electrons to the number of gamma quanta emitted per unit time for a given transition. The usefulness of the internal conversion coefficient stems from its dependence on the transition energy, the nuclear charge  $Z$ , the angular momentum change and the parity change

involved in the transition. The usefulness is further augmented by the coefficient's insensitivity to nuclear structure.

In the history of our understanding of the internal conversion process, Ellis<sup>76</sup> and Meitner<sup>77</sup> were the first investigators to give an empirically correct interpretation of the "line spectrum" of beta rays. Taylor and Mott<sup>78</sup> were the first to point out that the internal conversion process cannot be accounted for by photoelectric effect mechanisms, but has to be considered as a direct coupling of the electrons with the electromagnetic field of the nucleus. Taylor and Mott<sup>78</sup> and Hulme<sup>79</sup> also performed some of the earliest reasonably precise calculations of the internal conversion coefficients. The interim years since the nineteen thirties have seen the full development of the theory with the inclusion of complete relativistic treatment of the process, magnetic and screening effects<sup>80</sup> and finally allowances for finite nuclear size.<sup>81</sup>

In the post war years several sets of calculations based on approximate models were made, such as that of Gellman, et al.,<sup>107</sup> for example, who used a point nucleus and relativistic unscreened electrons. The first extensive set of tables was published by Rose, et al.,<sup>82</sup> in 1951. In these calculations the nucleus is still assumed to be a point and therefore no details of nuclear structure enter into these computations. The nucleus is assumed to be screened by the atomic electrons. As Rose pointed out

later,<sup>72</sup> such calculations lead to virtually exact results. Nuclear size, however, was found to play a more important part than originally thought. The point nucleus coefficients were found to be high by some 30-40 percent, particularly for the higher Z elements and for magnetic transitions.

Calculations of conversion coefficients with the finite size of the nucleus taken into account were first published by Sliv and Band<sup>81</sup> for a limited number of Z values and energies. Subsequently, extensive tables were prepared both by Sliv and Band<sup>74</sup> and by Rose.<sup>73</sup> The difference between these two compilations concerns the finite nucleus corrections. Sliv and Band use a special nuclear model which assumes that all nuclear currents flow on the surface of the nucleus. Rose, on the other hand, corrects the electron wave functions for finite nuclear size. The difference between the two sets of tables is approximately ten percent. Finite nuclear size effects lower the values of the conversion coefficients as compared to the point nucleus calculations, especially for magnetic multipole transitions and in the region of heavy elements. A further refinement, a method for correcting the calculations to take account of different nuclear models, has been worked out by Green and Rose.<sup>83</sup>

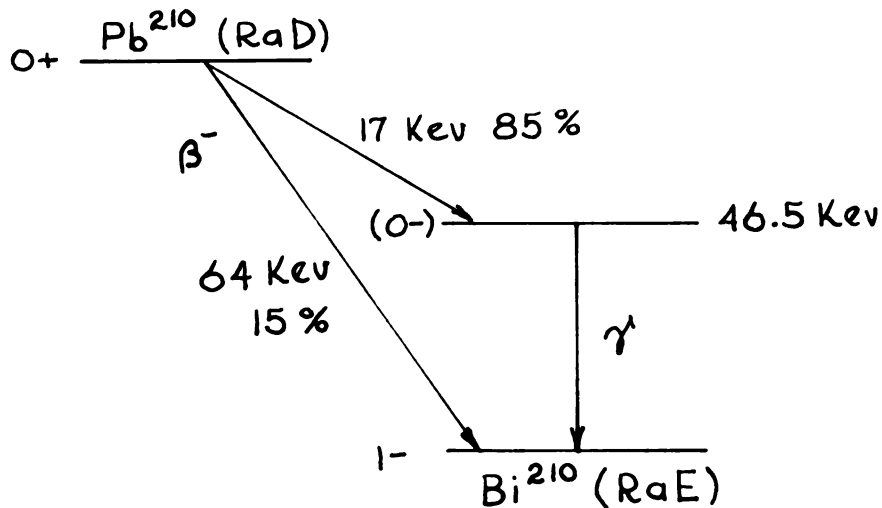
The validity of the finite nuclear size assumption and the nuclear structure corrections are supported by experimental evidence of Wapstra and Nijgh,<sup>84</sup> McGowan and Stelson,<sup>85</sup> Nordling, et al.,<sup>86</sup> Church and Weneser<sup>87</sup> and

others. The dependence of the internal conversion coefficients on the assumed nuclear model is a mixed blessing, for although it allows new information to be gained concerning the nuclear levels involved in a transition, the conversion coefficients are no longer as perfectly clear cut a tool for the determination of the multipolarities of the competing gamma radiations as was originally thought. Nevertheless, this does not destroy the value of the coefficients, for their sensitivity to nuclear structure is low, of the order of a few percent, whereas their variation with energy, multipolarity of the transition and the  $Z$  value is quite large.<sup>88</sup>

## 10.2 The Decay of Radium D

The history of investigations concerning the decay of Ra D presents a rather curious picture. From its discovery at the turn of the twentieth century until 1939 its decay was thought to be a simple beta-ray decay followed by a single gamma ray. Then in subsequent years the decay scheme gradually grew in complexity, reaching a peak in 1949 when seven distinct gamma rays were thought to be present. After this time the number of gamma rays attributed to radium D began to diminish as more carefully performed experiments and improvements in the experimental technique identified many of them as spurious (for example: fluorescent X-rays from the walls of the counters used). At present we are essentially back to the simple decay of

the nineteen thirties, with the exception of having two beta transitions instead of the original one. The contemporary decay scheme is:



The low energy of the predominant beta ray presents a rather difficult measurement problem. The first definitive measurements were done by Richardson and Leigh-Smith<sup>89</sup> who give two possible values for its end point energy: 16 Kev by fitting the spectrum to Fermi's shape predictions, assuming a  $(0,0)$  transition, or 24 Kev by assuming a  $(0,1)$  transition and fitting the shape to Konopinsky's shape predictions. Lee and Libby<sup>90</sup> used magnetic deflection methods and obtained  $25.5 \pm 1$  Kev for the end point energy of the beta spectrum. Kinsey<sup>91</sup> in 1948 and Cranberg<sup>92</sup> in 1950 suggested that there may be branching in the beta decay, and estimated the two components to have end point energies of 15 Kev and 60 Kev. Considering that at that time the 64 Kev beta ray had not been observed yet, the prediction



was remarkably good. Insch, Balfour and Curran<sup>93</sup> measured the end point energy of the low energy beta spectrum as  $18 \pm 2.5$  Kev and determined the disintegration energy of radium D as  $64.5 \pm 2.5$  Kev, using a proportional counter. Their analysis identifies the 18 Kev beta ray emission as allowed, unfavored, with log ft value of 5.5. They assume the 64.5 Kev beta transition to the ground state of Bi<sup>210</sup> to be absent, saying that if it exists at all, it will have low intensity.

Jaffe and Cohen<sup>94</sup> offer the first tentative experimental evidence of branching of the beta decay. Their results show the low energy beta ray end point to be  $16.7 \pm 1$  Kev. They conclude that at least ten percent of the decays proceed by a 55.6 Kev end point beta transition to a 7.8 Kev level of Bi<sup>210</sup>. In a later paper,<sup>95</sup> however, they report that the 7.8 Kev state of Bi<sup>210</sup> does not really exist, the "gamma ray" being actually a fluorescent X-ray of copper excited in the walls of the counter. Their final conclusion is that the evidence for the existence of a higher energy beta ray was inconclusive. The same year (1953) Wu, et al.,<sup>96</sup> suggest, still tentatively, that on the basis of measurements of the number of unconverted 46.5 Kev gamma rays per disintegration of the parent RaD, there may be  $8 \pm 5$  percent beta transitions proceeding to the ground state of Bi<sup>210</sup>.

The first definitive evidence of the existence of the higher energy component of the beta decay and a

measurement of its intensity were obtained by Stanners and Ross<sup>97</sup> in 1956, using electron sensitive emulsions impregnated with citrate of radium D. Their results show the 64 Kev component to have an intensity of  $15.5 \pm 3.5$  percent. In a later measurement Tousset and Moussa<sup>98</sup> obtained a branching of  $19 \pm 4\%$  and  $81 \pm 4\%$  for the high and low energy components respectively.

The values accepted at the present time by the compilers of nuclear data tables are  $15 \pm 4\%$  for the 64 Kev component and  $85 \pm 4\%$  for the 17 Kev component of the beta decay.

The study of the gamma rays following the decay of RaD presents an even more varied and interesting picture: Early investigators, between the years of 1912 and 1935, essentially agreed on the existence of one gamma ray of approximate energy of 47 Kev.<sup>90</sup> In 1939, however, Amaldi and Rasetti<sup>99</sup> reported an additional weak gamma ray with energy of 43 Kev. This experiment was repeated and expanded after the war in 1945 by Tsien<sup>100</sup> who reported six gamma rays. A crystal diffraction experiment by Frilley<sup>101</sup> likewise gave six gamma rays and suggested a seventh at 65 Kev. The energies, as reported by Tsien, were 46.7, 43, 37, 32, 23.2 and 7.3 Kev. A later study by Cork, et al.,<sup>102</sup> in which the gamma ray spectrum was studied via the observation of conversion electrons, is in direct conflict with the results of Tsien and Frilley, for it reports that there is no evidence of gamma rays other than the 47 Kev one.

The authors feel that any other gamma ray with intensity as low as one percent of the 47 Kev one would have been detected. On the other hand, Butt and Brodie,<sup>103</sup> while performing a similar experiment using a lens beta-ray spectrometer, conclude that at most 70 percent of the decays proceed via the 46.7 Kev transition. They suggest the existence of four other gamma rays having energies of 31.3, 23.2, 16.1 and 7.3 Kev. In 1953 Damon and Edwards<sup>104</sup> point out that, aside from the 46.5 Kev gamma ray, only one other could be found that gives rise to a weak conversion line and that conversion electrons from the other gamma rays have never been observed. Their measurements, using a brass proportional counter, verify the existence of the gamma rays reported by Tsien, except for the 7.8 Kev one which they suggest to be due to X-rays of copper in the walls of the counter. The gamma rays (and their intensities per hundred disintegrations) thought to be in existence at this time are:

46.7 $\pm$ 0.1 Kev	3.5 $\pm$ 0.4 %
41.5 $\pm$ 1 Kev	0.1 %
37.0 $\pm$ 0.5 Kev	0.1 %
30.7 $\pm$ 0.5 Kev	0.4 %
24 $\pm$ 0.5 Kev	0.3 or less %
16.1 $\pm$ 0.3 Kev	0.5 %

An extensive systematic study of the RaD gamma ray spectrum was undertaken in the same year (1953) by Wu, Boehm and Nagel.<sup>96</sup> They showed the  $7.3 \pm 0.7$  Kev line to be due to copper or nickel fluorescence radiation, by performing experiments with proportional counters made wholly of brass

and aluminum, and by backing the source with a copper sheet while using an all aluminum counter. The 7.3 Kev line appeared whenever copper or nickel were near the source, and was absent when the experiment was performed with an aluminum counter. The 23 Kev gamma line was identified as a pile-up effect of the L X-rays of Bi<sup>210</sup>. If the proportional counter registers two L X-rays as a single sum pulse the energy would be in the correct range, i.e., the sums  $L_{\alpha} + L_{\alpha}$ ,  $L_{\alpha} + L_{\beta}$  and  $L_{\beta} + L_{\beta}$  give energies in the range 22 to 26 Kev. The 16.1 Kev line is tentatively identified by Wu as the  $L\gamma$  X-ray line of Bi. The remaining lines, the 42.6, 37 and 31 Kev gamma rays were not resolved in this experiment due to their close proximity to the 46.5 Kev line and its escape peak at 34.2 Kev. From conversion electron studies, however, they place an upper limit on the intensity of all three of these lines as less than 0.5 percent. Thus Wu, et al., conclude that the 46.5 Kev line is the only gamma ray of significant intensity present in the decay of RaD, a conclusion which is also supported by the lack of conclusive evidence for the presence of conversion electrons for any of the other gamma transitions.

Subsequent work by Damon and Edwards<sup>105</sup> confirms the findings of Wu, et al., and a very carefully done experiment with freshly chromatographically separated carrier free sources of RaD by Fink, et al.,<sup>106</sup> shows that if other gamma rays exist their combined intensity would have to be

less than 0.2 percent of the 46.5 Kev photons.

The story has, therefore, come a full circle and the decay of RaD may once again be regarded to be simple.

### 10.3 The Conversion Electrons of Radium D

The first post-war investigator of the conversion electron spectrum of RaD was Cranberg,<sup>92</sup> who used a 180 degree spectrograph with calibrated electron sensitive emulsions. In his spectrum he does not resolve any of the subshell lines of the M, N and O shells and has some difficulty resolving the lines of the L shell. He measures the number of decays accompanied by L shell conversion as 54 percent. Using a value of 3.5 percent for the number of unconverted gamma rays, he obtains for the L shell conversion coefficient a value of 15.5. Cranberg also presents in this paper a brief summary of previous work dating from 1912 to 1926.

A summary of the results of this and other papers discussed in this section is presented in Table VIII at the end of the section.

Butt and Brodie<sup>103</sup> examined the conversion electrons from RaD by a lens spectrometer. Their resolution, however, was very poor. No L subshell structure is apparent in their spectrum, nor do they resolve the M, N, O shells. From their data they find  $46.7 \pm 4$  percent of the decays accompanied by L shell conversion, leading to the conversion coefficient value of 13.5. Their discussion leading to

the assignment of spins and parities to the various levels involved in the decay is rather interesting (though wrong). They suggest that since RaD and RaF are both even-even nuclei, with ground state spins  $0(+)$ , that the ground state of RaE ought to be  $2(+)$  on the basis of Gamow-Teller selection rules, taking the RaE beta spectrum as second forbidden beta decay. They assign  $1(+)$  to the excited state of RaE, which gives the 46.5 Kev gamma ray a  $\Delta l = 1$  and  $\Delta \pi$ , no, suggesting that M1 radiation should be in even competition with E2. Experimentally, though, they agree that the conversion coefficient  $\alpha_L = 13.5$  suggests a rather heavy contribution from the M1 part.

Butt and Brodie report no evidence for conversion lines other than those associated with the 46.5 Kev gamma ray.

As a part of their very thorough study of RaD, Wu, et al.,<sup>96</sup> include a magnetic analysis of its conversion electrons. The resolution is good enough to resolve the L subshell lines and at least partially resolve the M shell components. The experimental value of the conversion coefficient for the L shell is  $\alpha_L = 9.1$ . Wu compares this value with the theoretical conversion coefficient calculated by Gellman, et al.,<sup>107</sup> for an unscreened nucleus. Gellman's value is approximately 30, a considerable disagreement. Wu points out, however, that the line intensity ratios are in excellent agreement with Gellman's calculations. The results of the experiment are the following:

		$L_I$	$L_{II}$	$L_{III}$	$M_{I-III}$	$M_{IV-V}$	$N_{I-V}$	$N_{VI,VII+O_I}$
Wu		100	$7.5 \pm .5$	$0.7 \pm .3$	$25 \pm 2$	$0.6 \pm .2$	$7 \pm 1$	$0.7 \pm .3$
Gellman	M-1	100	8.5	0.11	----	-----	---	-----
	E-1	100	84.8	112	----	-----	---	-----
	E-2	100	3450	3450	----	-----	---	-----

Wu concludes that the 46.5 Kev gamma ray must be a magnetic dipole radiation.

In the discussion concerning the spins and parities of the levels involved in the decay Wu points out that the shell model predicts the 83rd proton of RaE to be in one of the states  $h_{9/2}$ ,  $f_{7/2}$  or  $p_{3/2}$ , all of which have odd parity, and the 127th neutron in  $i_{11/2}$ ,  $g_{9/2}$  or  $d_{5/2}$  whose parity is even. The ground state of RaE therefore has odd parity and, since RaF is an even-even nucleus with a ground state  $0(+)_{\text{g}}$ , the RaE beta decay must involve a parity change and should be first forbidden. If a  $0-0$ , "yes" type of transition is assumed for the 64 Kev beta transition of RaD to the ground state of RaE and also for the RaE beta decay, then the excited state of RaE should be  $1(-)$ . Wu continues that the other alternative is to assign to the ground state of RaE a spin value of 1. In that case the excited state could be either 0 or 2. She concludes that, although the  $ft$ -value for the low energy beta ray of RaD ( $10^5$ ) seems too short for a  $(0-2 \text{ "yes"})$  transition, there are not enough  $ft$ -values known for  $(0-0 \text{ "yes"})$  transitions to exclude the possibility of the  $2(-)$  assignment.

The problem of RaE decay was resolved by Plassmann

and Langer<sup>108</sup> in 1954. They report a direct measurement of the ground state spin of RaE of  $1(-)$  by K. F. Smith via a private communication.\* They fit the spectrum to a first forbidden shape. The current model of the RaD - RaE decay dates approximately from this time.

To continue with the history of the conversion line measurements: In 1953 Bashilov, et al.,<sup>109</sup> suggested, on the basis of his measurements, that the 46.5 Kev gamma ray is mostly of M-1 multipolarity with a small admixture of E-2.

In 1956, Fink, et al.,<sup>106</sup> obtained  $13.3 \pm 2$  for the L conversion coefficient and compared it to the point nucleus calculation of Rose:<sup>82</sup> 17.85 (for pure M-1) and the finite nuclear size calculations of Sliv,<sup>74,81</sup> which give 12.7, confirming the predominantly M-1 character of the transition.

Frilley and Valadares<sup>110</sup> used a photographic recording spectrograph of good resolving power and concluded, on the basis of Sliv's calculations and communications with M. E. Rose, that the 46.5 Kev gamma ray is a pure M-1 transition. On the other hand, Krause,<sup>111</sup> having determined the number of unconverted 46.5 Kev gamma rays as  $4.05 \pm 0.08$  percent, finds the L conversion coefficient to be  $\alpha_L = 15.6 \pm 0.8$  which is somewhat higher than the theoretical value for a finite nucleus and pure M-1 radiation (Rose

---

\*Another reference to Smith is made by Wu in Siegbahn's book (reference 13).



gives a value 13.3).

Lee<sup>112</sup> lists the relative intensities of the conversion lines in a RaD spectrum obtained on the Vanderbilt  $\pi\sqrt{2}$  spectrometer (the M shell is still unresolved) and, in addition, reports seeing the  $L_I$  and  $L_{II}$  conversion lines of a 31.3 Kev gamma ray for the first time.\*

Table VIII presents a summary of the RaD conversion line intensity data and, where available, the conversion coefficients.

#### 10.4 The Experiment

##### (a) Source Preparation

The source material was obtained from Atomic Energy of Canada, Limited, Ottawa, Canada, in the form of  $Pb^{210}$  metal plated onto a platinum substrate and contained one millicurie of RaD ( $Pb^{210}$ ). The source was prepared by the process of vacuum evaporation. Slivers cut from the platinum foil containing the source material were placed onto a ribbon filament and heated to boil off the lead deposit. Experience has shown that the boil-off is very rapid, even at relatively low temperatures. Some of the early attempts resulted in heavy contamination of all internal surfaces of the evaporator, probably due to such rapid evolution of lead vapor that the pumping system was not able to handle it. The source used in this experiment was prepared

---

\*There are some indications that the errors reported by Lee are rather optimistic.<sup>113</sup>

TABLE VIII. Summary of Rad Conversion Electron Data

Line	Relative Intensity									
	100	100	100	100	100	100	100	100	100	100
L <sub>I</sub>										100 $\pm$ 3.4
L <sub>II</sub>	9.0 $\pm$ 1.5	7.5 $\pm$ .5	15 $\pm$ 3	10.5	8.8	5.4 $\pm$ .3				11.1 $\pm$ 0.7
L <sub>III</sub>	1.9 $\pm$ 0.4	.7 $\pm$ .3	.86 $\pm$ .05	1.0	0.8	0.8 $\pm$ .2				.94 $\pm$ .28
M <sub>I</sub>	$\uparrow$	$\uparrow$	$\uparrow$	29.4	$\uparrow$	$\uparrow$	$\uparrow$			22.9 $\pm$ 0.7
M <sub>II</sub>		25 $\pm$ 2		3.2						2.3 $\pm$ 0.3
M <sub>III</sub>	29 $\pm$ 2	$\downarrow$	27 $\pm$ 3	0.3	24	23.8 $\pm$ .6	26.6			0.29 $\pm$ 0.22
M <sub>IV</sub>	$\downarrow$	$\uparrow$	$\downarrow$	weak	$\downarrow$	$\downarrow$	$\downarrow$			-----
M <sub>V</sub>		.6 $\pm$ .2	$\downarrow$	weak	$\downarrow$	$\downarrow$	$\downarrow$			-----
N <sub>I</sub>	$\uparrow$	$\uparrow$	$\uparrow$	$\uparrow$	$\uparrow$	$\uparrow$	$\uparrow$			5.97 $\pm$ 0.38
N <sub>II</sub>										0.69 $\pm$ 0.11
N <sub>III</sub>										0.12 $\pm$ 0.05
N <sub>IV</sub>	8.5 $\pm$ 1	7 $\pm$ 1	5.8 $\pm$ .1	6.7	6	5.3 $\pm$ .3				-----
N <sub>V</sub>	$\downarrow$	$\downarrow$	$\downarrow$	$\downarrow$	$\downarrow$	$\downarrow$	$\downarrow$			-----
N <sub>VI, VII</sub>	$\downarrow$	$\downarrow$	$\downarrow$	$\downarrow$	$\downarrow$	$\downarrow$	$\downarrow$			-----
O <sub>I</sub>	2.1 $\pm$ .7	.7 $\pm$ .3	2.1 $\pm$ .2	1.6	1.4	1.4 $\pm$ .2				1.5 $\pm$ 0.3
L Conv. Coeff.	15.5	9.1	--	15.6	--	--	13.5	13.3	15.6	
Reference	92	96	109	110	98	112	103	106	111	Present
	Cranberg	Wu	Bashilov	Frilley	Tousset	Lee	Butt	Fink	Krause	Work

by evaporating the lead very slowly, over a period of minutes, and at very low temperature.

The source dimensions were 1 mm x 25 mm. The source was sufficiently thin to show no appreciable thickness effects down to approximately 7 Kev. The resolution, full width at half maximum, on the  $L_I$  conversion line is 0.18 percent.

#### (b) Data Collection

Approximately eight passes were made over the entire conversion spectrum of RaD, running both upward and downward in momentum. The data were collected in essentially the same way as in the case of the  $Cs^{137}$  experiment described in the previous chapter. The upper sideband of the  $L_I$  conversion line was used as a calibration reference point.

#### (c) Data Analysis

The data were corrected for background and for spectrometer drifts in much the same way as described in section 9.3(c).<sup>\*</sup> The lower resolution used in this experiment makes most of the drifts negligible in comparison to the line width. Figure 54 shows the final form of the data. All the runs were averaged and the points represent counts per minute divided by the potentiometer setting.

---

<sup>\*</sup>Fairly frequent background readings were taken. The source material tended to contaminate the spectrometer vacuum tank gradually raising the background level.

## THE CONVERSION ELECTRON SPECTRUM OF RaD

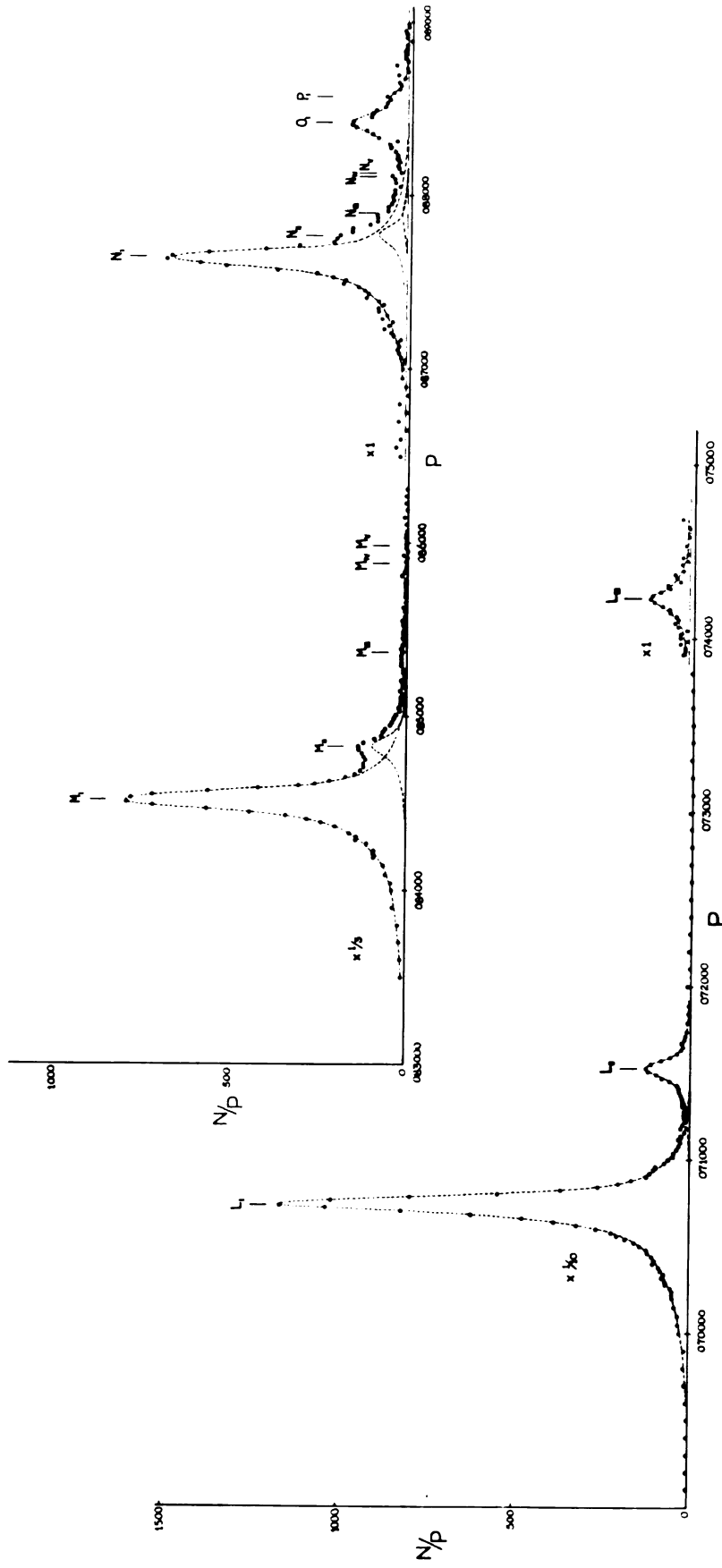


Figure 54. The conversion electron spectrum of RaD.

Before line fitting could be carried out, it was necessary to subtract the small, but nevertheless detectable, contributions of the continuous beta ray components. The procedure used was the following: First, the shapes of the 64 Kev and the 17 Kev end point beta transitions were calculated. The transitions were assumed to be allowed. Using the branching ratio of 15% for the 64 Kev and 85% for the 17 Kev components, the calculated spectra were combined with (100%) RaE beta spectrum whose forbidden shape was taken from the data published by Wu, et al.<sup>96</sup> Second, the low energy maximum (at Br = 250 gauss.cm) of the combined continuous spectra was matched to the experimentally observed value. Finally, the area under the 17 Kev spectrum alone was checked against the total area under the conversion lines. For the total conversion rate value of 0.81 (nuclear data tables) the areas matched within slightly less than four percent. The confidence level of the continuum subtraction is therefore extremely good. The error in the normal background is by far the larger of the two. The four percent error in the beta spectrum represents only a small fraction of a count per minute in the background under the conversion lines, while the normal background rate is about 8-10 counts per minute.

For line fitting, the  $L_I$  line shape was assumed as a standard. The lifetime of the 46.5 Kev state of  $\text{Bi}^{210}$  was measured experimentally as  $\tau < 3 \cdot 10^{-9}$  sec. by Lewis.<sup>114</sup> Weisskopf estimate gives  $2 \cdot 10^{-11}$  sec. for the lifetime.

Since our resolution is approximately 0.2 percent, the above assumption is likely to be good.

The  $L_I$ ,  $L_{II}$  and  $L_{III}$  lines are well separated. In the M shell only the  $M_I$  and the  $M_{II}$  can be seen clearly. There is just a trace of  $M_{III}$ . The rest of the M lines are too weak to be detected. In the N shell the first three lines can be fitted, although the  $N_{III}$  is very weak. The  $N_{IV}$  and the  $N_V$  lie under the low energy tail of the O shell group and thus cannot be seen at all. The remainder of the N shell lines, the  $N_{VI}$  and the  $N_{VII}$ , fall under the  $O_I$  line. The  $O_I$  and  $P_I$  lines are also in evidence and are partially resolved (see Figure 54).

The errors in the relative intensities of the conversion lines are primarily due to statistics. As in the previous chapter, they represent the latitude with which the individual lines may be fitted, while their sum remains within the probable error of the experimental points. Undetected systematic errors may also be present.

## 10.5 Results and Conclusions

Some of the results of this experiment are shown in Figures 55 and 56 and in Table IX. The figures show the theoretical values of the conversion line intensity ratios in the L and the M shells, plotted against transition energy. Both Rose's and Sliv's values are presented for the L shell. The only available theoretical values for the M shell are those calculated by Rose, who used a point nucleus without screening to obtain these values.

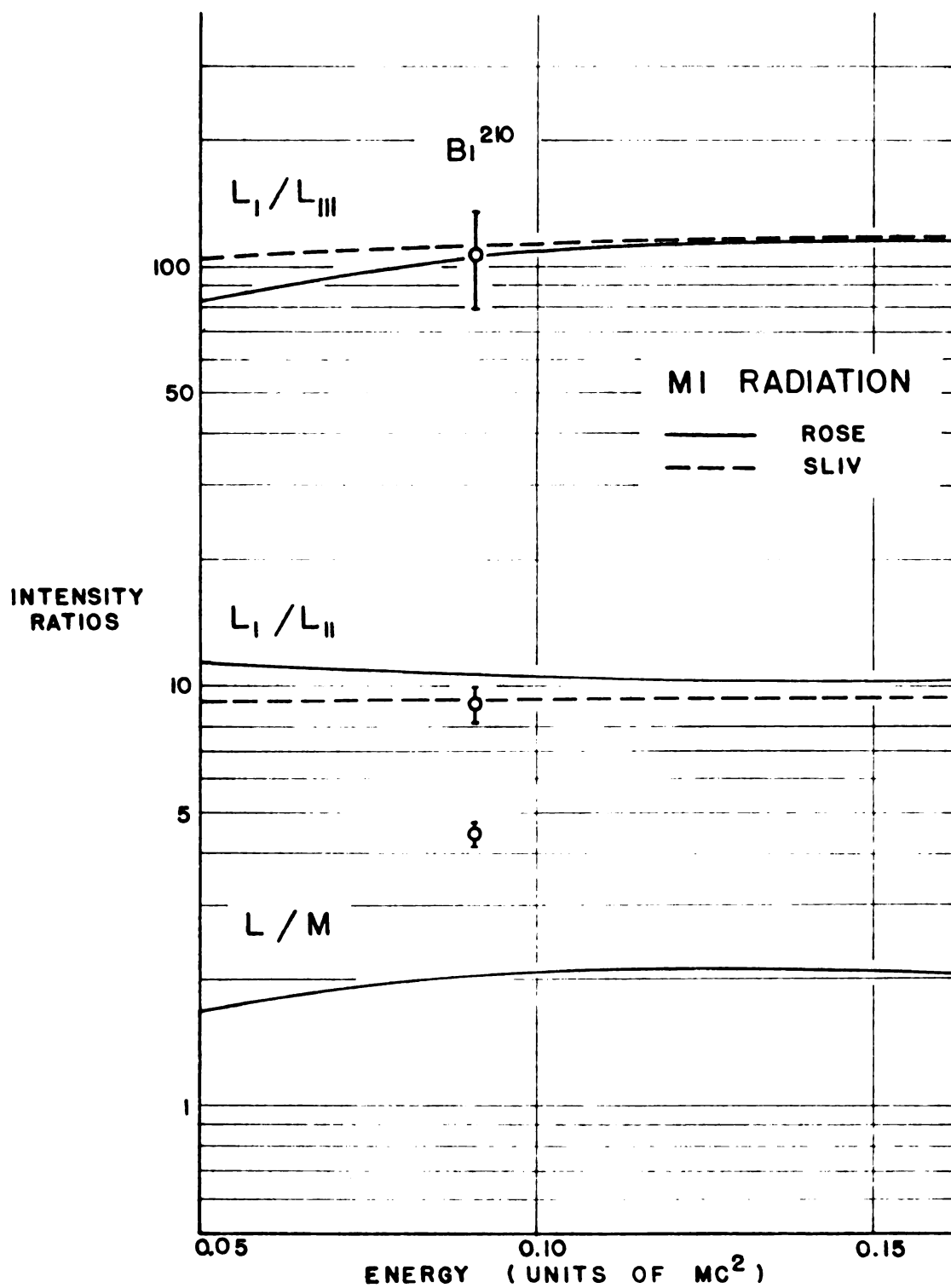


FIGURE 55. CONVERSION LINE INTENSITY RATIOS AS A FUNCTION OF TRANSITION ENERGY.

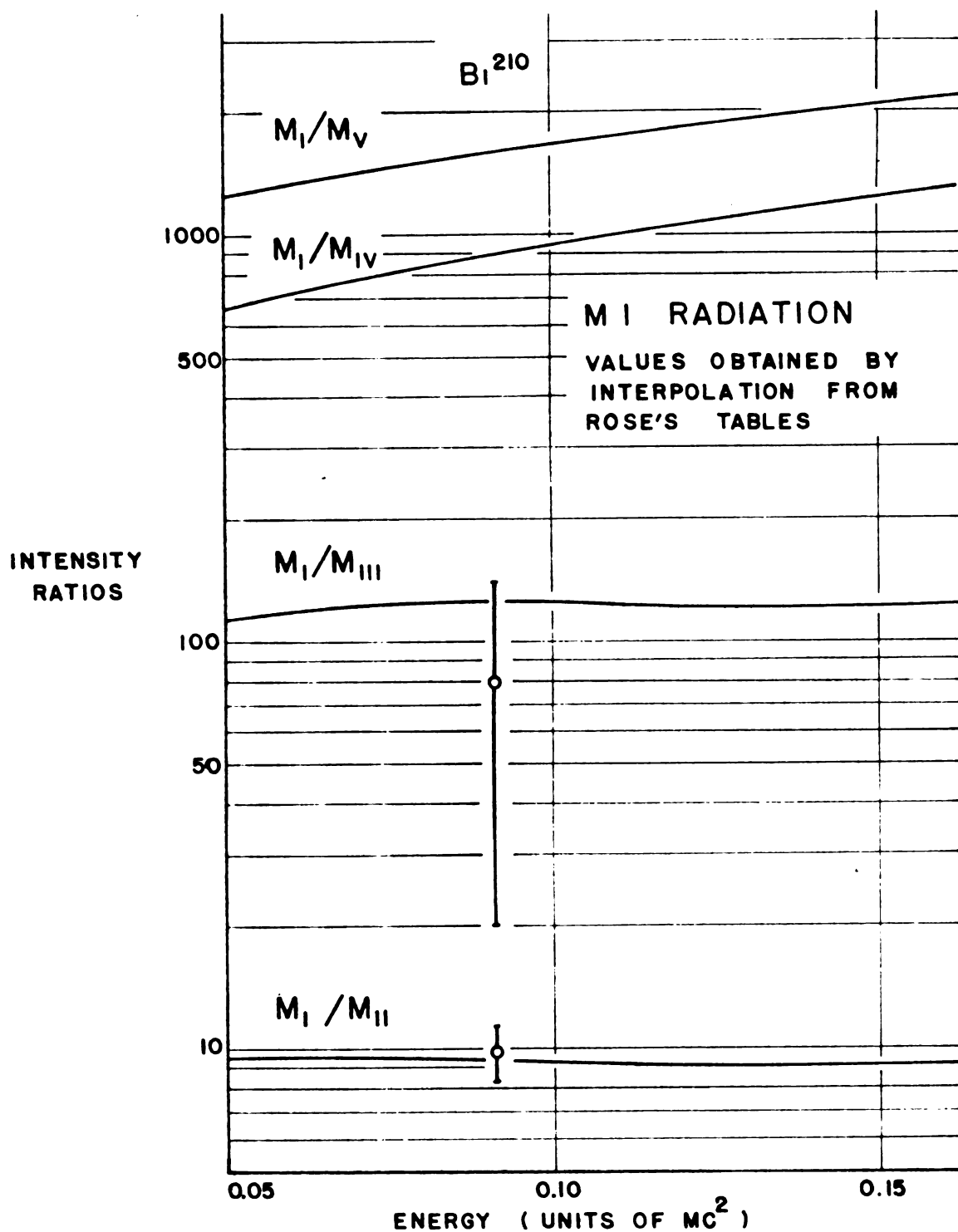


FIGURE 56. CONVERSION LINE INTENSITY RATIOS AS A FUNCTION OF TRANSITION ENERGY.



TABLE IX. Relative Intensities of the RaD Conversion Lines

Line	Rose	Sliv	Present work
$L_I$	1	1	$1 \pm 0.034$
$L_{II}$	0.0962	0.111	$0.111 \pm 0.007$
$L_{III}$	0.00979	0.00922	$0.0094 \pm 0.0028$
$\Sigma L$	1.106	1.120	$1.120 \pm 0.035$
$M_I$	0.511	-----	$0.229 \pm 0.007$
$M_{II}$	0.0549	-----	$0.023 \pm 0.003$
$M_{III}$	0.0042	-----	$0.0029 \pm 0.0022$
$M_{IV}$	0.00057	-----	-----
$M_V$	0.00032	-----	<del>-----</del>
$\Sigma M$	0.571	-----	$0.256 \pm 0.010$
$N_I$	-----	-----	$0.0597 \pm 0.0038$
$N_{II}$	-----	-----	$0.0069 \pm 0.0011$
$N_{III}$	-----	-----	$0.0012 \pm 0.0005$
$\Sigma N_{I-III}$	-----	-----	$0.067 \pm 0.004$
$\Sigma N_{IV-VII}$	-----	-----	$0.015 \pm 0.003$
$\Sigma O+P$	-----	-----	
$L_I/L_{II}$	10.4	9.08	$9.0 \pm 0.7$
$L_I/L_{III}$	102.2	108.5	$107 \pm 29$
$M_I/M_{II}$	9.3	-----	$10.0 \pm 1.4$
$M_I/M_{III}$	128	-----	$79 \pm 59$
$N_I/N_{II}$	-----	-----	$8.7 \pm 1.5$
$N_I/N_{III}$	-----	-----	$52 \pm 22$
$\Sigma L / \Sigma M$	1.94	-----	$4.44 \pm 0.22$
$\Sigma M / \Sigma N_{I-III}$	-----	-----	$3.72 \pm 0.28$
$\Sigma N_{I-III}$	-----	-----	$4.43 \pm 0.95$
$\Sigma N_{IV-VII}^{+O+P}$	-----	-----	

During the interpolation of the L shell coefficients it was found that, while the  $L_I$  and the  $L_{III}$  subshell coefficients of Rose and Sliv (for M-1 radiation) agree quite closely, there is a substantial disagreement in the values for the  $L_{II}$  subshell. Our experimental results of the  $L_{II}$  line intensity are in excellent agreement with Sliv. We are slightly more than two experimental errors off Rose's value.

Table IX summarizes the theoretical relative intensities of the RaD conversion lines and compares them to the values obtained in this experiment. In addition, the experimental values for the N and O shells are presented together with the total shell conversion intensity ratios. It is interesting to note that the L/M, M/N and N/O+P ratios are quite consistent.

Comparison with other workers can be made by the examination of Tables VIII and IX. The resolution used in this experiment is about five times better than the resolution used by Wu, et al.,<sup>96</sup> about the best previously obtained spectrum. In particular, the L subshell lines have been obtained with better separation and better statistics than ever before. In this experiment, the  $L_{II}$  peak rises to approximately 8-10 times background, while in Wu's case it is only about 3 times background. Examination of Wu's spectrum shows very prominent low energy tails on the conversion lines which suggest the possibility of source thickness. The tails would make fitting of the lines more

difficult and could result in the reported discrepancies between Wu and other workers.

Aside from Bashilov, et al.,<sup>109</sup> whose reported experimental errors are hard to understand, and Lee,<sup>112</sup> whose errors are purported to be optimistic, this experiment presents the most complete and statistically reliable picture of the RaD conversion spectrum up to date.

The experimental  $L_I/L_{II}$ ,  $L_I/L_{III}$  and  $M_I/M_{II}$  ratios are in excellent agreement with the theoretical values for pure M-1 radiation. The  $M_I/M_{III}$  ratio has too great an error in the  $M_{III}$  line intensity to be taken too seriously. It is clear that, while the theoretical values of the M shell conversion coefficients do not agree with the experimental values, the ratios of the subshell lines are in good agreement. We note here, as in the case of the Cs<sup>137</sup> decay (chapter 9), that Rose's values of the M shell conversion coefficients are too high. The experimental value of the

$\sum L / \sum M$  ratio is in good agreement with that of the Cs - Ba experiment and the data collected by Bäckström, et al.,<sup>75</sup> for the  $\sum L / \sum M$  ratios of Hg<sup>199</sup>. The summary of these data, presented in Section 9.4, can now be augmented by the RaD result:

	Energy	Multipolarity	L/M (theory)	L/M (experiment)
Ba <sup>137m</sup>	662 Kev	M-4	2.40	4.43
Hg <sup>199</sup>	158 Kev	E-2	2.06	3.85
Hg <sup>199</sup>	50 Kev	M-1	2.11	3.97
Pb <sup>210</sup>	47 Kev	M-1	1.94	4.44

It appears, therefore, that Rose's values of the M shell conversion coefficients should be revised downward by about a factor of two. Rose points out that, as these coefficients were calculated on the basis of an unscreened point nucleus, the individual values may be off by as much as a factor of two. Taken relatively, however, they should be much more accurate. Our two experiments and that of Bäckström confirm this statement and indicate the amount of correction needed to bring theory and experiment into agreement for these energies and particular values of Z.

A comment concerning the conversion lines of a 31.3 Kev gamma ray, reported by Lee<sup>112</sup> may be in order at this point: The energies of the  $L_I$ ,  $L_{II}$  and  $M_I$  lines would be 14.91 Kev, 15.49 Kev and 17.30 Kev respectively. Our experimental coverage of the  $L_I$  line position is very thorough. The  $L_{II}$  and the  $M_I$  line positions are also covered, but with poor statistics. Our data fail to show the presence of any lines at any of these energies.

In conclusion, it can be said that the results of this experiment: Indicate the 46.5 Kev gamma transition to be a pure M-1 radiation, add to the evidence concerning deviations in the tabulation of the M shell conversion coefficients and present the most complete picture of the RaD internal conversion spectrum up to date.

# REFERENCES

1. H. Becquerel, Compt. rend., 122, 420 (1896). *discovery of radioactivity*
2. E. Rutherford and F. Soddy, Phil. Mag., 5, 576 (1903). *discovery of alpha*
3. E. Rutherford and T. Royds, Phil. Mag., 17, 281 (1909). *discovery of alpha*
4. E. Rutherford, Phil. Mag., 21, 661 (1911). *scint. exp.*
5. J. J. Thomson, Proc. Roy. Soc. London, 89, 1 (1913). *discovery of electrons*
6. M. Curie and F. Joliot, C. R. Acad. Sci. Paris, 194, *experimental*  
pages 273, 708, 876 and 2208 (1932).
7. J. Chadwick, Nature, 129, 312 (1932) and Proc. Roy. Soc. London, A136, 692 (1932). *discovery of neutrons*
8. F. Joliot and Irene Curie, Nature, 133, 201 (1934). *artificial radioactivity*
9. E. Schroedinger, Phys. Rev., 28, 1049 (1926). *wave mechanics*
10. E. H. S. Burhop, "The Auger Effect and Other Radiationless Transitions," Cambridge University Press, 1952.
11. M. A. Listengarten, Izvestia Akad. Nauk SSSR, (Physics) 25, 792 (1961).
12. Evelyn Sokolowski, C. Nordling and K. Siegbahn, Phys. Rev., 110, 776 (1958). *from beta*
13. Kai Siegbahn, Editor, "Beta and Gamma Ray Spectroscopy," North Holland Publishing Company, 1955.
14. J. A. Jungerman, M. E. Gardner, C. G. Patten and N. F. Peek, Nuclear Instr. and Methods, 15, 1 (1962). *discovery of*
15. M. S. Freedman, F. Wagner, Jr., F. T. Porter, J. Terandy and P. P. Day, Nuclear Instr. and Methods, 8, 255 (1960). *discovery of*
16. T. R. Gerholm, "Beta-Ray Spectroscopes," in the "Encyclopedia of Physics," edited by S. Flügge, Volume 33, 609, Springer-Verlag 1956.
17. N. Svartholm and K. Siegbahn, Arkiv för Mat. Astr. och Fys., 33A, No. 21, 17 (1946). *discovery of*
18. N. Svartholm, Arkiv för Mat. Astr. och Fys., 33A, No. 24, 12 (1946). *discovery of*

19. F. B. Shull and D. M. Dennison, Phys. Rev., 71, 681 (1947).
20. G. L. Lee-Whiting and E. A. Taylor, Atomic Energy of Canada, Ltd., Chalk River Project Report No. CRT 668, (1956). Chalk River Project Report No. CRT 668, higher order
21. K. Siegbahn and K. Edvarson, Nuclear Physics, 1, No. 3, 137 (1956).
22. C. DeVries and A. H. Wapstra, Nuclear Instr. and Methods, 8, 121 (1960).
23. M. Mladjenovic, Proc. of Rehovoth Conf., 537 (1957).
24. K. Siegbahn, C. L. Nordling, J. M. Hollander, Chemistry Div. Annual Report 1961, VCRL-10023, Jan., 1962.
25. A. Moussa and J. B. Bellicard, J. Phys. et Radium, 15, 85A (1954).
26. J. B. Bellicard and A. Moussa, J. Phys. et Radium, 15, 532 (1956).
27. G. E. Lee-Whiting and E. A. Taylor, Can. J. Phys., 35, 1 (1957).
28. R. L. Graham, G. T. Ewan and J. S. Geiger, Nuc. Instr. and Methods, 9, 245 (1960).
29. Q. L. Baird, J. C. Nall, S. K. Haynes and J. H. Hamilton, Nuc. Instr. and Methods, 16, 275 (1962).
30. T. R. Lyle, Phil. Mag., 3, (6), 310 (1902).
31. R. A. Parker, "A Low Background Geiger Mueller Counter for a Low Energy Beta-Ray Spectrometer," M.S. Thesis, Vanderbilt University, (1960).
32. H. S. Sommers, P. R. Weiss and W. Halpern, Rev. Sci. Instr., 20, 244 (1949) and 22, 612 (1951).
33. R. L. Garwin, D. Hutchinson, S. Penman and G. Shapiro, Rev. Sci. Instr., 30, 105 (1959).
34. J. C. Nall, "An Iron-Free, Double Focusing, Beta-Ray Spectrometer and the Analysis of the L-Auger Spectrum of Gold 199 - Mercury 199," Ph.D. Thesis, Vanderbilt University, 1958.
35. R. L. Garwin, Rev. Sci. Instr., 29, 223 and 900 (1958).
36. W. F. Brown and J. H. Sweer, Rev. Sci. Instr., 6, 276 (1945).

37. K. I. Williamson, J. Sci. Instr., 24, 242 (1947).
38. R. F. K. Herzog and O. Rischler, Rev. Sci. Instr., 24, 1000 (1953).
39. H. E. Hoeschel, Machine Design, 32, #3, 141 (1960).
40. G. Bäckström, A. Bäcklin, N. E. Holmberg and K. E. Bergkvist, "A Magnetic Spectrometer for Neutron Capture Experiments," private communication.
41. B. T. Smith, M.S.U. Cyclotron Project Report, MSUCP-8.
42. R. O. Lane and D. J. Zaffarano, Phys. Rev. 94, 960 (1954).
43. A. W. Smith, "Detection of Very Low Energy Electrons in a Beta-Ray Spectrometer," M.S. Thesis, Vanderbilt University, 1953.
44. A. O. Burford, "The L-Auger Spectrum of Cesium-Barium 137," Ph.D. Thesis, Vanderbilt University, 1958.
45. K. Stroheimer, Ark. Naturf., 6a, 508 (1951).
46. L. Harris, J. Opt. Soc. Amer., 45, 27 (1955).
47. U. Hauser and W. Kerler, Rev. Sci. Instr., 29, 380 (1958).
48. K. Sevier and W. Parker, Nuc. Instr. and Methods, 6, 218 (1960).
49. G. Dearnaley, Rev. Sci. Instr., 31, 197 (1959).
50. E. Kashy, R. R. Perry and J. R. Risser, Nuc. Instr. and Methods, 4, 167 (1959).
51. W. Parker, M. DeCroës and K. Sevier, Nuc. Instr. and Methods, 7, 22 (1960).
52. J. S. Geiger, R. L. Graham and F. Brown, Can. J. Phys., 40, 1258 (1962).
53. C. L. Peacock and A. C. G. Mitchell, Phys. Rev., 75, 1273 (1949).
54. H. M. Agnew, Phys. Rev., 77, 655 (1950).
55. L. M. Langer and R. D. Moffat, Phys. Rev., 82, 635 (1951).
56. Y. Yoshizawa, Nuc. Physics, 5, 122 (1958).

57. J. S. Osoba, Phys. Rev., 76, 345 (1949).
58. A. C. G. Mitchell and C. L. Peacock, Phys. Rev., 75, 197 (1949).
59. M. A. Waggoner, Phys. Rev., 82, 906 (1951).
60. R. L. Heath and P. R. Bell, Phys. Rev., 87, 176A (1952).
61. V. M. Dolishnyuk, G. M. Drabkin, V. I. Orlov and L. I. Rusinov, Doklady Akad. Nauk SSSR, 92, 1141 (1953).
62. T. Azuma, J. Phys. Soc. Japan, 9, 1 (1954).
63. A. H. Wapstra, Arkiv Fysik, 7, 275 (1954).
64. F. K. McGowan and P. H. Stelson, Phys. Rev., 107, 1674 (1957).
65. R. A. Ricci, Physica, 23, 693 (1957).
66. S. Hultberg and R. Stockendahl, Arkiv Fysik, 14, 565 (1959).
67. C. deVries, E. J. Bleeker and N. Salomons-Grobbe, Nuclear Physics, 18, 454 (1960).
68. W. L. Bendel, F. J. Shore, N. H. Brown and R. A. Becker, Phys. Rev., 87, 195A (1952).
69. W. E. Kinney, AECU-2921, (1953).
70. J. Verhaege and J. Demuyne, Compt. rend., 239, 1374 (1954).
71. I. A. Antonova, Izvest. Akad. Nauk SSSR, Ser. Fiz. 20, 896 (1956).
72. M. E. Rose, "Beta and Gamma Ray Spectroscopy," K. Siegbahn, ed., see ref. 13.
73. M. E. Rose, "Internal Conversion Coefficients," North Holland Publishing Company, 1958.
74. L. A. Sliv and I. M. Band, "Coefficients of Internal Conversion of Gamma Radiation," Parts 1 and 2, Academy of Science of the U.S.S.R., 1958. Issued in U.S.A. as Report 58 ICC L1, Physics Department, University of Illinois, Urbana, Illinois.
75. G. Bäckström, O. Bergman and J. Burde, Nuclear Phys., 7, 263 (1958).



76. C. D. Ellis, Proc. Roy. Soc. (London), A99, 261 (1921) and A101, 1 (1922).
77. L. Meitner, Z. Physik, 9, 131 and 145 (1922).
78. H. M. Taylor and N. F. Mott, Proc. Roy. Soc. (London), A142, 215 (1933).
79. H. R. Hulme, Proc. Roy. Soc. (London), A138, 643 (1932).
80. N. Tralli and G. Goertzel, Phys. Rev., 83, 399 (1951).
81. L. A. Sliv and I. M. Band, Zhur. Eksp. i Teoret. Fiz., 31, 134 (1956).
82. M. E. Rose, G. H. Goertzel, B. I. Spinrad, J. Harr and P. Strong, Phys. Rev., 83, 79 (1951).
83. T. A. Green and M. E. Rose, Phys. Rev., 110, 105 (1958).
84. A. H. Wapstra and G. J. Nijgh, Nuclear Phys., 1, 245 (1956).
85. F. K. McGowan and P. H. Stelson, Phys. Rev., 103, 1133 (1956).
86. C. Nordling, K. Siegbahn, E. Sokolowski and A. H. Wapstra, Nuclear Phys., 1, 326 (1956).
87. E. L. Church and J. Weneser, Phys. Rev., 104, 1382 (1956).
88. M. A. Preston, "Physics of the Nucleus," Addison Wesley Publishing Company, 1962 (Chapter 11).
89. H. O. W. Richardson and A. Leigh-Smith, Proc. Roy. Soc., A160, 454 (1937).
90. D. D. Lee and W. F. Libby, Phys. Rev., 55, 252 (1939).
91. B. Kinsey, Canad. J. Res., 26, 421 (1948).
92. G. Cranberg, Phys. Rev., 77, 155 (1950).
93. G. M. Insch, J. G. Balfour and S. C. Curran, Phys. Rev., 85, 805 (1952).
94. A. A. Jaffe and S. G. Cohen, Phys. Rev., 86, 1041 (1952).
95. A. A. Jaffe and S. G. Cohen, Phys. Rev., 89, 454 (1953).
96. C. S. Wu, F. Boehm and E. Nagel, Phys. Rev., 91, 319 (1953).

97. W. Stanners and M. A. S. Ross, Proc. Phys. Soc., A69, 836 (1956).
98. J. Tousset and A. Moussa, Compt. Rend. 245, 1617 (1957).
99. E. Amaldi and F. Rasetti, Ricerca Scient., 10, 111 (1939).
100. San-Tsiang Tsien, Phys. Rev., 69, 38 (1946).
101. M. Frilley, Compt. Rend., 213, 505 (1944).
102. J. M. Cork, C. E. Branyan, A. E. Stoddard, H. B. Keller, J. M. LeBlanc and W. J. Childs, Phys. Rev., 83, 681 (1951).
103. D. K. Butt and W. D. Brodie, Proc. Phys. Soc. (London), A64, 791 (1951).
104. P. E. Damon and R. R. Edwards, Phys. Rev., 90, 280 (1953).
105. P. E. Damon and R. R. Edwards, Phys. Rev., 95, 1698 (1954).
106. R. W. Fink, G. W. Warren, R. R. Edwards and P. E. Damon, Phys. Rev., 103, 651 (1956).
107. Gellman, Griffin and Stanley, Phys. Rev., 85, 944 (1952).
108. E. A. Plassmann and L. M. Langer, Phys. Rev., 96, 1593 (1954).
109. A. A. Bashilov, B. S. Dzhelepov and C. S. Chervinskaya, Izv. Akad. Nauk SSSR, Ser. Fiz., 17, 428 (1953).
110. M. Frilley and M. Valadares, J. Phys. et Radium, 18, 468 (1957).
111. I. Y. Krause, Zeit. f. Physik, 152, 586 (1958).
112. N. K. Lee, "Auger and Conversion Spectrum of Radium D," M.S. Thesis, Vanderbilt University, 1958.
113. S. K. Haynes, Private communication.
114. G. M. Lewis, Proc. Phys. Soc. (London), A68, 735 (1955).

MICHIGAN STATE UNIVERSITY  
DEPARTMENT OF PHYSICS  
EAST LANSING, MICHIGAN

MICHIGAN STATE UNIV. LIBRARIES



31293017430038